Mitochondrial degradation by autophagy (mitophagy) in hepatocytes

Insil Kim

A dissertation submitted to the faculty of the University of North Carolina at Chapel Hill in partial fulfillment of the requirements for the degree of Doctor of Philosophy in the Department of Cell and Developmental Biology.

Chapel Hill
2008

Approved by

Advisor: John J. Lemasters, MD, PhD

Reader: Keith W. T. Burridige, PhD

Reader: Mohanish Deshmukh, PhD

Reader: Ann H. Erickson, PhD

Reader: Richard A. Rippe, PhD

Abstract

Insil Kim: Mitochondrial degradation by autophagy (mitophagy) in hepatocytes (under the direction of John J. Lemasters, M.D., Ph. D)

Mitochondria are the essential site of aerobic energy production in eukaryotic cells. Reactive oxygen species (ROS) are an inevitable by-product of mitochondria metabolism and can cause mitochondrial DNA mutations and dysfunction. Mitochondrial damage can also be the consequence of disease processes. Therefore, maintaining a healthy population of mitochondria is essential to the well-being of cells. Autophagic delivery to lysosomes is the major degradative pathway in mitochondrial turnover. I use the term mitophagy to refer to mitochondrial degradation by autophagy. Although long assumed to be a random process, increasing evidence indicates that mitophagy is a selective process. This study provides a description of a description of the process of mitophagy, the possible role of the mitochondrial permeability transition in mitophagy and the importance of mitophagy in turnover of dysfunctional mitochondria.

Acknowledgements

The work presented in this thesis was done under the supervision of Professor John J. Lemasters in the Department of Cell and Developmental Biology, University of North Carolina at Chapel Hill. I thank Dr. Lemasters for his support and advice.

I wish to thank Drs. Keith Burridige, Mohanish Deshmukh, Ann Erickson, and Richard Rippe for their advice.

I wish to thank Dr. Vytas A. Bankaitis and the staff of University Department of Cell and Development for their friendship and encouragement.

I wish to thank Dr. Rick G. Schnellmann, for his advice and support, and the staff of Department of Pharmaceutical Science at Medical University of South Carolina for their friendship and encouragement.

Finally, I wish to thank my parent, brother, aunt, uncle, Grace, and friends for their love and support.

Table of contents

List of figures

List of abbreviations

Abbreviation	
Atg	Autophagy related
Bcl-2	B-cell lymphoma 2
BimEL, L, and S	Bcl-2-interacting mediator extra long, long, and short
Calcine AM	Calcein acetoxymethyl ester
CsA	Cyclosporin A
DN-JNK	Dominant negative JNK
GFP-LC3	Green fluorescence protein fused microtubule-associated protein 1 light chain 3
HDM	Hormonally defined medium
JIP	JNK interacting protein
JNK	c-Jun NH_2-terminal kinase
JPI	JNK peptide inhibitor
KRH/G	Krebs-Ringer HEPES buffer plus glucagon
LC3	microtubule-associated protein 1 light chain 3
LTR	LysoTracker Red
MPT	Mitochondrial permeability transition
mtDNA	Mitochondrial DNA
MFFR	MitoFluoro Far Red
MTG	MitoTracker Green
NIM	NIM811, CsA analogue
PAS	Pre-autophagic structure
ROS	Reactive oxygen species

TMRM	Tetramethylrhodamine Methyl Ester
WM	Waymouth's complete growth medium MB 752/1
3-MA	3-methyladenine

Chapter 1. General introduction

(This work was published in Archives of Biochemistry and Biophysics as 'Selective degradation of mitochondria by mitophagy' and written by Insil Kim, Sara Rodriguez-Enriquez, and John Lemasters.)

1.1. Introduction

1.2. General features of autophagy

1.3. Molecular control of autophagy

1.4. Characteristics and possible structure of mitochondrial permeability transition pores

1.5. Selective autophagy and mitophagy

1.6. Mitophagy and cell death

1.7. Mitophagy in aging

Chapter 1. General introduction

1.1. Introduction

Autophagy is an adaptive process that maintains cellular homeostasis under various adverse conditions such as starvation (Mitchener et al., 1976; DE, 1963). During autophagy, cytoplasmic components are sequestered into vesicles called autophagosomes. After formation, autophagosomes fuse with lysosomes, which leads to lysosomal degradation of the autophagosomal content (Punnonen et al., 1992). Autophagic dysfunction is relevant in the pathogenesis of neurodegenerative diseases, aging, infectious diseases, and cancer (Yuan et al., 2003; Bergamini et al., 2003; Dorn et al., 2002; Nakagawa et al., 2004; Yue et al., 2003). Although autophagy has long been assumed to be a non-selective process, recent evidence indicates autophagy selectively removes damaged and dysfunctional mitochondria that might otherwise induce cell death signaling pathways (Elmore et al., 2001; Rodriguez-Enriquez et al., 2006; Kim et al., 2007). While yeast genetic screens have increased our understanding of the molecular mechanisms of autophagy, the mechanism for mitochondrial autophagy (mitophagy) remains poorly understood. This chapter is written to give an in depth understanding of mitophagy and possible mechanisms involved in mitophagy.

1.2. General features of autophagy

The balance between anabolism and catabolism is a fundamental element of life. There are two major degradation systems -- proteasomal proteolysis and autophagy. Proteasomal degradation is involved in selectively removing short-lived proteins as well as abnormal proteins; whereas autophagy is responsible for degrading long-lived proteins and organelles (Goldberg, 2003; Cuervo, 2004; Gronostajski et al., 1985). Three types of autophagy have

been described: chaperone-mediated autophagy, microautophagy, and macroautophagy (Cuervo, 2004). Chaperone-mediated autophagy involves direct translocation of proteins with specific protein motifs across lysosomal membranes through recognition by chaperone proteins that interact with lysosomal membrane proteins to facilitate translocation. Microautophagy is the direct intake of cytoplasm by invagination of lysosomal membranes. Macroautophagy, often referred to simply as autophagy, involves formation of double membrane vesicles around organelles and other cytoplasmic components that then fuse with lysosomes (Levine and Klionsky, 2004).

Autophagy is ongoing in nucleated cells and is typically activated by fasting and nutrient deprivation. In the liver particularly, glucagon promotes autophagy, whereas insulin negatively regulates autophagy (Arstila and Trump, 1968; Schworer and Mortimore, 1979). During fasting, autophagy is important for generating amino acids, fueling the tricarboxylic cycle and maintaining ATP energy production. Autophagy also removes toxic protein aggregates and unneeded organelles. Both insufficient and excess autophagy seem capable of promoting cell injury (Levine and Yuan, 2005). Appropriate regulation of autophagy is thus essential for cellular well-being.

During autophagy, an isolation membrane forms a cup-shaped membranous structure called a phagophore that eventually envelopes the autophagic target (Figure 1.1) (Seglen et al., 1996; Suzuki et al., 2001; Reggiori et al., 2005). The origin of isolation membranes is controversial. One proposed source is ribosome-free regions of the rough endoplasmic reticulum (ER), but others suggest that isolation membranes are novel structures devoid of Golgi and ER markers (Suzuki et al., 2001). As isolation membranes envelop and seal around their targets, double–membrane vesicles called autophagosomes form. These

autophagosomes then fuse with lysosomes to form autolysosomes. Their sequestered contents are degraded by lysosomal hydrolases and recycled.

As first characterized in yeast, a machinery of genetically conserved autophagy-related proteins regulates and participates in autophagy (Ohsumi and Mizushima, 2004). These Atg proteins are grouped into different categories depending on their function, including 1) a serine-threonine kinase complex, such as Atg1, involved in autophagic induction, 2) a Class III phosphatidyl inositol-3-kinase (PI3K) complex which functions in vesicle nucleation, 3) Atg9 which functions in membrane protein recycling, and 4) a pair of novel ubiquitin-like protein conjugating systems, the Atg12 and Atg8 systems, which produce vesicle extension and completion (Yorimitsu and Klionsky, 2005)

During sequestration and formation of autophagosomes, an Atg12-Atg5 complex binds to Atg16, which translocates to the isolation membrane and functions as a linker involved in formation and elongation of the isolation membrane (Figure 1.1). An E1-like enzyme, Atg7, activates Atg12, which is transferred to Atg10, an E2-like enzyme. Atg12 then becomes conjugated to Atg5 to form an autophagosomal precursor in complex with Atg16 (Ohsumi and Mizushima, 2004; Matsushita et al., 2007)

LC3 is a mammalian autophagosomal ortholog of yeast Atg8. In mammalian cells, newly synthesized proLC3 is cleaved to its cytosolic form, LC3-I, by Atg4B exposing its C-terminal glycine 120. Then LC3-I is activated by Atg7p, a E1-like enzyme, and conjugated to phosphatidylethanolamine (PE) by Atg3p, an E2-like enzyme (Kabeya et al., 2000; Tanida et al., 2004). LC3-II (16kDa) has slightly higher mobility than LC3-I (18kDa) when run in SDS-PAGE gels. LC3-II selectively incorporates into forming and newly formed autophagosomes making LC3-II a useful autophagosomal marker. Some LC3-II becomes

entrapped on the inner surface of double membrane autophagosomes. After fusion with lysosomes, this LC3-II is degraded. Surface LC3-II also disappears due to its deconjugation from PE by Atg4B (Figure 1.1). Recently, a transgenic mouse strain was created that expresses a green fluorescent protein (GFP)-LC3-II fusion protein. In cells and tissues of this mouse, GFP fluorescence selectively identifies the membranes of forming autophagosomes and newly formed autophagosomes (Mizushima et al., 2004).

1.3. Molecular Control of Autophagy.

Phosphoinositide 3-kinases (PI3Ks) phosphorylate phosphotidylinositol at position 3 of the inositol ring and play an important role in the regulation of autophagy (Meijer and Codogno, 2006). PI3K inhibitors, such as 3-methyladenine, wortmannin, and LY294002, potently block autophagy. However, different classes of PI3K exert opposing effects on autophagy: Class III PI3K promotes sequestration of autophagic vacuoles, whereas class I PI3K inhibits autophagy. Class III PI3K/p150 associates with Beclin1, a mammalian homologue of Atg6 discovered by yeast two hybrid screening for its interaction with Bcl-2. Recruitment of PI3K-Beclin1 complexes together with Atg12-Atg5 is an initial step in autophagosome formation (Tassa et al., 2003). Mammalian target of rapamycin (mTor) is a kinase downstream of Class I PI3K whose activation suppresses autophagy. Rapamycin, which inhibits mTOR, induces autophagy apparently by activating protein phosphatase 2A (PP2A) (Noda and Ohsumi, 1998). PP2A also dephosphorylates proapoptotic BH3 only Bcl-2 family proteins, such as Bad and Bcl-2, that associate with mitochondrial membranes (Simizu et al., 2004). Moreover, overexpression of Bcl-2 inhibits starvation-induced

autophagy (Pattingre et al., 2005). Thus, a functional relationship between autophagic proteins and mitochondrial proteins may exist.

The mammalian Bcl-2 family consists of more than 20 different proteins that are divided into anti- and proapoptotic members in accordance with the presence of different Bcl-2 homology domains (BH1, BH2, BH3, and BH4) (Lutz, 2000). Anti-apoptotic members contain all four of these domains include Bcl-2, Bcl-xl, and Mcl-1. These proteins are located on the mitochondrial outer membrane and some other endomembranes, such as endoplasmic reticulum. Proapoptotic Bcl-2 family proteins, often thought to contain only BH3 regions or BH1, BH2, and BH3 regions, reside primarily in the cytoplasm and translocate to the outer membrane of mitochondria during apoptotic signaling. Bim is one of these proapoptotic BH3-only proteins, which forms a heterodimer with other members of anti-apoptotic proteins, such as Bcl-2, Bcl-xl, and Mcl-2, and other pro-apoptotic proteins, such as Bax. In this way, Bim may elicit either survival or death responses. Three main isoforms of Bim, Bim EL (extra long), Bim L (long), and Bim S (short), are detected in a various tissues and cell types (O'Reilly et al., 2000). These isoforms contain a BH3 domain and a hydrophobic tail which is required their interaction with mitochondria, but they differ at their N-terminus regions. Under normal conditions, BimEL is associated with cytoplasmic dynein light chain (LC8) which is tightly sequestered into microtubule-associated dynein motor complexes. This interaction is disrupted by apoptotic stimuli, which leads to BimEL translocation to mitochondria where it activates Bax or binds to Bcl-2 protein (Puthalakath et al., 1999; Liu et al., 2003). BimEL is phosphorylated by Erk1/2 at different sites, which have not been identified and which promote proteasomal degradation and prevent the interaction of BimEL with Bax (Harada et al., 2004; Luciano et al., 2003). BimEL expression increases during

proapoptotic withdrawal of growth factors and starvation (Austin and Cook, 2005; Quadros et al., 2006).

JNK (c-Jun NH_2-terminal kinase) is a stress-induced kinase that may be involved in autophagy (Rodriguez-Enriquez et al., 2006; Aubel et al., 2001; Leicht et al., 2003). JNK is a mitogen-activated protein kinase (MAPK), a class of kinases that responds to cellular stresses such as pH changes, cytokines, UV exposure, hypoxia, heat shock, and ethanol. When phosphorylated, JNK activates nuclear substrates such as c-Jun and ATF2 and cytosolic substrates such as Bcl-2 family proteins leading to cellular proliferation, transformation, and programmed cell death (Minden et al., 1994a; Minden et al., 1994b; Maundrell et al., 1997). JNK consists of JNK1, JNK2 and JNK3. JNK1 and JNK2 are expressed ubiquitously; whereas, JNK3 is mainly expressed in the brain (Gupta et al., 1996). Although JNK isoforms are similar in structure, they have distinct functions. For example, JNK1 deficiency enhances tumor growth, whereas JNK2 deficiency suppress tumor growth (Chen et al., 2001; She et al., 2002). JNK1 mediates insulin resistance by phosphorylating IRS-1 (insulin receptor substrate-1) in animal models, whereas JNK2 is recruited by apoptotic signaling pathways causing mitochondrial dysfunction (Coffey et al., 2002; Hirosumi et al., 2002; Eminel et al., 2004). In TNF-dependent hepatotoxicity, caspase-8 activation and Bid cleavage are elicited by JNK2 (Wang et al., 2006). JNK2 is also proposed to translocate to mitochondria mediating cytochrome *c* release in 6-hydroxydopamine-induced neuronal cell death (Eminel et al., 2004). Translocation of active JNK to mitochondria also occurs in HeLa cells after treatment with paclitaxel. In this model, JNK associates with PP1 (protein phosphatase 1) and Bcl-2 on the mitochondria (Brichese et al., 2004). Such activation of JNK is required for zVAD-induced autophagic cell death (Yu et al., 2004).

Heterotrimeric guanine nucleotide-binding proteins are also involved in autophagy. Nonhydrolyzable GTP analogs, such as GTPγS, inhibit autophagy (Kadowaki et al., 1996). The G_{α}-interacting protein (GAIP) elicits autophagic sequestration by accelerating GTP hydrolysis and activating $G_{\alpha i3}$. In addition, Rab24, Rab22, and Rab7, small GTP binding proteins that regulate vesicular transport, participate in processing of late autophagosomes (Jager et al., 2004; Petiot et al., 2002).

1.4. Characteristics and Possible Structure of Mitochondrial Permeability Transition Pores

Recent evidence suggests a possible involvement of the MPT in autophagy (Elmore et al., 2001; Rodriguez-Enriquez et al., 2006). In the MPT, opening of PT pores causes mitochondria to become permeable to all solutes up to a molecular mass of about 1500 Da, an event leading to mitochondrial depolarization and activation of the mitochondrial ATPase (ATP synthase operating in reverse) (Hunter et al., 1976; Gunter and Pfeiffer, 1990; Zoratti and Szabo, 1995; Forte and Bernardi, 2005). After the MPT, mitochondria undergo large amplitude swelling driven by colloid osmotic forces, which culminates in rupture of the outer membrane and release of proapoptotic mitochondrial intermembrane proteins into the cytosol, including cytochrome *c*, apoptosis inducing factor, Smac/Diablo and others. The immunosuppressant compound, cyclosporin A (CsA), and various of its analogs inhibit the MPT through interaction with cyclophilin D (CypD) (Waldmeier et al., 2003; Halestrap and Davidson, 1990).

In one model, PT pores are composed of the voltage dependent anion channel (VDAC) in the outer membrane, the adenine nucleotide translocator (ANT) in the inner

membrane and CypD in the matrix space (Figure 1.2A) (Halestrap and Davidson, 1990; Crompton et al., 1998; Beutner et al., 1996; Marzo et al., 1998). Other proteins, such as creatine kinase (intermembrane space), hexokinase (outer membrane) and Bax (outer membrane), are also proposed to contribute to the composition of PT pores. However, the MPT still occurs in cells types like hepatocytes that lack creatine kinase and hexokinase and in ANT-deficient mitochondria isolated from conditional double ANT knockout mice (Kokoszka et al., 2004). Most recently, CypD knockout mice have been developed, and mitochondria from these mitochondria still display an MPT, but the MPT observed is insensitive to cyclosporine A (CsA) and requires higher concentrations of calcium for induction (Basso et al., 2005).

An alternative model of the MPT has been proposed that accounts for these observations (Figure 1.2B) (He and Lemasters, 2002). This model postulates that PT pores form as a consequence of misfolding of integral membrane proteins caused by ROS, reactive chemicals and other stresses. Because misfolding exposes hydrophilic surfaces to the hydrophobic membrane bilayer, the proteins aggregate at these hydrophilic surfaces to enclose channels that conduct all aqueous solutes smaller in size than the channel diameter. Since such permeabilizatoin would be catastrophic to mitochondrial function, chaperones have evolved, including cyclophilin D, that block conductance through these nascent channels. Other chaperones remain to be identified, although indirect evidence suggests that the small heat shock protein, Hsp25/27, and the Rieske iron sulfur protein may be involved (He and Lemasters, 2005; He and Lemasters, 2003). When matrix calcium rises to high levels, PT pores open to induce the MPT, an effect mediated by CypD and blocked by CsA. When formation of nascent PT pores from misfolded protein aggregates exceeds the number

of chaperones that can regulate and close these pores, an unregulated MPT occurs that is CsA-insensitive and calcium-independent. This change from a regulated to an unregulated PT pore occurs as the time and strength of MPT induction increases.

On a molar basis, ANT is the most abundant inner membrane protein and thus is often a target of stresses causing protein misfolding. However, other proteins can also misfold, which explains MPT onset in ANT knockout mice. Since CypD participates in calcium sensing, the model also explains the greater requirement for calcium for the MPT in CypD deficient mitochondria. Lastly, the model explains why completely exogenous pore-forming peptides like mastoparan and alamethicin induce a CsA-sensitive and calcium-dependent MPT at low concentrations, but CsA-insensitive and calcium-independent mitochondrial swelling at higher concentrations (Pfeiffer et al., 1995; He and Lemasters, 2002). At low concentration, chaperones recognize the pore-forming peptides as misfolded protein aggregates and block their conductance, but as the chaperone supply becomes exhausted conductance can no longer be blocked, and mitochondrial swelling, depolarization and uncoupling ensue.

Autophagic stimulation of rat hepatocytes by serum deprivation and glucagon (a hormone released to the liver during fasting) increases the rate of spontaneous depolarization of mitochondria by 5-fold to about 1% of mitochondria per hour (Elmore et al., 2001). These depolarized mitochondria move into acidic vacuoles, which also increase in number after nutrient deprivation. The acidic structures containing mitochondrial remnants are autophagosomes and autolysosomes, and serial imaging reveals an average mitochondrial digestion time of about 7 min after autophagic sequestration (Rodriguez-Enriquez et al., 2006). CsA, the MPT blocker, suppresses both mitochondrial depolarization during nutrient

deprivation and the proliferation of autophagosomes and autolysosomes. Tacrolimus, an immunosuppressant that does not block the MPT, does not block autophagosomal proliferation, whereas NIM811, a CsA analog and MPT inhibitor that is not immunosuppressive, does block MPT (Elmore et al., 2001; Rodriguez-Enriquez et al., 2006).

1.4. Selective Autophagy and Mitophagy

Whether autophagy is selective or non-selective has been controversial. Autophagosomes observed by EM often contain a variety of different cytoplasmic elements, including cytosolic proteins and organelles such as ER, peroxisomes and mitochondria (Kopitz et al., 1990). Moreover, the degradation of cytoplasmic proteins was demonstrated to be nonselective (Kopitz et al., 1990). Such findings led to the assumption that autophagy is a non-selective form of lysosomal digestion. However, more recent findings indicate that autophagy can be a selective process. In yeast grown on methanol as a carbon source, peroxisomes proliferate. Changing the nutrient broth to glucose- or ethanol-containing medium results in specific degradation of peroxisomes by autophagy, a selective process termed pexophagy (Kim and Klionsky, 2000). Moreover, withdrawal of treatment of hepatocytes with indi-(2-ethylhexyl)phthalate (DEHP), a peroxisome proliferator, in the presence of protease inhibitors leads to accumulation of peroxisomes in autophagosomes indicating selective removal of peroxisomes in mammalian cells (Yokota, 2003). Peroxin 14 is required for recognition of peroxisomes for the pexophagy process in yeast (Bellu et al., 2001)

Some pathogens selectively regulate autophagy in mammalian cells for their survival. *Shigella flexneri* produces the protein, IscB, which inhibits the binding of bacterial VirG to

Atg5 in cytoplasm, which would otherwise induce autophagy (Ogawa et al., 2005). In this way, shigella escapes recognition for autophagic sequestration and elimination. In addition during the postnatal period, glycogen is selectively sequestered into autophagosomes to enhance glycolytic substrate generation after interruption of transplacental nutrition (Kuma et al., 2004). Autophagosomes formed postnatally contain large amounts of glycogen and rarely contain mitochondria or other organelles (Kotoulas et al., 2006).

Increasing evidence indicates that autophagy of mitochondria also occurs selectively, and the term mitophagy has been suggested for this selective mitochondrial autophagy (Lemasters, 2005). For example, in Uth1p deficident yeast, nutrient dprivation stimulates normal autophagy of various organelles but not mitochondria (Kissova et al., 2004). However, a corresponding mammalian protein is yet to be identified. Additionally, mutation in Aup1, which is a mitochondrial phosphatase homologue localized to mitochondrial intermembrane space, leads to reduction of mitophagy in yeast during stationary phase (Tal et al., 2007).

1.6. Mitophagy and Cell Death

Controversy exists as to whether autophagy promotes or prevents cell death (Gozuacik and Kimchi, 2004; Debnath et al., 2005; Levine and Yuan, 2005). If autophagy removes damaged mitochondria that would otherwise activate caspases and apoptosis, then autophagy should be protective. In agreement, disruption of autophagic processing and/or lysosomal function promotes caspase-dependent cell death (Debnath et al., 2005; Boya et al., 2005). However, excessive and dysregulated autophagy may promote cell death, since enzymes leaking from lysosomes/autolysosomes, such as cathepsins and other hydrolases, can initiate

mitochondrial permeabilization, caspase activation and apoptosis (Bursch, 2001; Turk et al., 2002). In some models, deletion of autophagy genes decreases apoptosis (Boya et al., 2005). Indeed, autophagy is often a prominent feature of programmed cell death to the extent that autophagic cell death has been proposed as a distinct mode of cell death (Debnath et al., 2005; Tsujimoto and Shimizu, 2005).

The MPT may provide a common pathway leading to mitophagy, apoptosis and necrosis (Figure 1.3). With low intensity stresses, limited MPT onset increases mitophagy to rid cells of damaged mitochondria as a repair mechanism. With more stress, mitophagy may no longer contain proapoptotic factors being released from mitochondria undergoing the MPT, in which case apoptosis begins to occur. Additionally, an overburdened autophagic apparatus may release lysosomal enzymes and possibly other factors to promote cell death signaling. Lastly when extreme stress causes MPT onset in virtually all cellular mitochondria, ATP levels plummet. Because of bioenergetic failure, neither autophagy nor apoptosis can progress, and only necrotic cell death ensues. The progression from mitophagic repairs to apoptosis and then to necrosis after increasing MPT onset has been termed necrapoptosis (Figure 1.3). Interventions that modulate the extent of MPT onset after stresses, therefore, affect the relative amount of autophagy, apoptosis, and necrosis that follows (Lemasters et al., 1998; Malhi et al., 2006).

1.7. Mitophagy in Aging

Aging seems to affect mitochondria particularly. Because of mitochondrial ROS generation, protein damage occurs in mitochondria, and mutations of mtDNA accumulate. mtDNA is more susceptible to oxidative damage than nuclear DNA since histones are not

present in mitochondria to protect mtDNA and because DNA repair mechanisms in mitochondria are less robust than in the nucleus (Yakes and Van, 1997; Bohr, 2002). Moreover, virtually all mtDNA is transcriptionally active compared to 2 or 3% of nuclear DNA, which also makes mtDNA relatively more vulnerable to damage. mtDNA mutations lead to synthesis of abnormal mitochondrial proteins or block synthesis altogether, which further exacerbates mitochondrial dysfunction. Thus, in postmitotic cells of aged organisms, morphological abnormalities of mitochondria are often observed, including swelling, loss of cristae, and destruction of inner membranes (Ermini, 1976; Beregi et al., 1988; Terman, 1995). Moreover, ATP production and respiration in mitochondria from aged animals are lower than in mitochondria from young animals.

Mitochondria of non-proliferating tissues like heart, brain, liver, and kidney constantly turnover with a half-life of 10 to 25 days. Mitochondrial biogenesis occurs by fission of pre-existing mitochondria analogously to bacterial division, but loss of mitochondria during turnover is primarily due to mitophagy (Menzies and Gold, 1971; Attardi and Schatz, 1988). Such mitophagy may be important to the elimination of dysfunctional mitochondria and mutated mtDNA. Certain mtDNA mutations may decrease recognition signals for mitophagy and, therefore, accumulate with age (de Grey, 1997; Lemasters, 2005). For example, a mtDNA mutation causing respiratory defects leading to decreased ROS generation might make a mitochondrion less likely to be targeted for mitophagy, which would promote retention and amplification of the mutation.

Many studies show that mtDNA mutations accumulate with age at an accelerating rate, a phenomenon that may represent an age-related diminishment of autophagic activity (Bergamini, 2006). Indeed, formation and processing of autophagosomes diminish with

aging (Terman, 1995). Another link between mitophagy and aging is Uth1p. Deletion of Uth1p leads to a selective defect in mitophagy and decreased longevity in yeast during nutrient deprivation (Camougrand et al., 2004; Kissova et al., 2004; Kennedy and Guarente, 1996). Uth1p also confers resistance to superoxide- and H_2O_2-induced injuries (Kissova et al., 2004). Caloric restriction is well known to increase longevity in rodents and other animals (Bergamini et al., 2003; Bergamini, 2006). Such caloric restriction is an inducer of autophagy, and increased longevity might thus be due, at least in part, to enhanced removal of oxidatively damaged mitochondria and their mutated mtDNA. These hypotheses and speculations relating mitophagy and aging need further investigation.

Chapter 2. Mitochondrial degradation by autophagy (mitophagy) and mitochondrial permeability transition (MPT) in GFP-LC3 transgenic hepatocytes during nutrient deprivation.

Chapter 2. Mitophagy and mitochondrial permeability transition in GFP-LC3 transgenic hepatocytes during nutrient deprivation-induced autophagy.

2.1. Abstract

Fasting *in vivo* and nutrient deprivation *in vitro* enhance sequestration of mitochondria and other organelles for autophagy and recycling of essential nutrients. Here our goal was to use a transgenic mouse strain expressing GFP fused to rat microtubule-associated protein 1 light chain 3 (LC3), a marker protein for autophagy, to characterize the dynamics of mitochondrial turnover by autophagy (mitophagy) in hepatocytes during nutrient deprivation. In complete growth medium, GFP-LC3 fluorescence was distributed diffusely in the cytosol and in small (0.2 - 0.5 μm) patches in proximity to mitochondria. After nutrient deprivation plus 1 μM glucagon to simulate fasting, the number of GFP-LC3 patches decreased as individual GFP-LC3 patches developed into green crescents (isolation membrane or phagophores) and eventually into ring structures (autophagosomes) that mostly surrounded individual mitochondria labeled with tetramethylrhodamine methylester (TMRM), a potential-indicating fluorophore. Sequestration of mitochondria took place in 6.5 ± 0.4 min. Mitochondrial fission often occurred coordinately with sequestration such that only portions of individual mitochondria were sequestered. Partial mitochondrial sequestration occurred both at the ends (43%) and middle parts (9%) of mitochondria with sequestration of whole mitochondria occurring in the remainder. 3-Methyladenine (3MA), a specific inhibitor of autophagy, blocked GFP-LC3 ring formation, and decreased GFP-LC3 patches during nutrient deprivation. After ring formation, mitochondria depolarized in 11.8 ± 1.4 min, as indicated by loss of TMRM fluorescence. After ring formation, labeling with LysoTracker

Red (LTR), a marker of acidification, occurred gradually. Acidification was maximal after 9.9 ± 1.9 min and was sometimes associated with fusion with pre-formed acidic vesicles. After acidification, GFP-LC3 fluorescence dispersed, leaving behind LTR-labeled autolysosomes. PicoGreen labeling of mitochondrial DNA (mtDNA) showed that mtDNA was also sequestered and degraded in autophagosomes. CsA and NIM811, MPT blockers, did not inhibit the formation of GFP-LC3 crescent structures nor rings around TMRM-labeled mitochondria. Bim, a pro-apoptotic Bcl-2 family protein, was dephosphorylated during nutrient deprivation plus glucagon. The results are consistent with the conclusions that GFP-LC3 protein patches (pre-autophagosomal structures, PAS) serve as nucleation sites for mitophagy and that the initial steps of sequestration precede rather than follow mitochondrial depolarization.

2.2 Introduction

Autophagy refers to 'self-eating' where cells degrade their cellular constituents to maintain cellular homeostasis during normal physiological conditions, starvation, aging, and pathological conditions, such as cancer, muscular disorders, neurodegenerative diseases, and pathogen infections (DE, 1963; Mitchener et al., 1976; Gozuacik and Kimchi, 2004). In liver, glucagon released from the pancreas during fasting promotes autophagy. In contrast, insulin released after feeding suppresses autophagy (Yu and Marzella, 1988). Autophagy acts to salvage amino acids, fatty acids and other molecular building blocks essential for cell survival during nutrient deprivation. Autophagy also removes protein aggregates and unwanted and dysfunctional organelles, such as mitochondria (Meijer and Codogno, 2004). In particular, prompt elimination of aged, damaged, and dysfunctional mitochondria may be important to protect cells against release of pro-apoptotic mitochondrial proteins, mitochondrial formation of toxic reactive oxygen species and futile hydrolysis of ATP after uncoupling.

The term mitophagy has been introduced to refer specifically to the autophagic degradation of mitochondria (Lemasters, 2005). In non-proliferating tissues like heart, brain, liver, and kidney, mitochondria turn over with a half-life of 10 to 25 days (Menzies and Gold, 1971; Pfeifer, 1978). Mitochondrial degradation associated with this turnover is predominantly by mitophagy. Although some studies support the conclusion that autophagy of mitochondria and other organelles occurs randomly (Seglen et al., 1990), other evidence supports the concept that autophagy of mitochondria and other organelles occurs selectively. For example, in cells where apoptosis is inhibited by caspase inhibitors, mitochondria are eliminated in specific and regulated manner (Xue et al., 1999). The mitochondria undergoing

mitochondrial permeability transition are involved in mitophagy (Rodriguez-Enriquez et al., 2006; Elmore et al., 2001)

During autophagy, phagophores form that sequester and enclose components of the cytoplasm yielding double membrane vesicles known as autophagosomes (Seglen and Bohley, 1992). Subsequently, autophagosomes undergoes fusion with lysosomes and/or late endosomes to mature into autophagolysosomes where degradation by lysosomal hydrolases occurs. The process of autophagy requires several evolutionally conserved Atg (autophagy-related) proteins (Tsukada and Ohsumi, 1993; Thumm et al., 1994; Harding et al., 1996). For example, Atg5, Atg12, and Atg8 are required for autophagosome formation in yeast. LC3 is a mammalian homologue of yeast Atg8. LC3 (LC3 I) is proteolytically cleaved to LC3 II by Atg4B, conjugated with phosphotidylethanolamine (PE) and recruited to isolation membranes, which form into autophagosomes (Kuma et al., 2002; Kabeya et al., 2000). LC3 remains on autophagosomes until after autophagosomal fusion with lysosomes. Afterwards, LC3 entrapped inside autophagosomes is degraded, whereas LC3 on the surface is released and presumably recycled (Mizushima et al., 2004). .

Although mitochondria are constantly renewed in non-dividing cells, mitochondrial degradation by autophagy has not been studied in depth in mammalian cells. Here, using hepatocytes isolated from GFP-LC3 transgenic mice, we show that pre-autophagosomal structures-like structures (PAS-like structures) containing LC3 appear to serve as nucleation sites for formation of isolation membranes that sequester all or parts of single polarized mitochondria. At or after sequestration, mitochondria lose their membrane potential. Subsequent processing leads to vesicular acidification and degradation of mitochondrial contents, such as mitochondrial DNA (mtDNA).

The mitochondrial permeability transition (MPT) is caused by opening of pores in the mitochondrial inner membrane that takes up solutes up to 1.5 kDa in size (Hunter et al., 1976; Gunter and Pfeiffer, 1990; Zoratti and Szabo, 1995). As a consequence, mitochondria undergo large amplitude swelling driven by colloid osmotic forces that leads to rupture of the outer membrane. MPT is regulated by many factors. Ca^{2+}, reactive oxygen species (ROS), various oxidants, and inorganic phosphate induce PT pore opening, whereas acidic pH, ubiquinone analogues, and cyclosporin A (CsA) inhibit onset of the MPT. PT pores are suggested to be composed of voltage-dependent anion channels (VDAC) in the outer membrane, the adenine nucleotide translocator (ANT) in the inner membrane, cyclophilin D (CypD) in the matrix space and possible other ancillary proteins (Halestrap and Davidson, 1990). CsA inhibits PT pores through an interaction with CypD (Hsu and Armitage, 1992). In addition, creatine kinase and Bcl-2 family proteins have been proposed to contribute to PT pore formation. Bcl-2 family proteins such as Bim may bind to VDAC and thus serve as gate keepers for PT pores (Tsujimoto and Shimizu, 2000).

In this study, I investigated the dynamics of mitophagy and the role of the MPT and Bcl-2 family proteins during nutrient deprivation-induced autophagy. To investigate mitophagy, we used hepatocytes from GFP-LC3 transgenic mice loaded with mitochondrial and lysosomal probes during nutrient deprivation-induced autophagy. Our results show that LC3 initially forms complexes (PAS-like structure) that serve as nucleation sites on mitochondria. After nutrient deprivation, PAS grow to form cup-shaped isolation membranes that sequester single mitochondria or part mitochondria into autophagosomes (mitophagosomes). With sequestration, or shortly after, mitochondria depolarize and the mitophagosomes mature into autolysosomes. CsA and NIM811, MPT inhibitors, did not

block mitophagosome formation nutrient deprivation-induced mitophagy. Dephosphorylation of Bim also occurred, but this event did not appear to be necessary for nutrient deprivation-induced mitophagy. These data illustrates dynamics of mitophagy during nutrient-deprivation induced autophagy.

2.3. Material and methods

2.3.1 Materials.

Collagenase A was obtained from Roche (Penzberg, Germany); 3-methyladenine, protease cocktail, and phosphatase inhibitor cocktail from Sigma Chemical (St. Louis, MO); Lysotracker Red (LTR), tetramethylrhodamine methylester (TMRM), and PicoGreen from Molecular Probes (Carlsbad, CA); bicinchoninic acid (BCA) reagents from Pierce (Rockford, IL); 4%-12% Bis-Tris gels from Invitrogen (Carlsbad, CA); nitrocellulose membranes from Whatman (Dassel, Germany); rabbit anti-Bim antibody and rabbit anti-LC3 antibody from MBL International (Wobrun, MA); goat anti-rabbit antibody from Chemicon (Billerica, MA); and chemiluminescence reagents from GE Sciences (Buckinghamshire, UK). Lamda phosphatase phurchased from cell signaling (Danvers, MA)

2.3.2. Hepatocyte isolation and culture.

Primary hepatocytes from Sprague-Dawley rat and wildtype, GFP-LC3 transgenic, or Bim knockout C57BL/6 mice were isolated by two-step collagenase perfusion, as described (Qian et al., 1997). Hepatocytes were cultured overnight in 5% CO_2/95% air at 37°C on Type 1 collagen-coated, 35-mm glass-bottom dishes (300,000 cells per dish) in Waymouth's MB-752/1 growth medium supplemented with 27 mM $NaHCO_3$, 10% fetal bovine serum, 100 nM insulin, and 100 nM dexamethasone.

2.3.3. Loading of fluorophores and induction of autophagy.

Hepatocytes were incubated with 300 nM tetramethylrhodamine methylester (TMRM), a potential-indicating fluorophore, or 500 nM LysoTracker Red (LTR), a probe of acidic organelles, for 30 min at 37°C in complete growth medium supplemented with 25 mM Na-HEPES buffer, pH 7.4. After loading, one-third of the initial concentration of TMRM or LTR was added to subsequent incubation media to maintain steady-state loading. Hepatocytes from wildtype and Bim knockout were loaded with 500 nM LTR, 300 nM Mitofluoro Far Red (MFFR) and 300 nM MitoTracker Green (MTG), as indicated above. In all experiments, one-third of the initial concentration of TMRM, LTR and/or MFFR was added after washes in subsequent incubation media to maintain equilibrium distribution of the fluorophores. In other experiments, wildtype hepatocytes were labeled with 3 μl/ml PicoGreen to label mtDNA (Ashley et al., 2005). To induce autophagy by nutrient deprivation, hepatocytes were placed in Krebs-Ringer-HEPES buffer (KRH, containing in mM: 115 NaCl, 5 KCl, 1 $CaCl_2$, 1 KH_2PO_4, 1.2 $MgSO_4$, and 25 HEPES buffer) plus 1 μM glucagon (KRH/G).

2.3.4. Laser scanning confocal microscopy.

Hepatocytes isolated from GFP-LC3 transgenic mice were loaded with red-fluorescing tetramethylrhodamine methylester (TMRM, 200 nM) or MitoFluor Far Red (MFFR, 200 nM) for 30 min in the absence or presence of 10 mM 3MA or 100 nM wortmannin at 37°C in Waymouth's MB-751/1 growth medium supplemented with 25 mM Na-HEPES buffer, pH 7.4. TMRM and MFFR are membrane-permeable monovalent cations that accumulate electrogenically into mitochondria (Zahrebelski et al., 1995). In other experiments, acidic compartments were labeled with LysoTracker Red (LTR, 500 nM) under identical conditions.

After TMRM, MFFR and LTR loading, one-third of the initial loading concentration was maintained in the medium to maintain steady-state.

2.3.5. LTR multiwell assay.

LTR uptake, a measure of cellular content of acidic organelles, was assessed by a multiwell fluorescence reader assay, as described previously (Rodriguez-Enriquez et al., 2006). Briefly after 70 min incubation of hepatocytes in WM or KRH plus 1 μM glucagon (KRH/G), 50 nM LTR was added. After 20 min at 37ºC, the hepatocytes were fixed with 2% paraformaldehyde for 10 min at 4ºC. The red fluorescence of LTR was measured using a 544-nm (15-nm band pass) excitation filter and a 590-nm long pass emission filter with Novostar multi-well fluorescence plate reader (BMG LabTechnologies, Offenburg, Germany). LTR fluorescence after experimental treatment was expressed as the percentage of LTR fluorescence of hepatocytes incubated in WM.

2.3.6. Quantitative analysis of autophagic structures.

The number of GFP-labeled LC3 dots, cup-shaped structures, rings with TMRM (red), and rings only were counted in three independent confocal experiments from three different hepatocytes isolations. The results were expressed as the mean ± SD.

2.3.7. Western blot analysis.

Hepatocytes were harvested by scrapping in RIPA buffer (20 mM Tris-HCl buffer, pH 7.5, 150 mM NaCl, 1% sodium dodecyl sulfate, and 0.1% NP-40 containing protease inhibitor cocktail, as recommended by the manufacturer) and sonicated using an ultrasonic cell disruptor (Misonex, Farmingdale, NY) on ice. Lysates were centrifuged at 13,000g for 10 min at 4ºC. Protein concentration was measured using a BCA procedure, as recommended by the manufacturer. The cell lysates were resolved on 4 to 15%

polyacrylamide gels or 20% polyacrylamide gels and electrotransferred onto the nitrocellulose membranes. After blocking with 5% non-fat milk in TBST (10 mM Tris-HCl buffer, pH. 7.6, 150 mM NaCl, and 0.1% Tween-20) for 1 h, membranes were immunoblotted with anti-LC3 antibody diluted 1:1000 in TBST, or anti-Bim antibody diluted 1:1000. Primary antibody was detected with a horseradish peroxidase-conjugated anti-rabbit secondary antibody using a chemiluminescence kit according to the manufacturer's instructions.

For phosphatase treatment, the cell lysates from hepatocytes starved were harvested with or without sodium orthovanadate (Na_3VO_4), a phosphatase inhibitor, in WM or KRH/G for 90 min. A portion of cell lysate harvested without sodium orthovanadate was under dialysis overnight to eliminate detergents and treated with lamda phosphatase as recommended by the manufacturer. Samples were subjected for immunoblotting for anti-Bim antibody.

2.4. Results

2.4.1. Nutrient deprivation stimulates autophagosome formation and mitophagy in cultured GFP-LC3 hepatocytes.

To evaluate the dynamics of mitochondrial autophagy (mitophagy), we examined hepatocytes isolated from GFP-LC3 transgenic mice. When GFP-LC3 hepatocyes were incubated in Waymouth's growth medium (WM), GFP-LC3 was distributed relatively diffusely throughout the cytosol. GFP-LC3 fluorescence also extended into and was slightly concentrated into the nucleus. Some GFP-LC3 fluorescence was present in small patches of about 0.2 to 0.5 μm in diameter and occasional rings (Figure 2.1A, left panel), which likely

correspond to pre-autophagosomal structures (PAS) (Kuma et al., 2002). After 90 min of placing GFP-LC3 hepatocytes in nutrient-free KRH plus 1 μM glucagon (KRH/G), GFP-LC3 patches (arrowhead) decreased in number by 69% as GFP-labeled cup-shaped structures (isolation membrane or phagophores, arrow), GFP-labeled rings (autophagosomes, double arrow), and solid GFP-labeled disks (autophagosomes, double arrowhead) increased in the confocal images (Figure 2.1A). The majority of autophagosomes were GFP-labeled rings (empty green vesicles), which represented optical sections through the middle of the structures. A few autophagosomes were observed as GFP-labeled disks (filled green vesicles), which likely represented optical sections including the edges of autophagosomes extending from one lateral margin to the other. These results illustrate induction of autophagy in cultured GFP-LC3 transgenic hepatocytes by nutrient deprivation.

During autophagy, LC3-I is cleaved, processed, and recruited to the sites of forming autophagosomes (Kabeya et al., 2000). Consequently, cleaved LC3 (LC3-II) increases during autophagy. To confirm stimulation of autophagy, wildtype hepatocytes from the same breeding colony as the GFP-LC3 transgenic mice were incubated in Waymouth's complete medium (WM) or KRH/G with and without 3-methyladenine (3MA) for 0 to 90 min. LC3-I (18 kDa) and –II (16 kDa) protein expression were then determined by Western analysis. During incubation in WM, the intensity of LC3-I bands were relatively unchanged after 5, 20, 50 and 90 min, and the intensity of LC3-II bands was very faint (Figure 2.1B, top gel). By contrast, during incubation in KRH/G, the intensity of LC3-II bands progressively increased for at least 50 min; whereas the intensity of LC3-I bands remained relatively unchanged (Figure 2.1B, bottom gel). 3-Methyladenine (3MA), an inhibitor of autophagy, prevented increases of LC3-II stimulated by KRH/G (data not shown). Taken together, these results

showed that incubation of hepatocytes in KRH/G induces robust autophagy with LC3 processing and recruitment of GFP-LC3 from PAS patches into isolation membranes and autophagosomes.

2.4.2. GFP-LC3-labeled isolation membranes sequester polarized mitochondria during nutrient deprivation.

To investigate mitophagy during nutrient deprivation, hepatocytes from GFP-LC3 mice were co-labeled with TMRM, a red-fluorescing cationic fluorophore that accumulates electrophoretically into mitochondria and which labels individual mitochondria with bright red fluorescence (Figure 2.2A). Images of the hepatocytes were taken after 90 min in WM, KRH/G or KRH/G in the presence of 3MA. In WM, a few green rings were present, but GFP-LC3 was predominately observed as small green patches (Figure 2.2A, left panel). In KRH/G, GFP-LC3 patches decreased in number, as GFP-labeled cup-shaped structures, -rings, and -disks increased in confocal images (Figure 2.2A, middle panel). Frequently, TMRM-labeled polarized mitochondria occupied the interior of GFP-labeled rings, discs, and cup-shaped structures, and time lapse imaging revealed that GFP-labeled cup-shaped structures formed around TMRM-labeled mitochondria (Figure 2.2A, middle panel). 3MA completely suppressed internalization of polarized mitochondria into GFP-LC3-labeled structures after incubation in KRH/G. Rather in the presence of 3MA, GFP-LC3 remained as diffuse fluorescence and small patches (Figure 2.2A, right panel).

A statistical analysis was performed to quantify the distribution of GFP-LC3 into various structures from images of random fields from three independent experiments. Figure 2.2C illustrates the GFP-LC3-labeled autophagic structures that were scored: PAS patches (autophagic dots, arrowhead), cups (phagophores or isolation membrane, arrow) and rings

and disks containing TMRM (early mitophagosomes, double arrow) and not containing TMRM (late mitophagosomes, double arrowhead). Based on TMRM-labeling, rings and disks were categorized as TMRM positive (early) and TMRM negative (late) mitophagosomes. After 90 min in WM, GFP-LC3 was predominantly diffuse or incorporated into PAS patches dispersed throughout the cytosol. In KRH/G, PAS patches decreased 69% compared to WM. In addition, PAS-like patches were frequently located near polarized mitochondria in KRH/G (Figure 2.2C, arrowhead). At the same time, phagophores, and early and late mitophagosomes increased 1.55, 11.1, and 8.1-fold. Overall, about 40% of total autophagosomes contained TMRM-labeled mitochondria (Figure 2.2B). 3MA virtually completely inhibited formation of phagophores and mitophagosomes after 90 min KRH/G with retention of PAS patches.

Newly formed autophagosomes fuse with lysosomes to mature into acidic autolysosomes (Arstila and Trump, 1968). To characterize intravesicular acidification after autophagic induction by nutrient deprivation, GFP-LC3 hepatocytes were loaded with LTR, a red-fluorescing weak base that accumulates into acidic compartments. In WM, a relatively small number of red-fluorescing LTR-labeled structures were present that presumably corresponded to lysosomes and late endosomes. These LTR-labeled vesicles did not colocalize with GFP-LC3-labeled PAS (Figure 2.2D, left panel). After 90 min incubation in KRH/G, LTR-labeled red-fluorescing structures increased dramatically. About 12.4% of LTR-labeled vesicles were surrounded by GFP-LC3 rings, whereas 59.8% of GFP-LC3 rings contained an LTR-labeled interior (Figure 2,2D, middle panel). About 27.8% of GFP-LC3 rings did not contain LTR. Green cup-shaped structures (phagophores) increased after nutrient deprivation but did not colocalize with LTR. After 90 min in KRH/G plus 3MA,

these changes were prevented, and the images were virtually indistinguishable from those obtained for hepatocytes incubated in WM (Figure 2.2D, right panel).

2.4.3. After autophagic sequestration, mitochondria depolarize and the mitophagosomes acidify.

To investigate the dynamics of mitophagosome formation and processing, time lapse images were collected of GFP-LC3 hepatocytes loaded with TMRM. As illustrated in Figure 2.3A (arrow), mitophagy began with growth of PAS (GFP-LC3 patches) into phagophores (GFP-LC3-labeled cup-shaped structure). Phagophores then enveloped and sequestered individual TMRM-labeled mitochondria, resulting in the formation of mitophagosomes (GFP-labeled ring) (Figure 2.3A, bottom left and middle panels). The time from PAS-like to fully formed phagophore averaged 3.3 ± 0.3 min (n=28), whereas the time from phagophore to closed ring was 3.5 ± 0.4 min (n=28). In favorable sections viewing phagophore formation laterally, depolarization of mitochondria (loss of TMRM fluorescence) appeared to occur coordinately with ring closure (Figure 2.3A, bottom right panel). More often, mitophagosomal formation was observed obliquely or end on, and TMRM was frequently retained inside GFP-LC3 rings (Figure 2.3A). However, whether such rings represented truly closed vesicles could not be determined. Overall, TMRM fluorescence was lost 11.8 ± 1.4 min (n=11, Figure 2.4) after apparent ring formation, suggesting that mitochondrial depolarization was indeed following completion of sequestration.

In some instances, GFP-LC3 formed isolation membranes that did not sequester polarized mitochondria (data not shown). Such events were the minority (14.7%) with the remainder of sequestrations involving polarized mitochondria. Consistently, the mitophagic

process during nutrient deprivation began from a single PAS in association with a target mitochondrion. Moreover, as autophagy progressed, the number of PAS in the cytoplasm decreased (Figure 2.2A). Taken together, these data are consistent with the conclusion that PAS serve as nucleation and initiation sites for mitophagy.

In other experiments, time lapse images of GFP-LC3 hepatocytes loaded with LTR were collected during incubation in KRH/G. Again, PAS grew into cup-shaped isolation membranes and then into rings with a time course similar to that observed for TMRM-labeled hepatocytes (Figure 2.3B, top right panel). LTR consistently did not localize to PAS and isolation membranes. Rather, LTR uptake occurred only after ring formation. The time after apparent ring closure of onset of LTR accumulation was difficult to assess because uptake was gradual (Figure 2.3B, top right and bottom left and middle panels). However, maximal LTR accumulation indicating acidification was observed after an average of 9.9 ± 1.9 min (n=28) after apparent GFP-LC3 ring closure (Figure 2.3B and diagrammed in Figure 2.4). After maximal LTR labeling, GFP-LC3 fluorescence was frequently lost altogether.

2.4.4. Mitochondrial fission occurs coordinately with mitophagy.

Frequently, phagophores sequestered pieces of individual mitochondria rather than whole mitochondria into mitophagosomes (Figure 2.5). This mitochondrial fission occurred in close coordination with the formation of LC3-labeled rings as if isolation membranes were pinching off portions of mitochondria. Fission events during mitophagy occurred from both the middles (Figure 2.5A) and ends of individual mitochondria (Figure 2.5B). Fission during mitophagy from middles and ends occurred 9.1% and 43.1% of the time, respectively, with sequestration of whole mitochondria occurring in the remainder. The intensity of TMRM fluorescence did not appear to differ between sequestered and non-sequestered portions of

mitochondria being targeted for mitophagy. Only after fission and sequestration were complete did TMRM release occur. Overall, these findings indicated that mitochondrial fission occurred in close coordination with autophagosome formation.

2.4.5. Mitophagy degrades mitochondrial DNA (mtDNA).

Mitochondria are a major source of reactive oxygen species (ROS), which can lead to mutations in mitochondrial DNA (mtDNA). mtDNA lacks of histones and has limited DNA repair capacity compared to nuclear DNA, which makes mtDNA more vulnerable to oxidative damage (Yakes and Van, 1997). To investigate a role of mitophagy in mtDNA degradation and turnover, hepatocytes from wildtype mice were co-labeled with PicoGreen and TMRM or LTR. PicoGreen is a green DNA-intercalating fluorophore that penetrates mitochondrial membranes labeling mtDNA. PicoGreen (green)- and TMRM (red)-loaded hepatocytes were incubated in WM or KRH/G for 90 min and imaged. Virtually every TMRM-labeled mitochondria contained PicoGreen-labeled mtDNA nucleoids in WM (Figure 2.6A). In WM, virtually no PicoGreen-labeled DNA was found in the cytoplasm outside polarized mitochondria (data not shown)

In hepatocytes co-loaded with PicoGreen and LTR and incubated in KRH/G, LTR-labeled autolysosomes proliferated. Many of these autolysosome contained PicoGreen-labeled DNA (Figure 2.6B). DNA in these autolysosomes was mtDNA, since in time-lapse confocal imaging individual clusters of mtDNA nucleoids became surrounded by LTR fluorescence (Figure 2.6C). Subsequently, the intensity of PicoGreen decreased, indicating degradation of mtDNA after acidification. Overall, these results show that each individual polarized mitochondrion in hepatocytes contains several copies of mtDNA. During mitophagy, mitochondria and their mtDNA are sequestered into mitophagosomes that

become acidic autolysosomes in which the mtDNA is degraded. Thus, mitophagy is an important mechanism for mtDNA degradation and turnover.

2.4.6. Cyclosporin A and NIM811 do not inhibit Mitophagy

In previous studies, cyclosporin A (CsA) and NIM811 (NIM), MPT pore inhibitors, suppressed mitochondrial depolarization and proliferation of acidic autophagosomes/autolysosomes after nutrient deprivation plus glucagon treatment to rat hepatocytes (Elmore et al., 2001; Rodriguez-Enriquez et al., 2006). To evaluate the role of the MPT in GFP-LC3 hepatocytes, we treated TMRM or LTR-loaded GFP-LC3 hepatocytes with CsA or NIM811. In WM, GFP-LC3 was incorporated into green PAS patches (Figure 2.7A). In KRH/G, GFP-LC3-labeled phagophores and autophagosomes formed TMRM-labeled mitochondria proliferated. CsA and NIM treatment, however, did not appear to inhibit the formation of phagophores and autophagosomes (Figure 2.7A).

The distribution of GFP-LC3-decorated PAS-like patches, phagophores, TMRM-loaded rings, and empty rings was quantified in images of random fields from three independent experiments with and without CsA or NIM811 treatment (Figure 2.7B). After 90 min in KRH/G, the number of PAS patches decreased by 69%, whereas phagophores, polarized mitophagosomes, and depolarized autophagosomes increased by 1.5, 11.1, and 8.1-folds. The magnitude of these changes was not blocked by CsA or NIM811 (Figure 2.7B). Taken together, these data support the conclusion that MPT does not precede initiation of mitophagic sequestration.

In LTR-loaded GFP-LC3 hepatocytes, LTR-labeled autolysosomes proliferated after 90 min incubation in KRH/G. Some of these LTR-labeled autolysosomes were surrounded by GFP-LC3-labeled rings; whereas others were not (Figure 2.8). CsA and NIM811 did not

block the formation of LTR-labeled autophagosomes or autolysosomes in GFP-LC3 hepatocytes incubated in KRH/G.

2.4.7. Pro-apoptotic Bcl-2 familt protein, Bim EL is dephosphorylated during mitophagy

Bcl-2 family proteins play a role in autophagy. For example, in different studies Bcl-2 inhibits starvation-induced autophagy as well as the MPT (Adams and Cory, 2001; Tsujimoto, 2003; Pattingre et al., 2005). We tested whether Bcl-2 family proteins were involved in nutrient deprivation-induced autophagy. Bcl-2 itself is not expressed in normal hepatocytes (Charlotte et al., 1994), which I confirmed by Western blotting in rat hepatocytes incubated in the complete growth medium and KRH/G (data not shown). Additionally, protein expression assessed by Western blotting of Bcl-xl, Bax, Bid, and Bnip did not change in during incubation of hepatocytes WM or KRH/G with and without 3MA (Figure 2.9A). By contrast, incubation in KRH/G altered BimEL expression from a wide 2-3 kDa width bands to a narrow 1 kDa width (Figure 2.9B). After 0 to 20 min of incubation in KRH/G, BimEL was weakly detected as broad bands, whereas after incubation of 50 min or more in KRH/G, BimEL migrated as a narrower and more intense band on 4 to 15% polyacylamide gels (Figure 2.9B). When cell lysates of hepatocytes incubated in complete WM were resolved in 20% polyacylamide gel, Bim EL was detected as two bands (23 kDa and 27 kDa) that were equal in intensity (Fig. 2.9C). By contrast, cell lysates after KRH/G incubation only showed a fainter 23kDa band and a stronger 27 kDa band. This result leaded us a speculation that Bim may be undergoing post-transmodification either cleavage or phosphorylation during nutrient deprivation-induced autophagy.

To investigate whether the difference between two bands were due to phosphorylation, cell lysates of WM and KRH/G were treated with lamda phosphatase. The two bands (23 kDa and 27 kDa) observed in WM extracts were converted to a single band at 27 kDa after phosphatase treatment; whereas, the 27 kDa band found in KRH/G extracts remained unchanged (Figure 2.9D). These findings were consistent with the conclusion that the 27 kDa band of BimEL represented a phosphorylated form, whereas the 23 kDa band represented unphosphorylated BimEL.

To investigate further a possible role of Bim in mitophagy, we assessed autophagy and mitophagy in hepatocytes isolated from Bim knockout (Bim -/-) mice. After 90 min in KRH/G, lysosomal proliferation assessed by LTR uptake increased to a similar extent in wildtype and Bim -/- hepatocytes in LTR plate assay data (Figure 2.10A)**,** and this increased LTR uptake was inhibited by 3MA in both wildtype and Bim -/-, confirming that autophagy was being assessed. Wildtype and Bim -/- hepatocytes were also loaded with LTR, MitoFluor Far Red (MFFR), and MitoTracker Green (MTG). MFFR is a far red-fluorescing cationic fluorophore that accumulates electrophoretically into polarized mitochondria and is released upon mitochondrial depolarization (Sakanoue et al., 1997). MTG is a green-fluorescing cationic fluorophore that accumulate electrophoretically into mitochondria. However unlike TMRM and MFFR, MTG covalently binds with mitochondrial proteins after accumulation is not released after mitochondrial depolarization (Elmore et al., 2001). After 90 min in KRH/G, LTR-labeled vesicles (acidified autophagosomes and autolysosomes) increased in hepatocytes from both wildtype and Bim -/- mice. Some LTR-labeled vesicles contained MTG and MFFR-labeled mitochondria (mitophagosomes) in both wildtype and

Bim -/- mice hepatocytes (Figure 2.10). Overall, these results indicate that Bim may not be required to activate nutrient deprivation-induced autophagy and mitophagy.

2.5. Discussion

Mitophagy is suggested to be a major degradative mechanism by which mitochondria turn over. In hepatocytes, 20% of mitochondria are degraded 12 h after nutrient deprivation indicating removal of mitochondria by autophagy (Kawai et al., 2006). However, the dynamic and signaling pathways of mitophagy have not been clarified. In this study, we characterized mitophagy in GFP-LC3 expressing hepatocytes. In GFP-LC3 expressing hepatocytes incubated in complete growth medium, GFP-labeled LC3 was diffuse in the cytosolic space or incorporated into small patches of 0.2 to 0.5 μm in diameter, or occasionally into green rings characteristic of autophagosomes (WM, Figure 2.1). The small patches likely represent pre-autophagic structures (PAS), as described in yeast (Kim et al., 2002). PAS contain complexes of Atg proteins forming a perivacuolar structure in yeast (Kim et al., 2002; Suzuki et al., 2001). PAS elongate into cup-shaped structures called isolation membranes (phagophores) and then into autophagosomes. However, it is not clear whether PAS simply relocates or reorganized to the mitochondria that are targeted for mitophagy.

The origin of isolation membranes has been controversial. In some studies, ribosome-free regions of the rough endoplamic reticulum (ER) or Golgi complex have been proposed as the source of these membranes (Dunn, Jr., 1990; Furuno et al., 1990; Yamamoto et al., 1990). However, the lipid and protein composition of autophagosomal membranes differ from membranes of ER and Golgi complex (Kim et al., 2002). Other studies suggest that

isolation membranes originate from a novel membranous structure that is neither ER nor Golgi (Fengsrud et al., 1995). One other speculation is membranous structure of isolation membrane is donated from a specific part of an organelle such as mitochondria where the marker proteins, Atg9, are rapidly recycled back to the donor organelle, mitochondria (Reggiori et al., 2005). A recent study shows that Atg9 cycles between PAS and mitochondria, suggesting that mitochondria may supply the lipids and proteins for forming autophagosomes in yeast (Reggiori et al., 2005). In the present study, GFP-labeled patches that corresponded to PAS decreased 69% during nutrient deprivation plus glucagon compared to the hepatocytes in the complete medium. Loss of PAS was accompanied by a corresponding increase in the number of isolation membranes (green cup-shaped structures) and autophagosomes (GFP-LC3 rings and disks, Figure 2.1A). LC3-II formation also increased during nutrient deprivation plus glucagon (Figure 2.1B), which is also consistent with autophagosome formation (Kabeya et al., 2000).

Of all GFP-LC3-labeled autophagosomes, about 40% contained TMRM-labeled polarized mitochondria (mitochondria containing autophagosomes) (Figure 2.2). This is an underestimate of the true percentage of autophagosomes containing mitochondria or mitochondrial remnants since mitochondria depolarize after autophagic sequestration. As expected the autophagy inhibitor, 3MA, suppressed the formation of GFP-LC3-labeled phagophores and mitophagosomes (Figure 2.2A and B). After autophagic sequestration of mitochondria, mitophagosomes acidified as assessed by LTR uptake (Figure 2.2D). In these experiments, mitochondrial depolarization occurs at or after the completion of autophagic sequestration. Thus, mitochondrial depolarization itself was not the signal initiating autophagic sequestration.

Previously in rat hepatocytes, we observed that nutrient deprivation plus glucagon induced a 5-fold increase of mitochondrial depolarization and a corresponding proliferation of acidic lysosomes and autolysosomes. Moreover, the depolarized mitochondria became localized to the acidic organelles (Elmore et al., 2001). Cyclosporin A (CsA), an inhibitor of mitochondria permeability transition (MPT), inhibited both mitochondrial depolarization and proliferation of lysosomes (Rodriguez-Enriquez et al., 2006). Moreover, NIM811, a non-immunosuppressive CsA analog that is not a calcineurin inhibitor, inhibited autophagy, whereas immunosuppressive tacrolimus, a calcineurin inhibitor that does not block the MPT, does not block autophagy (Elmore et al., 2001; Rodriguez-Enriquez et al., 2006). However, in my experiments using hepatocytes from GFP-LC3 transgenic mice, CsA and NIM811 did not appear to inhibit the proliferation of autophagosomes and their acidification (Fig. 2.7 and Fig. 2.8). The reason for the difference in my results in mice from the previous work in rats is unclear. One reason may be species differences. For example, in rat hepatocytes cyclosporin blocks the MPT occurring during TNFα-induced apoptosis, whereas in mouse hepatocytes CsA plus trifluoperazine is required to block the MPT (Bradham et al., 1998; Hatano et al., 2000). Moreover with time, the regulated MPT that is block by CsA can transform to an unregulated MPT that is not subject to inhibition by CsA (He and Lemasters, 2002; Kon et al., 2004). Thus, CsA may suppress autophagy at earlier time points but not at the later times ($\geq$90 min) assessed in the present work. Lastly, CsA may be acting subsequent to mitophagic sequestration by suppressing MPT dependent processing of mitophagosomes. Further studies are needed to be clarified this issue. However, from the present work we can conclude that mitochondrial depolarization and hence any MPT during nutrient deprivation is occurring at or following the completion of mitochondrial sequestration. If the MPT is

playing a role in mitophagy, then this role must be at or beyond this first step in autophagic processing.

In time-lapse images, some GFP-LC3 patches became closely associated with TMRM-labeled mitochondria prior to formation of phagophore (Figure 2.2C and 2.3A). Patches elongated into typical cup-shaped phagophore and enveloped the mitochondria in 3.3 ± 0.3 min and then into ring structures in another 3.4 ± 0.4 min (Figure 2.3A). However, not all rings represented completely formed autophagosomes. In favorable sections through long axis of the phagophores, cup shaped isolation membranes formed surrounding polarized mitochondria which if viewed from another angle would appear to be entirely enclosed by a ring of GFP-LC3 despite remaining open at one end. In such favorable sections, depolarization appeared to occur at or very shortly following completion of sequestration. Overall, depolarization occurred 11.8 ± 1.4 min after the first appearance of rings, but the time of depolarization after complete closure of the forming autophagosomes is likely substantially less (Figure 2.3A). After ring formation, maximal acidification as assessed by LTR uptake occurred after 9.9 ± 1.9 min (Figure 2.3B and Figure 2.4). In a previous study, the lifetime of LTR-labeled autolysosome was measured to be about 9 min (Rodriguez-Enriquez et al., 2006). However, the end point of autolysosomes is difficult to measure since degradation of autolysosomes cannot be easily distinguished from movement of autolysosomes out of the confocal plane. However, the morphometric analysis in EM images indicate that the lifetime of autophagosome is about 9 min in liver, which is consistent with results in hepatocytes by confocal microscopy (Pfeifer, 1978).

During nutrient deprivation-induced mitophagy, sometimes only a part of an individual mitochondria was sequestered for autophagic degradation. Ends (43.1% of events), middle

part (9.1%) or whole mitochondria (47.8%) were engulfed. As judged by the intensity of TMRM fluorescence, the membrane potential of the sequestering and non-sequestering parts was not different (Figure 2.5). These findings show that mitochondrial fission often occurs coordinately with mitophagosome formation. How partial autophagic engulfment of mitochondria occurs remains to be determined. One possibility is that an Atg proteins may be directly involved in mitochondrial fission. For example, Atg5-Atg12/Atg16 protein complexes, which function in forming sequestering membranes, may also assist in dividing mitochondria. Atg9 is suggested to supply lipid for autophagosomal membranes and may act to insert lipids into mitochondria membrane to assist in fission (Suzuki et al., 2001; Reggiori et al., 2005). Another possibility is that LC3 and other Atg proteins collaborate with mitochondrial fusion and fission proteins, such as mitofusin 1 (Mfn1) and dynamin-related protein 1 (Drp1). In primary neurons, nitric oxide (NO)-induced mitochondrial fission was accompanied by mitophagy and was inhibited by Mfn1 and dominant negative Drp1 expression (Barsoum et al., 2006). Further analysis is required for in depth understanding of the mechanism by which mitochondrial fission occurs during mitophagy.

On average, mitochondria of hepatocytes contain four to five copies of mtDNA (Chen and Butow, 2005). In complete growth medium, PicoGreen labeling confirmed that each polarized mitochondrion of hepatocytes contained several copies of mtDNA (Figure 2.6A). After autophagic induction, PicoGreen-labeled mtDNA moved into autolysosomes as mitophagy occurred (Figure 2.6B and C). mtDNA has 10 to 20 fold higher mutation rate than nuclear DNA due to the proximity of mtDNA to the reactive oxygen species-generating respiratory chain, the limited DNA repair capacity of mitochondria, and lack of protective histones in mtDNA (Yakes and Van, 1997). Mutation of mtDNA will lead to mitochondrial

dysfunction due to absent or abnormal synthesis of one of more of the 13 key protein subunits of oxidative phosphorylation that are encoded by mtDNA. Defective mtDNA in mice leads to a shortened life span and to signs of aging, such as hair loss, osteoporosis, and reduced fertility (Trifunovic et al., 2004). Deletion in mtDNA is observed in some diseases, including Pearson's syndrome and sideroblastic anemia (Fontenay et al., 2006). Our study shows mtDNA is degraded as mitochondria undergo autophagy, which suggests that mitophagy may play an important role in the elimination of mutated mtDNA from cells.

Bcl-2 is implicated as a regulatory protein in autophagy, but hepatocytes do not normally express Bcl-2. Of several Bcl-2 family members examined, Bcl-xl, Bid, and Bnip3 did not change during nutrient deprivation-induced mitophagy (Figure 2.9A). However, Bim became dephosphorylated about 50 min after nutrient deprivation. Nonetheless, this event was not required for mitophagy, since formation of mitochondria-containing autophagosomes and autolysosomes was not inhibited in hepatocytes from Bim knockout mice (Figure 2.10). ERK1/2 phosphorylates Bim EL at Ser69, Ser59, and Ser104 and possibility additional sites. As a consequence, Bim EL becomes targeted for the proteasomal degradation (Weston et al., 2003; Seward et al., 2003). After interleukin-2 (IL-2) withdrawal in Bal17 cells, at least two sites on Bim EL becomes de-phophorylated (Seward et al., 2003). JNK also weakly phosphorylates Bim EL at Ser69 after neuronal growth factor withdrawal, the effect which facilitates apoptosis (Putcha et al., 2003). My data shows that Bim dephosphorylation occurs after nutrient deprivation. However, Bim was not necessary for autophagy to occur, and Bim dephosphorylation during autophagy was not associated with induction of apoptosis.

In summary, mitophagy was induced during nutrient deprivation. PAS in association with polarized mitochondria appeared to serve as nucleation sites for autophagosome

formation and grew in just a few minutes into cup-shaped phagophore and then fully formed autophagic vesicles. Mitophagy often occurred coordinately with mitochondria fission. Sequestration was followed by relatively abrupt mitochondrial depolarization and then gradual vesicular acidification and conversion of mitophagosomes to autolysosomes in which mitochondrial components, including mtDNA, were degraded. These findings will provide a framework for analyzing mitophagy in disease.

Chapter 3. JNK (c-Jun NH_2-terminal kinase) as a positive regulator of mitophagy

Chapter 3. JNK (c-Jun NH_2-terminal kinase) as a positive regulator of mitophagy

3.1. Abstract

Diverse stimuli, including TNF-α, IL-1, UV radiation, and oxidative stress, activate a stress-activated protein kinase, c-Jun N-terminal kinases (JNK). Recent evidence indicates that JNK also participates in autophagic cell death. In this study, we examined the role of JNK in mitochondrial autophagy. Autophagic induction of GFP-LC3 transgenic mice and wildtype mice hepatocytes by nutrient deprivation plus glucagon caused an increase of LTR fluorescence uptake. In wildtype hepatocytes, SP600125, a JNK-specific small molecule inhibitor, decreased LTR uptake in a dose-dependent manner with maximal inhibition at 100 μM. SP600125 treatment of GFP-LC3 hepatocytes during nutrient deprivation also inhibited proliferation of isolation membranes, autophagosomes, and autolysosomes. In addition, SP600125 decreased formation of mitophagosomes (mitochondria-containing autophagosomes). After autophagic stimulation, JNK was phosphorylated transiently between 5 and 20 min, whereas total JNK was unchanged. However, JIP (JNK peptide inhibitor) and DN-JNK (dominant-negative) expression did not inhibit LTR fluorescence uptake or inhibit proliferation of autophagosomes or mitophagosomes. Moreover, autophagosome and mitophagosome formation was not blocked in JNK1 and JNK2 knockout hepatocytes. Here, we conclude that JNKs may not play a direct role in nutrient deprivation-induced autophagy. The effect of SP600125 may be via inhibition of another unidentified kinase.

3.2. Introduction

Autophagy is a cellular process by which portions of the cytosol and individual organelles become sequestered into double membrane vesicles called autophagosomes. Autophagosomes subsequently fuse with lysosomes forming autophagolysosomes whose contents undergo hydrolytic lysosomal degradation. Autophagy is an important catabolic mechanism activated by nutrient deprivation and growth factor withdrawal. Autophagy also can be important as a defense against intracellular microbial infections and may have a role in the pathogenesis of many diseases, including cancer (Yue et al., 2003; Dorn et al., 2002). At least 27 autophagy proteins (Atg) have been discovered that participate in autophagy (Ohsumi and Mizushima, 2004). LC3, a mammalian homologue of yeast Atg8, is among the best characterized of these and used as a tool to study autophagy in the mammalian cells (Kabeya et al., 2000).

c-Jun NH_2-terminal kinases (JNK) belongs to a family of mitogen-activated protein kinase (MAPK) that are activated by various stresses and mitogenic stimuli, including hypoxia, UV radiation, cytokines, osmotic shock, toxic compounds, and pathogen-derived antigens (Rosette and Karin, 1996). Phosphorylated JNK phosphorylates transcription factors such as c-Jun, p53, and Elk-1, and non-transcriptional factors such as Bcl-2 family proteins (Tsuruta et al., 2004; Hibi et al., 1993; Davis, 2000). Three genes (JNK1, 2, and 3) encode JNK family proteins. At least 10 splicing variants are expressed from these genes. JNK3 is expressed mostly in brain, whereas JNK1 and JNK2 is expressed ubiquitously (Gupta et al., 1996). Mice lacking both JNK1 and JNK2 die around embryonic day 11 (E11). These double knockout mice exhibit open neural tube with reduced apoptosis in the hindbrain at E9.25 and increased apoptosis in the hindbrain and forebrain at E10.5 (Sabapathy et al., 1999). However, the mice lacking either JNK1 or JNK2 survived suggesting their redundant

overlapping activities. Other findings indicate that JNK1 and JNK2 also have distinctive functions (Kuan et al., 1999). JNK1 seems to serve as a mediator of obesity-induced insulin resistance, whereas JNK2 is more closely associated with apoptotic signaling pathways . JNK3 expressed in brain is also a mediator of neuronal apoptosis (Coffey et al., 2002; Brecht et al., 2005).

Several lines of evidence suggest that the JNK cascade participates in mitochondrial signaling pathways. JNK activates the intrinsic pathway by phosphorylation of Bcl-2 family proteins such as Bcl-2, Bax, and Bim (Yamamoto et al., 1999; Maundrell et al., 1997; Lei and Davis, 2003). JNK-medicated phosphorylation suppresses the anti-apoptotic function of Bcl-2, whereas JNK activates the pro-apoptotic function of Bax and Bim. After paclitaxel-induced mitotic arrest in Hela cells, phosphorylated JNK translocates to mitochondria and forms a complex with Bcl-2 and protein phosphatase 1 (PP1) (Brichese et al., 2004).

JNK is suggested to play a positive role in autophagy. A JNK inhibitor, SP600125, reduced a proteasomal inhibitor, bortezomib-induced autophagy (Ding et al., 2007). A caspase inhibitor, zVAD-induced autophagy was partially inhibited by a JNK peptide inhibitor and c-Jun knockdown (Yu et al., 2004). Previously, we reported that the JNK inhibitor, SP600125, partially blocked the proliferation of autophagosomes after nutrient deprivation (Rodriguez-Enriquez et al., 2006). In this study, we used GFP-LC3 transgenic hepatocytes to monitor autophagy and mitophagy directly in relation JNK signaling after nutrient deprivation. Although we confirmed that SP600125 inhibits autophagy and that JNK becomes transiently activated after nutrient deprivation, autophagy and mitophagy were not affected by a JNK specific peptide inhibitor and dominant negative JNK. Moreover, autophagy was unchanged in hepatocytes deficient of a specific JNK isoform, JNK1 or JNK2.

Thus, JNK activation occurs as a stress response to nutrient depletion in hepatocytes, but appears not to promote induction of autophagy.

3.3. Materials and methods

3.3.1. Materials

Collagenase A was obtained from Roche (Penzberg, Germany), 3-methyladenine, protease cocktail, propidium iodide, phosphatase inhibitor cocktail, and ITS+3, a media supplement for serum-free cell culture, from Sigma Chemical (St. Louis, MO), SP600125 from A.G. Scientific (San diego, CA), and JNK peptide inhibitor 1 (JIP) from EMD chemicals (San Diego, CA). Ad5LacZ was purchased from Genetherapy center (University of North Carolina at Chapel Hill, NC). Ad5TAM (dominant negative c-Jun) and Ad5DN-JNK (dominant negative JNK) were kindly provided from Dr. Richard Rippe (University of North Carolina, Chapel Hill, NC) and Dr. David Pimentel (Boston Univeristy, Boston, MA). Lysotracker Red (LTR), tetramethylrhodamine methylester (TMRM), and Mitotracker Green (MTG) were from Molecular Probes (Carlsbad, CA), BCA (bicinchoninic acid) reagents from Pierce (Rockford, IL), 4%-12% Bis-Tris gels from Invitrogen (Carlsbad, CA), nitrocellulous membrane from Whatman (Dassel, Germany), rabbit anti-LC3 antibody from MBL International (Wobrun, MA), goat anti-rabbit antibody from Chemicon (Billerica, MA), rabbit anti-P-JNK from Cell Signal (Danvers, MA), anti-total JNK from Santa Cruz (Santa Cruz, CA), mouse anti-actin from Sigma Chemical (St. Louis, MO), and chemiluminescence reagents from GE Sciences (Buckinghamshire, UK).

3.3.2. Hepatocytes isolation, culture, and adenovirus infection

Primary hepatocytes from Sprangue-Dawley rats and wildtype, GFP-LC3 transgenic, and JNK1 and JNK2 knockout mice on a C57BL/6 background were isolated by 2-step collagenase reperfusion, as described (Qian et al., 1997). Hepatocytes were incubated in Waymouth's growth medium supplemented with 10% fetal bovine serum, 100 nM insulin, and 100 nM dexamethasone (WM) on 40-mm collagen-coated glass bottomed dishes, or 48 well-plates or 6 well-plates for overnight in 5% CO_2/95% air at 37ºC.

For adenovirus infection, hepatocytes at 4 hours after seeding were incubated in hormonally defined medium, which is composed of Roswell Park Memorial Institute 1630 (RPMI-1630) medium supplied with ITS + 3 [1.0 mg/ml insulin, 0.55 mg/ml human transferrin, 0.5 μg/ml sodium selenite, 470 μg/ml linoleic acid, 470 μg/ml oleic acid and 50 mg/ml bovine serum albumin, 2 moles each of linoleic acid and oleic acid per mole of albumin], containing recombinant adenoviruses (Ad5LacZ, Ad5DN-JNK, or Ad5TAM) at 30 plaque-forming units/cell for 2 h at 37°C. Afterwards, the cells were washed and incubated in WM overnight in 5% CO_2/95% air at 37ºC.

3.3.3. Imaging and confocal microscopy

Cultured hepatocytes were loaded with 500 nM LysoTracker Red (LTR) with or without 100 nM MitoTracker Green or 100 nM tetramethylrhodamine methylester (TMRM) in WM for 30 min. To maintain equilibrium distribution of probes, cells were then incubated with 166 nM LTR and 33 nM TMRM in WM or KRH. Images were collected using a Zeiss LSM 510 NLO laser scanning confocal microscope (Carl Zeiss, Thornwood, NY) with a 63X N.A. 1.4 oil immersion planapochromat objective lens. Temperature of the microscope stage was maintained at 37°C using an environmental chamber. LTR and TMRM were excited at 543-nm by an argon laser attenuated to less than 2% full power and emission was collected

through a 560-nm long pass filter. GFP-LC3 fluorescence was excited at 488-nm by helium-neon laser less then 2% and collected through a 500-550-nm band pass filter.

3.3.4. LTR multiwell assay

LTR uptake, a measure of cellular content of acidic organelles, was assessed by a multiwell fluorescence reader assay, as described previously (Rodriguez-Enriquez et al., 2006). Briefly after 70 min incubation of hepatocytes in WM or KRH plus 1 μM glucagon (KRH/G), 50 nM LTR was added. After 20 min at 37ºC, the hepatocytes were fixed with 2% paraformaldehyde for 10 min at 4ºC. The red fluorescence of LTR was measured using a 544-nm (15-nm band pass) excitation filter and a 590-nm long pass emission filter with Novostar multi-well fluorescence plate reader (BMG LabTechnologies, Offenburg, Germany). LTR fluorescence after experimental treatment was expressed as the percentage of LTR fluorescence of hepatocytes incubated in WM.

3.3.5. Cell viability assay

Viability of hepatocytes cultured in 24-well plates was determined by propidium iodide (PI) fluorometry, as described previously . Briefly, fluorescence of PI (30 μM) from each well was measured using excitation and emission wavelengths of 544-nm (15-nm band pass) and 590 nm long pass emission, respectively. For each experiment, an initial fluorescence measurement (A) was made 30 min after adding PI to hepatocytes incubated in WM. Maintaining PI in the medium, the cells were exposed to various treatments and fluorescence (X) was measured again after 90 min. Individual experiments were then terminated by addition of 375 μM digitonin to permeabilize all cells, and a final fluorescence measurement (B) was obtained 20 min later. The percentage of viable cells (V) was calculated as $V = 100(B - X)/ (B - A)$.

3.3.6. Western blot analysis

Hepatocytes were harvested by scraping into RIPA buffer (20 mM Tris-HCl buffer, pH 7.5, 150 mM NaCl, 1% sodium dodecyl sulfate, and 0.1% NP-40 containing protease and phosphatase inhibitor cocktails as recommended by the manufacturer). Cell lysates were sonicated on ice using an ultrasonic cell disruptor (Misonex, Farmingdale, NY) and centrifuged at 13,000 x g for 10 min at 4ºC. Protein concentration was measured using a bicinchoninic acid (BCA) procedure, as recommended by the manufacturer. Aliquots (30 μg protein) were resolved on 4 to 15% Bis-Tris gels and electrotransferred onto nitrocellulose membranes. After blocking with 5% non-fat milk in TBST (10 mM Tris-HCl buffer, pH. 7.6, 150 mM NaCl, and 0.1% Tween-20) for 1 h, membranes were immunoblotted with anti-P-JNK, anti-JNK, anti-actin, and anti-LC3 antibody diluted 1:1000 in TBST. Primary antibody was detected using horseradish peroxidase-conjugated secondary antibody against rabbit using a chemiluminescence kit according to the manufacturer's instructions.

3.4. Results

3.4.1. JNK inhibitor, SP600125 inhibited nutrient deprivation-induced autophagy.

To investigate a possible role for JNK in autophagy, we used SP600125, a JNK-specific small molecule inhibitor that prevents the activation of JNK effector molecules. The effect of SP600125 on autolysosome proliferation after nutrient deprivation was determined from by LysoTracker Red (LTR) uptake. When autophagosomes form, they fuse with lysosomes to mature into acidic autolysosomes that accumulate LTR (Rodriguez-Enriquez et al., 2006). Cultured rat hepatocytes were incubated in WM or KRH/G in the absence and presence of 3MA or SP600125. Compared to WM, LTR uptake increased 4.4 fold in KRH/G

(Figure 3.1A). 3MA, the classical autophagy inhibitor, blocked autophagy completely. At 1 μM, SP600125 did not change LTR uptake in KRH/G, but at higher concentrations, SP600125 caused dose-dependent inhibition. At 100 μM, SP600125 inhibited LTR uptake by hepatocytes incubated in KRH/G by 41%. SP600125 did not decrease cell viability at any concentration used (Figure 3.1B). This data indicated that SP600125 inhibited nutrient deprivation-stimulated autophagy in a dose-dependent fashion.

The effect of SP600125 on nutrient deprivation-induced autophagy was also visualized by confocal microscopy of GFP-LC3 hepatocytes. GFP-LC3 identifies forming and newly formed autophagosomes. GFP-labeled rings (autophagosomes) and LTR-loaded vesicles (autolysosomes) increased after nutrient deprivation, which was completely blocked by 3MA (Figure 3.1C). SP600125 (25 μM) partially inhibited GFP-labeled ring and LTR-loaded vesicle formation.

To confirm the inhibitory effect of SP600125 on autophagy, LC3-II was detected with SP600125 treatment in nutrient deprivation. During autophagic induction, LC3-I (18 kDa) is cleaved to LC3-II (16 kDa), which associates with forming autophagosomes (Kabeya et al., 2000). The amount of LC3-II, therefore, is proportional to the number of forming and newly formed autophagosomes. After nutrient deprivation, LC3-II increased, as assessed by immunoblotting (Figure 3.2A). With SP6000125 treatment, the increase of LC3-II was partially blocked. Taken together, the results indicated that SP600125 inhibited the proliferation of autophagosomes, and suggested that JNK may play a role during autophagy.

3.4.2. JNK is phosphorylated during nutrient deprivation-induced autophagy

JNK becomes phosphorylated when activated (Hibi et al., 1993). To examine JNK activation after nutrient deprivation, wildtype mouse hepatocytes from same breeding colony

as the GFP-LC3 transgenic mice were incubated in KRH/G for 0 to 90 min, and phosphorylated-JNK (P-JNK) and total-JNK (T-JNK) was determined by Western analysis. For hepatocytes cultured in WM, P-JNK expression was low (time 0), but after nutrient deprivation in KRH/G, P-JNK increased prominently at 5 to 20 min. P-JNK then declined after 50 and 90 min in KRH/G (Figure 3.2 B). T-JNK expression level was unchanged over 0 to 90 min in KRH/G. These results indicated that nutrient deprivation caused a transient early activation of JNK.

3.4.3. SP600125 inhibits mitophagy during nutrient deprivation

Next, we determined the effect of SP600125 on mitophagy in GFP-LC3 hepatocytes. GFP-LC3 hepatocytes were loaded with red-fluorescing TMRM, which accumulated into mitochondria electrophoretically. When autophagy was induced by nutrient deprivation (KRH/G), the number of GFP-labeled dots (pre-autophagic structure [PAS]-like structures) decreased, whereas the number of GFP-labeled cup-shaped structures (phagophores) and GFP-labeled rings with and without TMRM increased as seen in previous chapter (Figure 2.2C). 3MA blocked these changes nearly completely. Polarized mitochondria were initially sequestered into autophagosomes (early mitophagosomes), but shortly afterwards mitochondria lost their polarization inside the autophagosomes (late mitophagosomes). However, in presence of SP600125, the number of GFP-labeled rings with and without TMRM decreased (Figure 3.2C). The number of autophagic structures - PAS, isolation membranes, polarized mitophagosomes, and depolarized mitophagosomes – was counted from the confocal images. In the presence of SP600125, the number of PAS partially increased compared to KRH/G, whereas the number of isolation membranes and polarized

and depolarized mitophagosomes decreased relative to KRH/G. Taken together, confocal microscopy confirmed that SP600125 partially inhibits mitophagy after nutrient deprivation.

3.4.4. Autophagy and mitophagy is not blocked by other form of JNK inhibitors

SP600125 also has inhibitor effects on other protein kinases, including serum and glucocorticoid-inducible kinase (SGK), p70 ribosomal protein S6 kinase (S6K1), AMP-activated protein kinase (AMPK), and pyruvate dehydrogenase kinase (PDK1) . To determine if the inhibitory effect of SP600125 on autophagy was due to JNK inhibition, we examined JNK inhibition with a JNK inhibitory peptide inhibitor (JIP) and with dominant negative JNKs (DN-JNK). LTR uptake was measured with different JIP concentrations from 0.2 to 10 μM. As shown in Fig. 3.3A, JIP did not inhibited LTR uptake at any concentration. Moreover, in confocal images, the number of GFP-labeled rings and LTR-labeled vesicles after nutrient deprivation was unchanged after JIP (2 μM) (Figure 3.3B). In addition, the number of GFP-labeled rings containing TMRM (mitophagosomes) remained same with and without JIP treatment (Figure 3.3C). Thus, JIP failed to inhibit nutrient deprivation-induced autophagy and mitophagy in cultured hepatocytes.

To further determine whether JNK modulates autophagy, we evaluated the effect of DN-JNK1 in nutrient deprivation. DN-JNK1 is JNK1 in which threonine 183 is replaced by alanine and tyrosine 185 by phenylalanine. Consequently DN-JNK1 cannot be phosphorylated at these sites, does not become activated and thus exerts a dominant-negative effect on native JNK. Hepatocytes were tranduced with either AdDN-JNK or AdLacZ as a control. DN-JNK expression did not inhibit LTR uptake after nutrient deprivation compared to AdLacZ-treated hepatocytes (Figure 3.4A). Moreover, the proliferation of GFP-labeled rings and LTR-labeled vesicles was the same in both LacZ expressing and DN-JNK

expressing GFP-LC3 hepatocytes (Figure 3.4B). Similarly, GFP-labeled rings containing TMRM increased in both LacZ and DN-JNK expressing hepatocytes during nutrient deprivation-induced autophagy (Figure 3.4C).

We also examined DN-c-Jun (TAM-67) in nutrient deprivation. C-Jun is an important substrate for JNK, and TAM-67 is a c-Jun mutant that has a 104 amino acid deletion from the trans-activation domain of c-Jun. The overexpression of TAM-67 inhibits downstream JNK signaling (Alani et al., 1991). The DN-c-jun expression also did not block autophagosome and mitophagosome formation (data not shown). These findings support the conclusion that JNK does not play a role in nutrient deprivation-induced autophagy and mitophagy. Thus, the inhibitory effect of SP600125 may be due to an effect on other kinases.

3.4.5. JNK1 and JNK2 are not required for autophagy and mitophagy

Another possibility is that SP600125 may be acting on a specific isoform of JNK. In liver, JNK1 and JNK2 are expressed. JIP and DN-JNK predominately inhibit JNK1, although JNK2 also becomes inhibited at the high concentrations used here. To clarify possible roles of specific JNK isoforms on autophagy, we assessed autophagy and mitophagy in hepatocytes from JNK1 and JNK2 knockout mice (JNK1-/- and JNK2-/-). In JNK1-/- hepatocytes, LTR fluorescence uptake after nutrient deprivation was not inhibited compared to wildtype hepatocytes (Figure 3.5A). Moreover, formation of LTR-labeled vesicles (autolysosomes) and MitoTracker Green (MTG)-labeled LTR vesicles (mitophagosomes) remained the same in JNK1-/- hepatocytes compared to the wildtype hepatocytes (Figure 3.5B and C). These findings indicate that JNK1 does not play an essential role in nutrient deprivation-induced autophagy and mitophagy.

Similar results were obtained in JNK2-/- hepatocytes. LTR uptake after nutrient deprivation (KRH/G) increased to a similar extent in both JNK2-/- and wildtype hepatocytes (Figure 3.6A). Similarly, confocal microscopy showed similar proliferation of autolysosomes (LTR-labeled vesicles) in KRH/G in JNK2 -/- vs. wildtype hepatocytes (Figure 3.6B and C). The number of MTG-containing LTR-labeled vesicles (mitophagosomes) was also similar in JNK2-/- and wildtype hepatocytes. These results indicate that JNK2 is not required to activate nutrient deprivation-induced autophagy and mitophagy. However, JNK1 or 2 may compliment one another's function in autophagy when either JNK1 or JNK2 is deleted during autophagy.

3.5. Discussion

Previously, we investigated the effects of different mitogen-activated protein kinases (MAPKs) inhibitors on nutrient-deprivation induced autophagy (Rodriguez-Enriquez et al., 2006). The JNK inhibitors, SCP25041 and SP600125, blocked LTR uptake, whereas ERK1 inhibitors, PD98059, and a p38 inhibitor, SB203580, did not inhibit LTR uptake (Rodriguez-Enriquez et al., 2006). This pharmacological data therefore suggested a role for JNK in stimulating nutrient deprivation-induced autophagy. Other studies also implicate a role of JNK in promoting ER stress-induced autophagy (Ding et al., 2007; Ogata et al., 2006). JNK also promotes growth factor withdrawal-induced autophagic cell death in T cells (Li et al., 2006). In addition, JNK plays a key role in proapoptotic mitochondrial signaling pathways. JNK1 and JNK2 double-knock out cells are resistant to UV-induced apoptosis and cytochrome c release from mitochondria (Tournier et al., 2000).

The overall goal of the present study was to demonstrate directly a role of JNK signaling in nutrient deprivation-induced mitophagy in hepatocytes. We confirmed and extended our previous finding of the inhibitory effect of the small molecule JNK inhibitor, SP600125, on nutrient deprivation-induced autophagy. SP600125 inhibits LTR uptake in a dose dependent manner, whereas 3MA completely inhibited LTR uptake (Figure 3.1A). Under nutrient deprivation plus glucagon, cell killing did not occur at 1 to 100 μM concentration of SP600125 (Figure 3.1B). In GFP-LC3 hepatocytes, SP600125 partially blocked the proliferation of GFP-labeled rings (autophagosomes) and LTR-labeled disc structures (autolysosomes) during nutrient deprivation plus glucagon suggesting a role of JNK in autophagy (Figure 3.1C). LC3 II processing, which is a standard method to measure autophagic stimulation, was partially inhibited by SP600125 (Figure 3.2A). Furthermore, JNK became transiently phosphorylated at 5 to 20 min after nutrient deprivation, which supported the hypothesis that JNK mediates nutrient deprivation-induced autophagy (Figure 3.2B). Then, we investigated the effect of SP600125 on mitophagy in GFP-LC3 hepatocytes during nutrient deprivation. Here, we showed that SP600125 inhibited the proliferation of phagophores and mitochondrial autophagosomes (mitophagosomes) (Figure 3.2C). Based on the effects of SP600125, we proposed that JNK may act in the induction of autophagy and mitophagy.

To extend these findings, we assessed other types of JNK inhibitors, including a cell permeable JNK peptide inhibitor (JIP) and an adenoviral dominant negative JNK. JIP is derived from JNK-interacting-protein 1 whose JNK-binding domain (JBD) directly interacts with JNK and specifically inhibits JNK without affecting other MAPK family proteins such as ERK or p38 (Barr et al., 2004b; Barr et al., 2004a; Barr et al., 2002; Bogoyevitch et al.,

2004). DN-JNK is a dominant negative JNK1 which is unable to be phosphorylated and, therefore, is inactive. Surprisingly, JIP did not inhibit LTR uptake after autophagic induction (Figure 3.3A). In GFP-LC3 hepatocytes, the proliferation of GFP-LC3 labeled autophagosomes and LTR-labeled autolysosomes was not inhibited by JIP (Figure 3.3B). The sequestration of mitochondria and proliferation of mitochondria-containing autophagosomes (mitophagosomes) also were not blocked by JIP (Figure 3.3C). Similar results were found in DN-JNK expressing hepatocytes. The LTR uptake was not decreased in DN-JNK expressing hepatocytes (Figure 3.4A). The number of LTR-labeled autolysosomes was not inhibited in DN-JNK compare to LacZ (used for vector control) -expressing GFP-LC3 hepatocytes (Figure 3.4B). The number of mitophagosomes not inhibited in DN-JNK expressing hepatocytes (Figure 3.4C). These data imply that JNK is not directly involved in mitophagy. The inhibitory effect of SP600125 on autophagy occurs not by interupting JNK function, but rather by inhibiting other kinases such as serum and glucocorticoid-inducible kinase (SGK), p70 ribosomal protein S6 kinase (S6K1), AMP-activated protein kinase (AMPK), and pyruvate dehydrogenase kinase (PDK1) (Bennett et al., 2001; Bain et al., 2003; Bain et al., 2007). Although we observed transient JNK activation in hepatocytes incubated in KRH/G, this may be a nonspecific response to the stress induced by nutrient deprivation. Previous studies shows that JNK is activated by extracellular stresses including serum and amino acid depletion (Leicht et al., 2003; Aubel et al., 2001).

Different JNK isoforms might be responsible for the inhibitory effect observed with SP600125. For instance, JNK1 and JNK2 have distinct functions despite their biochemical and structural similarities. For example, JNK1 promotes bile acid injury, but JNK2 attenuates such effect. By contrast, JNK2 promotes acetaminophen hepatotoxicity and

proapoptotic mitochondrial signaling cascades. JNK1 also mediates insulin resistance by phosphorylating IRS-1 (insulin receptor substrate-1) (Hirosumi et al., 2002). In TNF-dependent hepatotoxicity, caspase-8 activation and Bid cleavage are elicited by JNK2. JNK2 is also proposed to translocate to mitochondria to mediate cytochrome *c* release upon 6-hydroxydopamine-induced neuronal cell death (Eminel et al., 2004). In our study, loss of one of JNK isoforms did not prevent autophagy or mitophagy in hepatocytes. In hepatocytes from JNK1 knockout mice, LTR uptake was not decreased compare to hepatocytes from wildtype mice (Figure 3.5A). The number of solid LTR-loaded autolysosome and mitochondria-containing autolysosomes increased in both wildtype and JNK1 knockout hepatocytes (Figure 3.5B and C). JNK2 knockout (JNK2 -/-) hepatocytes showed similar effects. LTR uptake was increased in both hepatocytes from wildtype and JNK2-/- mice (Figure 3.6A). The LTR-loaded autolysosomes and mitochondria-containing autolysosomes were not inhibited in JNK2 knockout hepatocytes compare to the wildtype (Figure 3.6B and C). These results suggest that JNK1 or JNK2 is not necessary for autophagy and mitophagy in nutrient deprivation. However, the ability of JNK1 to substitue for the function of JNK2 or *vice versa* during autophagy needs to be clarified. These data indicate that JNK is not directly involved in autophagy. However, recently presented data from Levine's group indicated that JNK was phosphorylated and activated during nutrient deprivation leading to phosphorylation of Bcl-2. As a consequence, phosphorylated Bcl-2 was unable to bind and inhibit Beclin which promoted autophagy (Golstein and Kroemer, 2007). It is not clear why our data support a different conclusion. Technical issues such as differences in cell lines verses hepatocytes may play a role.

In summary, these results demonstrate that the inhibitory effect of SP600125 is not likely through JNK pathway during nutrient deprivation-induced mitophagy; rather the effect is secondary to other kinase pathways by which SP600125 inhibits. However, we were unable to determine the targets of SP600125 against autophagy in the timeframe of this study. JNK1 or JNK2 may not be necessary in nutrient deprivation-induced mitophagy. However, JNK1 or JNK2 may substitute for each other when one is absent. Additional experiments should be addressed to resolve this issue.

Chapter 4. Damaged mitochondria are selectively removed by mitophagy

Chapter 4. Damaged mitochondria are selectively removed by mitophagy

4.1. Abstract

Damaged and dysfunctional mitochondria are proposed to be removed by autophagy. However, selective degradation of damaged mitochondria by autophagy (mitophagy) has yet to be verified experimentally. In this study, we investigated the cellular fate of mitochondria damaged by photoirradiation in cultured hepatocytes isolated from transgenic mice expressing GFP fused to microtubule-associated protein 1 light chain 3 (GFP-LC3), a marker of forming and newly formed autophagosomes. Photoirradiation with 488-nm light from an argon laser induced mitochondrial depolarization (release of tetramethylrhodamine methylester [TMRM]) in a dose-dependent fashion. At lower light doses (photoirradiation below 160 μs per pixel at 100% transmission of 488-nm laser), mitochondria depolarized transiently with repolarization within 3 min. After more light photoirradiation (above 320 μs per pixel at 100% transmission of 488-nm laser), mitochondrial depolarization became irreversible. Irreversible, but not reversible, photodamage induced autophagosome formation after 32 ± 5 min, as revealed by GFP-LC3 labeling. Photodamage-induced mitophagy was independent of TMRM, since photodamage also induced mitophagy in the absence of TMRM. Photoirradiation with 543-nm light did not induce mitophagy. As revealed by uptake of LysoTracker Red (LTR), mitochondria weakly acidified after photodamage before a much stronger acidification following autophagosome formation. Photodamage-induced mitophagy was not blocked by PI-3-kinase inhibition with 3-methyladenine (10 mM) or wortmannin (100 nM). In conclusion, damaged mitochondria are selectively degraded by mitophagy, but photodamage-induced mitophagic sequestration occurs independently of PI-3-kinase

signaling pathway, the classical upstream signaling pathway of nutrient deprivation-induced autophagy.

4.2. Introduction

Autophagy refers to the process by which cellular constituents are sequestered into vesicles called autophagosomes and delivered to lysosomes for digestion. Insulin and other growth factors inhibit autophagy, whereas nutrient deprivation and glucagon promote autophagy (Arstila and Trump, 1968; Schworer and Mortimore, 1979). During the normal life of cells, autophagy may remove damaged and superfluous organelles, including dysfunctional mitochondria that could be detrimental to cells. Several studies show that both inadequate and excess autophagy lead to cell injury and death (Levine and Klionsky, 2004). Therefore, proper regulation of autophagy is fundamental to cellular well being.

During autophagy, a novel membranous structure called a phagophore elongates and encloses cellular components to form a double membrane vesicle known as an autophagosome (Seglen et al., 1996). Lysosomes then fuse with autophagosomes to form autophagolysosomes in which lysosomal hydrolases degrade the sequestered contents. Autophagosomes can contain virtually any cytoplasmic element, including cytosolic proteins and various membranous organelles, such as endoplasmic reticulum, peroxisomes and mitochondria (Arstila et al., 1972; Kopitz et al., 1990).

In yeast, genetic screens identified a series of evolutionally conserved autophagy (ATG) genes that are required for autophagy. Beclin1, a mammalian homologue of yeast Atg6, interacts with PI3K to form a complex, which is an initial step in autophagosome formation (Furuya et al., 2005). Microtubule-associated protein 1 light chain 3 (LC3) was

then identified as a mammalian ortholog of yeast Atg8 that is important for autophagy in higher vertebrates (Kabeya et al., 2000). In mammalian cells, newly synthesized ProLC3 is processed to its cytosolic form, LC3-I. LC3-I is activated by Atg7 and transferred to Atg3. During this process, LC3-I is conjugated with phosphatidylethanolamine, called as LC3-II (Tanida et al., 2004). LC3-II localizes selectively to forming and newly formed autophagosomes even after other Atg proteins dissociate. Thus, LC3-II is a marker of ongoing autophagy. After sequestration, some LC3-II becomes entrapped on the inner surfaces of the double membrane autophagosomes. After fusion with lysosomes, this LC3-II is degraded. The outer surface LC3-II also disappears, most likely by breakdown of the phospholipid conjugate and reutilized. Recently, a transgenic mouse strain was created that expresses a green fluorescent protein (GFP)-LC3 fusion protein. In cells and tissues of GFP-LC3 transgenic mice, GFP fluorescence selectively identifies the membranes of forming and newly formed autophagosomes (Mizushima et al., 2004).

Whether or not autophagy selectively targets specific organelles has been controversial. After withdrawal of peroxisome proliferators in the presence of protease inhibitors, peroxisomes are selectively accumulate in autophagosomes (Yokota, 2003). The removal of peroxisomes by autophagy is referred as pexophagy which is often found in yeast where methanol containing medium is switched to glucose or ethanol containing medium (Kiel et al., 2003; Tuttle et al., 1993). Similarly, selective autophagic degradation of hepatic glycogen, but not mitochondria and other organelles, occurs in early postnatal period (Kotoulas et al., 2006). Mitochondria of non-proliferating tissues like heart, brain, liver, and kidney constantly turn over with a half-life of 10 to 25 days (Stromhaug et al., 1998), and recent evidence supports selective autophagic removal of mitochondria, a process of mitophagy (Tal

et al., 2007). In cells where apoptosis is inhibited by caspase inhibitors, mitochondria are eliminated by mitophagy in specific and regulated manner (Xue et al., 2001).In yeast, the mitochondrial outer membrane protein Uth1p, is required for efficient mitophagy in nutrient-poor medium, but a corresponding mammalian protein has yet to be identified (Kissova et al., 2004). Also, a yeast protein phosphatase homologue, Aup1 in the mitochondrial intermembrane space is required for mitophagy (Tal et al., 2007). Although these data support mitophagy as a distinctive pathway from other autophagy of other cytoplasmic components, selectivity of mitophagy for damaged mitochondria has not been directly shown. The visible light of 400 to 500 nm wavelength excite and damage flavin-containing proteins in mitochondria leading to mitochondrial damage (Aggarwal et al., 1978; Alexandratou et al., 2002). In this study, we used 488 nm light to photoirradiate mitochondria of primary hepatocytes from GFP-LC3 transgenic mice to show that photodamage of mitochondria leads to selective mitophagy.

4.3. Materials and Methods

4.3.1. Materials.

3-Methyladenine and wortmannin were purchased from Sigma Chemical Co. (St. Louis, MO). Calcein, Lysotracker Red (LTR), MitofluorFar Red (MFFR), and tetramethylrhodamine methylester (TMRM) were obtained from Molecular Probes (Carlsbad, CA). Collagenase A was obtained from Roche (Penzberg, Germany).

4.3.2. Hepatocyte isolation and culture

Hepatocytes from GFP-LC3 transgenic C57BL/6 mice or C57/BL6 wildtype mice were isolated by collagenase perfusion and cultured overnight in 5% CO_2/95% air at 37°C on type

1 collagen-coated 35-mm glass bottom dishes at a density of 300,000 cells per plate in Waymouth's MB-752/1 growth medium supplemented with 27 mM $NaHCO_3$, 10% fetal bovine serum, 100 nM insulin, and 100 nM dexamethasone (Gores et al., 1988).

4.3.3. Loading fluorophores

Hepatocytes isolated from GFP-LC3 transgenic mice were loaded with red-fluorescing tetramethylrhodamine methylester (TMRM, 200 nM) or MitoFluor Far Red (MFFR, 200 nM) for 30 min in the absence or presence of 10 mM 3MA or 100 nM wortmannin at 37°C in Waymouth's MB-751/1 growth medium supplemented with 25 mM Na-HEPES buffer, pH 7.4. TMRM and MFFR are membrane-permeable monovalent cations that accumulate electrogenically into mitochondria (Zahrebelski et al., 1995). In other experiments, acidic compartments were labeled with LysoTracker Red (LTR, 500 nM) under identical conditions. After TMRM, MFFR and LTR loading, one-third of the initial loading concentration was maintained in the medium to maintain steady-state. Hepatocytes isolated from wildtype mice were loaded with LTR as described above. Subsequently, the cells were photoirradiated and loaded with 1 μM calcein acetoxymethyl (AM) for 10 min at 37°C to assess mitochondrial inner membrane permeabilization. After LTR and calcein loading, one-third of the initial LTR loading concentration was maintained in the medium.

4.3.4. Photodamage and confocal microscopy

Laser-induced photodamage and confocal microscopy were performed with a Zeiss LSM 510 NLO laser scanning confocal microscope (Carl Zeiss, Thornwood, NY) using a 63 X N.A. 1.4 oil-immersion planapochromat objective lens. To induced photodamage, selected areas of individual cells containing 5 to 10 mitochondria were exposed to 488-nm argon laser light at 100% power for times of 80, 160, 320, 640 and 1280 μs per pixel. Green (GFP-LC3),

red (TMRM and LTR) and far red (MFFR) fluorescence was excited by the 488-nm, 543-nm and 633-nm laser lines of argon and helium-neon lasers in the multitracking mode. To image green and red fluorescence simultaneously, emitted light was separated by a 545-nm dichroic mirror and directed to different photomultipliers through 500 to 530-nm (green) band pass and 560-nm (red) long pass filters. To image green, red and far red fluorescence simultaneously, emitted light was separated by a 635-nm dichroic mirror and directed to different photomultipliers through 500 to 530-nm (green) band pass, 565 to 615-nm (red) band pass and 650 to 710-nm (far red) band pass filters. For serial imaging at up to one frame a minute, laser illumination was attenuated to less than 0.1% transmission power for pixel dwell times of 3.2 μs. Temperature on the microscope stage was maintained at 37°C.

4.4. Results

4.4.1. Photodamaged mitochondria are selectively removed by mitophagy

To investigate possible mitophagy after photodamage to mitochondria, cultured hepatocytes from GFP-LC3 transgenic mice were first loaded with TMRM, a red-fluorescing fluorophore that labels polarized mitochondria and is released upon mitochondrial depolarization. Selected areas of hepatocytes containing 5 to 10 TMRM-loaded mitochondria were exposed to 488-nm argon laser light at 100% transmission for 80, 160, 320, 640 and 1280 μs. This illumination corresponded to 2.5 $x10^4$, 5 x 10^4, 1 x 10^5, 2 x 10^5, and 4 x 10^5 times greater than the pixel power used for imaging. These pixel powers are designated in ascending order as 1x, 2x, 4x, 8x, and 16x. After selected area photoirradiation, confocal images of red TMRM and green GFP-LC3 fluorescence were collected every minute for 120 min. After lower laser photoirradiation (below 2x), mitochondria released

TMRM, indicating depolarization, but subsequently recovered TMRM fluorescence (Figure 4.1, double arrow). This transient depolarization signified reversible photodamage. At higher laser power (above 2x), mitochondria became irreversibly depolarized, indicating permanent mitochondrial damage (Figure 4.1). At 16x laser power, adjacent mitochondria surrounding the illuminated mitochondria also became depolarized (Figure 4.1, arrow). Presumably, this bystander injury was due to free radical generation by regions of the hepatocytes actually exposed to light (Aggarwal et al., 1978). Overall, these data showed that photoirradiation with 488-nm laser caused sustained mitochondrial depolarization in a dose-dependent fashion. Nonetheless, the photoirradiated hepatocytes remained viable and healthy with no morphological evidence of injury, necrosis or apoptosis *(e.g.,* cell surface blebbing, chromatin condensation, nuclear lobulation) over the time course of the experiments.

At 32 ± 5 min after photoirradiation (4x and up), GFP-LC3 fluorescence began to associate with depolarized mitochondria as small granular structures that eventually coalesced into ring structures (autophagosomes) (Figure 4.2, bottom right panel). However, GFP-LC3 did not localize to mitochondria that transiently depolarized after a lower light exposure. Unlike nutrient deprivation-induced mitophagy (Kim et al., 2007), GFP-LC3-labeled cup-shaped phagophores did not grow around and sequester individual photodamaged mitochondria; rather GFP-LC3 started to decorate around the damaged mitochondria (Figure 4.2).

4.4.2. Photodamage-induced mitophagy is independent of TMRM loading

To determine whether light-induced mitophagy is dependent on the presence of TMRM as a photosensitizer, small regions of GFP-LC3 hepatocytes were exposed to 488-nm illumination at 16x laser power in the absence of TMRM. Similar to observations in the

presence of TMRM, the region exposed to 16x laser power became decorated by GFP-LC3 after about 27 min (Figure 4.3, middle panel). The GFP-LC3 fluorescence subsequently coalesced into green rings indistinguishable from the GFP-LC3 rings that formed after photodamage in the presence of TMRM. Thus, mitophagy after photoirradiation with 488-nm light occurred independently of TMRM, which is consistent with weak absorbance of 488-nm light by TMRM (Figure 4.3, right panel). In another experiment, hepatocytes were loaded with TMRM and subjected to photodamage with different doses of 543-nm laser light, a wavelength that is absorbed by TMRM. Green excitation light at 543-nm caused photobleaching of TMRM (Figure 4.4, top right panel). However, GFP-LC3 did not localize to the mitochondria that were exposed to 543-nm light (Figure 4.4, bottom panels). Taken together, these observations indicate that 488-nm induces mitochondrial photodamage that leads to mitophagy. The presence of TMRM did not sensitize the process.

4.4.3. Mitochondrial permeability transition is induced by photodamage

Photoirradiation generates ROS that can induce the mitochondrial permeability transition (MPT) in mitochondria (Jou et al., 2002). During the MPT, mitochondria become permeable to molecules up to 1.5 kDa, which causes mitochondrial depolarization. To investigate a role for the MPT in initiating photodamage-induced mitophagy, hepatocytes from wild type mice were loaded TMRM, exposed to 488-nm light and then loaded with calcein acetoxymethyl ester (AM). Calcein AM enters the cytosol (and nucleus) where esterases release green-fluorescing calcein free acid, which outlines mitochondria as round dark voids. When mitochondria undergo the MPT, calcein fluorescence fills the voids (Lemasters et al., 1998; Qian et al., 1997; Qian et al., 1999). After exposure to 488-nm light, mitochondria released TMRM transiently at lower doses and permanently at higher light

levels (Figure 4.5, top right panel). Subsequently, after loading with calcein AM, still polarized mitochondria excluded the green-fluorescing probe. By contrast, depolarized mitochondria that had been exposed to high power light (16x) filled with calcein AM (Figure 4.5, top right panel), but mitochondria exposed to lower power (8x) released TMRM but initially (within 10 min after the photodamage) did not take in calcein AM (data not shown). Over time, however, the TMRM-released mitochondria were the filled with calcein fluorescence. At still lower power (1x), mitochondria regained TMRM after depolarizing initially. These mitochondria did not take up calcein (Figure 4.5, bottom panel). Thus, photoirradiation with higher doses of 488-nm light led to inner membrane permeabilization which is the characteristic of the MPT.

4.4.4. Photodamage-induced mitophagosomes undergo acidification

In general after autophagic sequestration, autophagosomes fuse with lysosomes and acidify. To investigate acidification of mitophagosomes (autophagosomes containing mitochondria), GFP-LC3 transgenic hepatocytes were loaded with MFFR, a far red-fluorescing fluorophore that accumulates electrophoretically into polarized mitochondria (Sakanoue et al., 1997). MFFR-labeled mitochondria were photodamaged with 488-nm light at 16x power, and then red-fluorescing LTR, a weak basic fluorophore that accumulates into acidic compartments, was loaded. After photodamage, mitochondria released their MFFR fluorescence signifying depolarization (Figure 4.6, top panels). After 20 min, LTR started to accumulate weakly into the photodamaged mitochondria (Figure 4.6, middle left panel) and GFP-LC3 (green) particles began to decorate the photodamaged mitochondria (Figure 4.6, middle right panel). Red LTR fluorescence progressively intensified afterwards (Figure 4.6, bottom panel). Thus, after photodamage, mitochondria became weakly acidic as they began

to associate with GFP-LC3. Subsequently after envelopment by GFP-LC3, the structures strongly acidified.

4.4.5. Photodamage-induced mitophagy activates downstream of PI3Kinase signaling

3MA, the classical inhibitor of autophagy, and wortmannin block autophagy after nutrient deprivation by inhibition of Class III PI3-kinase (Seglen and Gordon, 1982; Blommaart et al., 1997). To determine the role of PI3-kinase on mitophagy after photodamage, GFP-LC3 hepatocytes were loaded with TMRM and treated with 10 mM 3MA prior to photoirradiation of a small group of mitochondria with 488-nm laser light at 16x laser power. Photodamaged mitochondria again irreversibly lost TMRM fluorescence, indicating loss of membrane potential (Figure 4.7A and 4.7B, top panels). In the presence of 3MA, green ring structures again started to form around photodamaged mitochondria after about 30 min (Figure 4.7A). To confirm further that photodamage–induced mitophagy occurred after inhibition of PI3K, GFP-LC3 hepatocytes were treated with 100 nM wortmannin prior to photoirradiation. Wortmannin did not inhibit photodamage-induced mitophagy (Figure 4.7B). In the presence of either 3MA or wortmannin, the number of GFP-LC3 rings and the strength of labeling were greater than in their absence (Figure 4.7).

4.5. Discussion

Our results provide direct evidence that mitophagy selectively removes and degrades damaged mitochondria. In hepatocytes incubated in nutritionally replete growth medium, only photoirradiated mitochondria that depolarized were sequestered into autophagosomes. When mitochondria were photoirradiated at lower laser power, mitochondria initially

depolarized, but then recovered polarization as indicated by reuptake of TMRM. Such mitochondria did not undergo mitophagy. Thus, photodamage leading to sustained mitochondrial depolarization was required to initiate sequestration into autophagosomes.

Mitochondrial depolarization occurred in dose-dependent manner after photoirradiation with 488-light (Figure 4.1). The lowest light exposure, namely that used to image hepatocytes, did not cause mitochondrial depolarization or induce mitophagy. Beginning at a light exposure about 2.5 $x10^3$ times greater than that used for imaging, mitochondria depolarized, but then recovered their membrane potential within about 3 min. At greater photoirradiation, mitochondria depolarized in a sustained fashion. At highest illumination, a bystander effect occurred in which depolarization not only occurred in mitochondria under the light beam but also in adjacent mitochondria outside the illuminated region (Figure 4.2). Bystander photodamage suggests that a toxic agent formed in illuminated regions diffused into immediately adjacent areas. This toxic agent is most likely ROS, such as singlet oxygen, which is produced during exposure to strong light.

Photoxicity-dependent mitophagy occurred in the absence of TMRM or other added fluorophore and thus did not require photosensitization of an exogenous absorber (Figure 4.3). In addition, mitophagy did not occur with 543-nm light (Figure 4.4). Previous work shows that photoirradiation of 400 to 500-nm light causes oxygen-dependent inactivation of flavoproteins and succinate dehydrogenases that is mediated by production of ROS (Aggarwal et al., 1978). Thus, photodamage to mitochondria in our experiments is likely via photoexcitation of succinate dehydrogenase and other mitochondrial flavoproteins.

ROS induce the MPT in mitochondria, leading to depolarization, uncoupling and more ROS formation (Nieminen et al., 1997). After photodamage, sustained mitochondrial

depolarization appeared to be a prerequisite for subsequent mitophagy. Mitochondria that depolarized transiently after light exposure did not undergo subsequent mitophagy, whereas photodamaged mitochondria that underwent sustained depolarization were reproducibly sequestered into autophagosomes (Figure 4.2). Moreover, this latter group of mitochondria became permeable to calcein, indicative of the inner membrane permeabilization of the MPT (Figure 4.5). Thus, sustained mitochondrial depolarization and associated inner membrane permeabilization seemed to be required for autophagy signaling. These results are consistent with involvement of the MPT in photodamage-induced mitophagy, as proposed previously for autophagy stimulated by nutritional deprivation (Elmore et al., 2001).

However, photodamage-induced mitophagy differed from nutrient deprivation-induced mitophagy in several ways. In nutrient deprivation-induced mitophagy, small (0.2-0.3 μm) pre-autophagosomal structures associate with polarized mitochondria and grow into crescent-shaped phagophores that envelope and enclose individual mitochondria into mitophagosomes (Kim et al., 2007). Mitochondrial depolarization only occurs at or after formation of mitophagosomes. Subsequently, as the mitophagosomal vesicles acidify and fuse with lysosomes, GFP-LC3 is released and/or degraded (Kim et al., 2004).

By contrast, in photodamage-induced mitophagy, only depolarized mitochondria were targeted for autophagic degradation. Moreover, instead of being enveloped by a crescent-shaped phagophore, the periphery of photodamaged mitochondria became decorated with small granular aggregates of GFP-LC3 that later coalesced into rings enveloping the entire mitochondrion (Figure 4.2 and Figure 4.6). Additionally, mild acidification of photodamaged mitochondria occurred before assembly of continuous GFP-LC3-decorated rings. Future studies will be needed to determine whether depolarized mitochondria

themselves undergo mild acidification or whether a sequestration membrane encloses photodamaged mitochondria before recruitment of GFP-LC3 (Figure 4.6). Subsequently, after completion of the GFP-LC3 ring, the mitophagosomal vesicle became more intensely acidic.

A particularly noteworthy difference between nutrient deprivation-induced mitophagy and photodamage-induced mitophagy is that the latter was not blocked by PI3 kinase inhibition with 3-methyladenine (10 mM) or wortmannin (100 nM) (Kim et al., 2006). Class III PI3 kinase/p150 interacts with Beclin1, a mammalian homologue of Atg6 which is required for early stage of autophagosome formation during nutrient deprivation (Tassa et al., 2003). Rather, PI3K inhibition appeared to augment GFP-LC3 association with photodamaged mitochondria (Figure 4.7). These findings indicate that activation of mitophagy after photodamage occurs independently of PI3K signaling. Indeed, photodamage-induced GFP-LC3 ring formation was more robust after PI3K inhibition, which suggests that subsequent processing of mitophagosomes may require PI3K, as shown recently for the processing of mitophagosomes in nutrient deprivation-induced autophagy (Kim et al., 2007; Mousavi et al., 2003; Tassa et al., 2003)

Mitochondria of non-proliferating tissues such as heart, brain, liver, and kidney turnover the half-life of 10 to 25 days (Pfeifer, 1978; Menzies and Gold, 1971). In this normal turnover, old and presumably dysfunctional mitochondria are removed by mitophagy and replaced by biogenesis of new mitochondria. Such mitophagy serves the physiological function of segregating and degrading dysfunctional mitochondria that might otherwise release ROS, pro-apoptotic proteins and other toxic mediators. Because mitochondria are a primary site of ROS generation, mitochondrial DNA (mtDNA) is prone to oxidative damage.

Due to limited mtDNA repair mechanisms, damaged mtDNA likely accumulates with time. Since mtDNA is nearly 100% active in transcription (compared to 2 or 3% for nuclear DNA), damage to mtDNA will lead quickly to mitochondrial dysfunction. Decreased mitophagy may promote accumulation of mtDNA mutations in aging (Bergamini, 2006; Terman, 1995), whereas caloric restriction, an inducer of autophagy, increases longevity in rodents (Bergamini et al., 2003).

In conclusion, photoirradiation by 488-nm light caused mitochondrial depolarization, inner membrane permeabilization and subsequent selective mitophagy, consistent with previous reports of photodynamic induction of the MPT and involvement of the MPT in mitophagy (Lam et al., 2001; Zorov et al., 2006; Elmore et al., 2001). However, upstream signaling for photodamage-induced mitophagy bypassed the classical PI3K signaling pathway of nutrient deprivation-induced autophagy, although PI3 kinase may still be needed for downstream processing of newly formed mitophagosomes. Thus, mitophagy is an important mechanism to sequester and degrade damaged mitochondria in otherwise viable and healthy cells.

Chapter 5. Summary

5.1. Mitophagy induced by nutrient deprivation and its possible signaling pathway

5.1.1. Process of mitophagy

5.1.2. MPT in mitophagy

5.1.3. Mitophagy and Bcl-2 family proteins

5.1.4. Role of JNK in mitophagy

5.2. Mitophagy after photodamage

5.2.1. 488-nm light induces damage in mitochondria leading to mitophagy

5.2.2. MPT and photodamage-induced mitophagy

5.2.3. PI3K and photodamage-induced mitophagy

5.3. Final Remarks

Chapter 5. Summary

5.1. Mitophagy induced by nutrient deprivation and its possible signaling pathways

5.1.1. Process of mitophagy

Autophagy is responsible for degradation and turnover of damaged and superfluous mitochondria during normal physiology, fasting, and pathological conditions. During nutrient deprivation, mitophagy maintains ATP energy production and generates amino acids to fuel the tricarboxylic acid cycle. In this dissertation, time-lapse confocal imaging of hepatocytes isolated from transgenic mice expressing GFP fused with LC3 allowed direct visualization of the progression of nutrient deprivation-induced mitophagy. In nutritionally replete culture medium, GFP-LC3 fluorescence was diffuse except for small (0.2-0.3 μm) dotted structures, which likely represent pre-autophagosomal structures (PAS) distributed randomly throughout the cytoplasm (Figure 2.1). After imposition of nutrient deprivation, PAS-like structures came in close association with mitochondria and grew into crescent-shaped structures, or phagophores, surrounding individual mitochondria (Figure 2.2). These phagophores went on to sequester completely individual mitochondria (Figure 2.2 and Figure 2.3). Sequestration occurred in about 6 min from the first appearance of a PAS next to a mitochondrion (Figure 2.4). In some instances, only a portion of an individual mitochondrion became sequestered, which indicated that mitochondrial fission occurred coordinately with autophagosome formation. Partial mitochondrial sequestration occurred from both the ends and middle parts of mitochondria (Figure 2.5).

After ring closure, mitochondria depolarized in about 11.8 min, as revealed by the release of TMRM (Figure 2.3). As mitochondria inside autophagosomes depolarized,

acidification began as revealed by uptake of LysoTracker Red (LTR) (Figure 2.3). After vesicle acidification, GFP-LC3 fluorescence was released or degraded. Acidification and loss of GFP-LC3 fluorescence mostly likely reflected fusion with lysosomal precursors at about this time, leading to formation of autolysosomes. In addition, mitochondria contained one to several copies of PicoGreen-labeled mtDNA, which was degraded by mitophagy (Figure 2.6).

5.1.2. MPT in mitophagy

A role for the MPT in mitophagy was implicated in cultured hepatocytes during nutrient deprivation. CsA, the MPT blocker, suppressed the proliferation of autolysosomes (Rodriguez-Enriquez et al., 2006). NIM811, a CsA analog and MPT inhibitor that is not immunosuppressive, also blocked autophagy (Elmore et al., 2001). However, CsA and NIM811 did not block formation of GFP-LC3-labeled structures containing mitochondria during nutrient deprivation-induced mitophagy (Figure 2.7). Rather, CsA may block acidification occurring after sequestration or possibly the completion of the sequestration process itself (Figure 2.8). Taken together, my results showed that LC3-containing membranes sequestered polarized mitochondria during nutrient deprivation-induced mitophagy.

5.1.3. Mitophagy and Bcl-2 family protein

Recent studies show involvement of Bcl-2 family proteins in autophagy (Pattingre et al., 2005; Tracy et al., 2007). I examined protein expression of the Bcl-2 family proteins, Bcl-2, Bcl-xl, Bax, Bid, Bnip3, and Bim, in cultured hepatocytes during induction of autophagy by nutrient deprivation plus glucagon. Bcl-2 expression was undetectable before and after autophagic stimulation (data not shown). Bcl-xl was

detected but its protein expression did not change after autophagic stimulation. Of other pro-apoptotic Bcl-2 family proteins examined, Bax, Bid, Bnip3, BimL and BimS were not affected by autophagic stimulation (Figure 2.9). BimEL, however, changed its pattern of expression after autophagic stimulation (Figure 2.9). In complete medium, BimEL was detected as two bands, an apparent phosphorylated form and a non-phosphorylated form. By contrast, after stimulation of autophagy only a single band of non-phosphorylated BimEL was observed (Figure 2.9). In hepatocytes from Bim knockout mice, the proliferation of mitophagosomes and autolysosomes were not inhibited after nutrient deprivation plus glucagon (Figure 2.10). These data indicate that Bim is dephosphorylated, but Bim dephosphorylation is not required for the formation of autophagosomes or mitophagosomes during nutrient deprivation.

5.1.4. Role of JNK in mitophagy

JNK has been suggested to promote autophagy (Ding et al., 2007; Ogata et al., 2006; Li et al., 2006). In my studies, the small molecular JNK inhibitor, SP600125, inhibited autophagy in a dose-dependent manner, as assessed by LTR uptake (Figure 3.1). Concentrations of SP600125 inhibiting autophagy did not cause cell killing (Figure 3.1). Moreover, LC3 II processing that occurred during autophagic stimulation was partially inhibited by SP600125 (Figure 3.2). JNK, which is phosphorylated when activated, was transiently phosphorylated between 5 and 20 min of onset of nutrient deprivation (Figure 3.2). Confocal microscopy of GFP-LC3 transgenic hepatocytes also revealed an inhibitory effect of SP600125 on autophagosome and mitophagosome formation (Figure 3.1C and 3.2C).

SP600125 inhibits JNK by competing with the ATP-binding site. However, SP600125 also inhibits upstream MAP kinases, such as MKK4, MKK7, MKK3, MKK6, and others to lesser extent (Bennett et al., 2001; Bain et al., 2003). Therefore, inhibition of autophagy by SP600125 may not be via a JNK signaling pathway. The cell permeable JNK peptide inhibitor (JPI) and dominant negative JNK (DN-JNK) have higher specificity for JNK signaling than SP600125. JPI is derived from the JNK-binding domain (JBD) of JNK-interacting-protein 1 (JIP1), which is a putative JNK scaffolding protein (Dickens et al., 1997). JIP1 directly interacts with JNK and specifically inhibits JNK without affecting other MAPK family proteins, such as ERK or p38 (Barr et al., 2004b; Barr et al., 2004a; Bogoyevitch et al., 2004). DN-JNK is a dominant negative mutant JNK1 that is unable to be phosphorylated and, therefore, is constitutively inactive. Unlike SP600125, neither JPI nor DN-JNK inhibited nutrient-deprivation-induced autophagy and mitophagy (Figure 3.3 and Figure 3.4). However, whether JPI is equally effective in blocking JNK binding to substrates other than c-Jun has not been established . DN-JNK is derived from JNK1 and may not inhibit JNK2. However, hepatocytes from JNK2 knockout mice (JNK2-/-) did block nutrient deprivation-induced autophagy as assessed by LTR uptake (Figure 3.6). Confocal microscopy of GFP-LC3 transgenic mice also indicated that mitophagy was not inhibited in JNK2-/- hepatocytes. Similarly, autophagy and mitophagy were not blocked in hepatocytes from JNK1-/- (Figure 3.5). Taken together, JNK signaling did not appear to regulate nutrient-deprivation-induced autophagy, and inhibition of autophagy by SP600125 may be due to an effect on another kinase signaling pathway.

5.2. Mitophagy after photodamage

5.2.1. 488-nm light induces damage in mitochondria leading to mitophagy

Autophagic processes have long been proposed to remove damaged and dysfunctional mitochondria. Damaged mitochondria generate reactive oxygen species (ROS) and release pro-apoptotic factors such as cytochrome *c* to the cytosol. Moreover, accumulation of damaged mitochondria leads to a decrease in the efficiency of ATP generation, and uncoupled mitochondria can futilely hydrolyze ATP. Direct experimental confirmation of a role of autophagy in removing damaged mitochondria came in experiments in which selected mitochondria inside living hepatocytes were subjected to laser-induced photodamage (Kim et al., 2006). When portions of GFP-LC3-expressing hepatocyes cells containing 5 to 10 mitochondria were exposed to a pulse of 488-nm light from an argon laser, mitochondrial depolarization occurred in a light dose-dependent fashion, as documented by release of TMRM (Figure 4.1). At lower doses of light, mitochondria depolarized transiently, but subsequently recovered TMRM fluorescence within a few minutes. After greater exposure, mitochondrial depolarization became irreversible. After irreversible, but not reversible photodamage, green GFP-LC3 fluorescence began to envelop and completely encircle depolarized mitochondria after about 30 min (Figure 4.1 and Figure 4.2). This photodamage-induced mitophagy was not dependent on TMRM as a photosensitizer, since photodamage also induced mitophagy in the absence of TMRM (Figure 4.3). After formation of these autophagosomes, or more specifically mitophagosomes, acidification occurred, as shown by uptake of LTR (Figure 4.6).

5.2.2. MPT and photodamage-induced mitophagy

Photoirradiation with 488-nm light leads to production of ROS (Aggarwal et al., 1978). ROS, in turn, induces the MPT in mitochondria which leads to depolarization of mitochondria and more ROS formation (Nieminen et al., 1997). When mitochondria were photodamaged with 488-nm light for longer than 320 μs at 100% transmission, only the mitochondria exposed to light depolarized permanently, whereas, photoirradiation for 1280 μs per pixel led to depolarization of the mitochondria around photodamaged mitochondria. However, ROS production may not be sufficient for mitophagy induction. Mitochondria that depolarized transiently after light exposure did not undergo subsequent mitophagy, whereas photodamaged mitochondria that underwent sustained depolarization were reproducibly sequestered into autophagosomes (Figure 4.1 and Figure 4.2). These latter groups of mitochondria became permeable to calcein which is consistant with the inner membrane permeabilization of the MPT (Figure 4.5). Thus, sustained mitochondrial depolarization and associated inner membrane permeabilization are likely required for mitophagy supporting the involvement of the MPT in damage-induced mitophagy.

5.2.3. PI3K and photodamage-induced mitophagy

Unlike autophagy induced by nutrient deprivation, photodamage-induced mitophagy was not blocked by PI3K inhibition with 3-methyladenine or wortmannin (Figure 4.7). Rather, PI3K inhibition appeared to augment accumulation of GFP-LC3-labeled autophagosomes containing photodamaged mitochondria. These findings suggested that light activates mitophagy downstream of PI3K signaling. However, photodamage-induced mitophagy appeared to bypass the classical upstream PI3K signaling pathways involved in nutrient deprivation-induced autophagy.

5.3. Final remarks

In normal physiology, cells utilize autophagy to rid themselves of damaged, dysfunctional and superfluous cytoplasmic components to maintain cellular homeostasis and adjust to changing physiological demands. In this respect, mitochondrial degradation by mitophagy may play an essential role in maintaining mitochondrial functional and genetic integrity. However, there is a need for a better understanding of the regulatory pathways that control mitophagy and the specific signals and markers that target individual mitochondria for autophagic degradation. Such information will likely lead to new insights into the aging phenomena and the pathogenesis of different diseases.

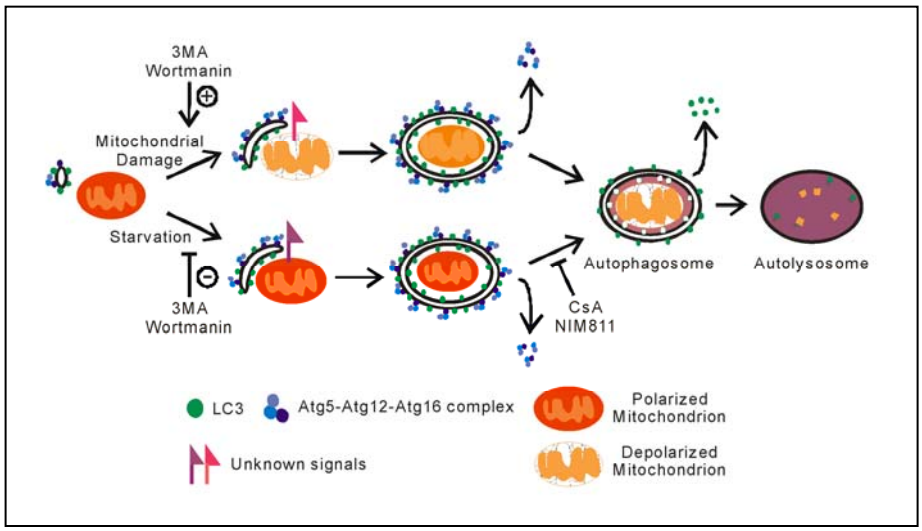

Figure 1.1. **Scheme of Mitophagy.** Atg12-Atg5-Atg16 and LC3 complexes localize to isolation membranes. In nutrient deprivation (starvation), isolation membranes target individual mitochondria by unknown signals in a process inhibited by the PI3K inhibitors, 3-methyladenine (3MA) and wortmannin. Isolation membranes completely envelop individual mitochondria to form double membrane vesicles (autophagosomes). After this sequestration, mitochondria depolarize in a CsA and NIM811 sensitive fashion, and Atg12-Atg5/Atg16 complexes are released from the autophagosomal surface. Autophagosomes then acidify and fuse with lysosomal vesicles to form autolysosomes. Lysosomal hydrolases digest the inner autophagosomal membrane and degrade LC3 trapped inside autophagosomes. Remaining LC3 on the surface of autophagosomes is released. After mitochondrial damage, mitochondria first depolarize and then are recognized and sequestered by isolation membranes recognizing unknown markers on the damaged mitochondria. 3MA and wortmannin do not inhibit this process but actually seem to augment it. In both pathways, sequestered mitochondria are completely digested and their molecular components recycled to the cytoplasm.

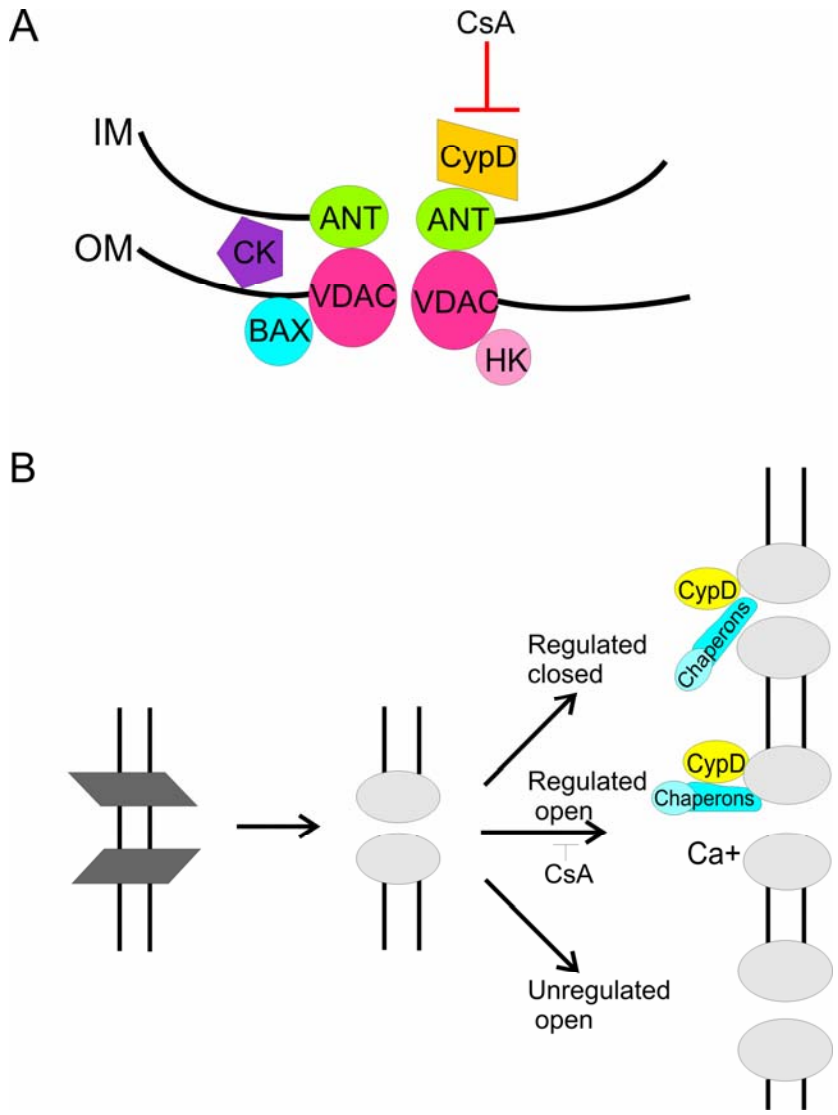

Figure 1.2. **Models of the permeability transition pore**. In **A**, the PT pore is composed of ANT from the inner membrane (IM) and VDAC from the outer membrane (OM) and other proteins, including CypD, hexokinase (HK), creatine kinase (CK) and Bax, a proapoptotic Bcl-2 family proteins. In **B** of an alternative model, misfolded mitochondrial membrane proteins organize forming the PT pores by exposing their hydrophilic surfaces facing the hydrophobic membrane bilayer. CypD and other chaperones bind to PT pores and block channel opening. However, high Ca^{2+} concentration leads opening of these regulated channels through CypD that can be blocked by CsA. When misfolded proteins exceed the number of chaperones, the channels can not on longer be regulated, therefore, become constitvtively opened where CsA has inhibitory effect.

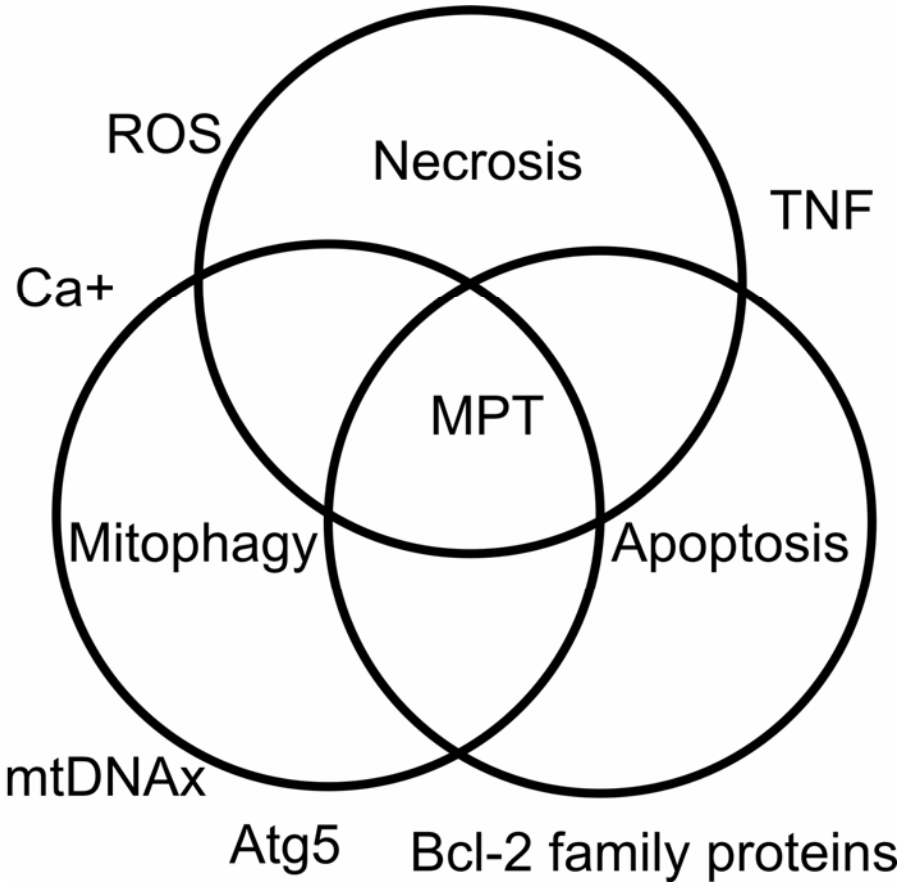

Figure 1.3. **Mitophagy, apoptosis and necrosis.** Ros, Ca^{2+}, TNF, Atg5, Bcl-2 fmaily proteins and mutations of mtDNA ($mtDNA_X$) leads to mitophagy, apoptosis, and necrosis. MPT may serve as central role in cellular responses progress from mitophagy, apoptosis and to necrosis due to ATP depletion which inhibit mitophagy and apoptosis.

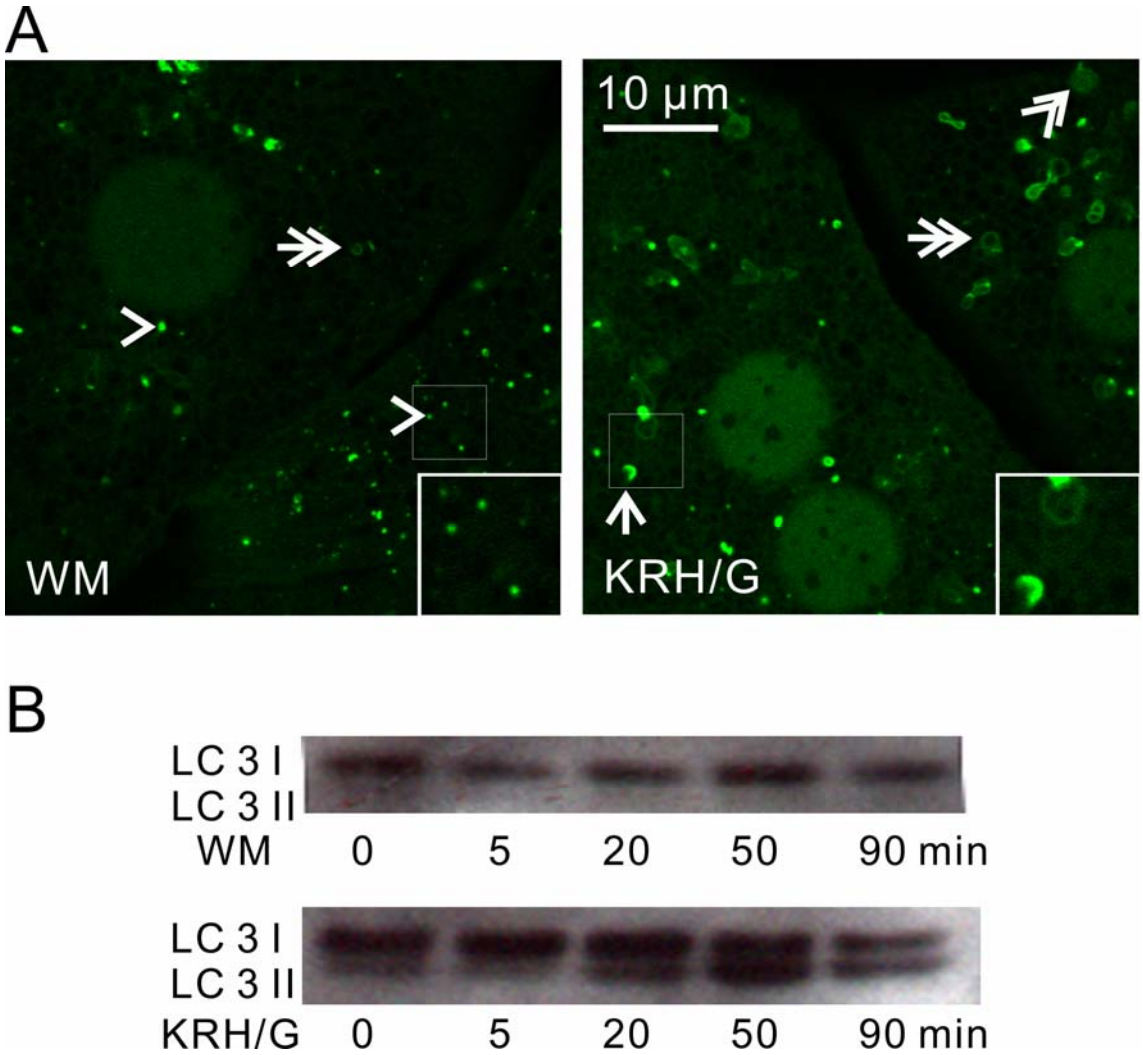

Figure 2.1. **Induction of autophagosomes during nutrient deprivation plus glucagon in GFP-LC3 hepatocytes.** In A, hepatocytes from GFP-LC3 mice were incubated either in Waymouth's growth medium/HEPES (WM) or nutrient-free Krebs-Ringer/HEPES buffer plus 1 µM glucagon (KRH/G). Images were taken after 90 min by confocal microscopy. Note that the number of green rings and disks (autophagosomes) increased in KRH/G compare to WM. In left panel (WM), arrows and double arrow identify PAS patches and a phagophore, respectively. In the left panel, arrow and double arrow identify a phagophore and autophagosomes, respectively. Insert is the magnified images of autophagic structures. In B, hepatocytes from wild type mice were incubated in WM or KRH/G for 0 to 90 min at which time LC3 I and LC3 II protein expression was assessed in cell extracts by Western blotting, as described in Materials and Methods.

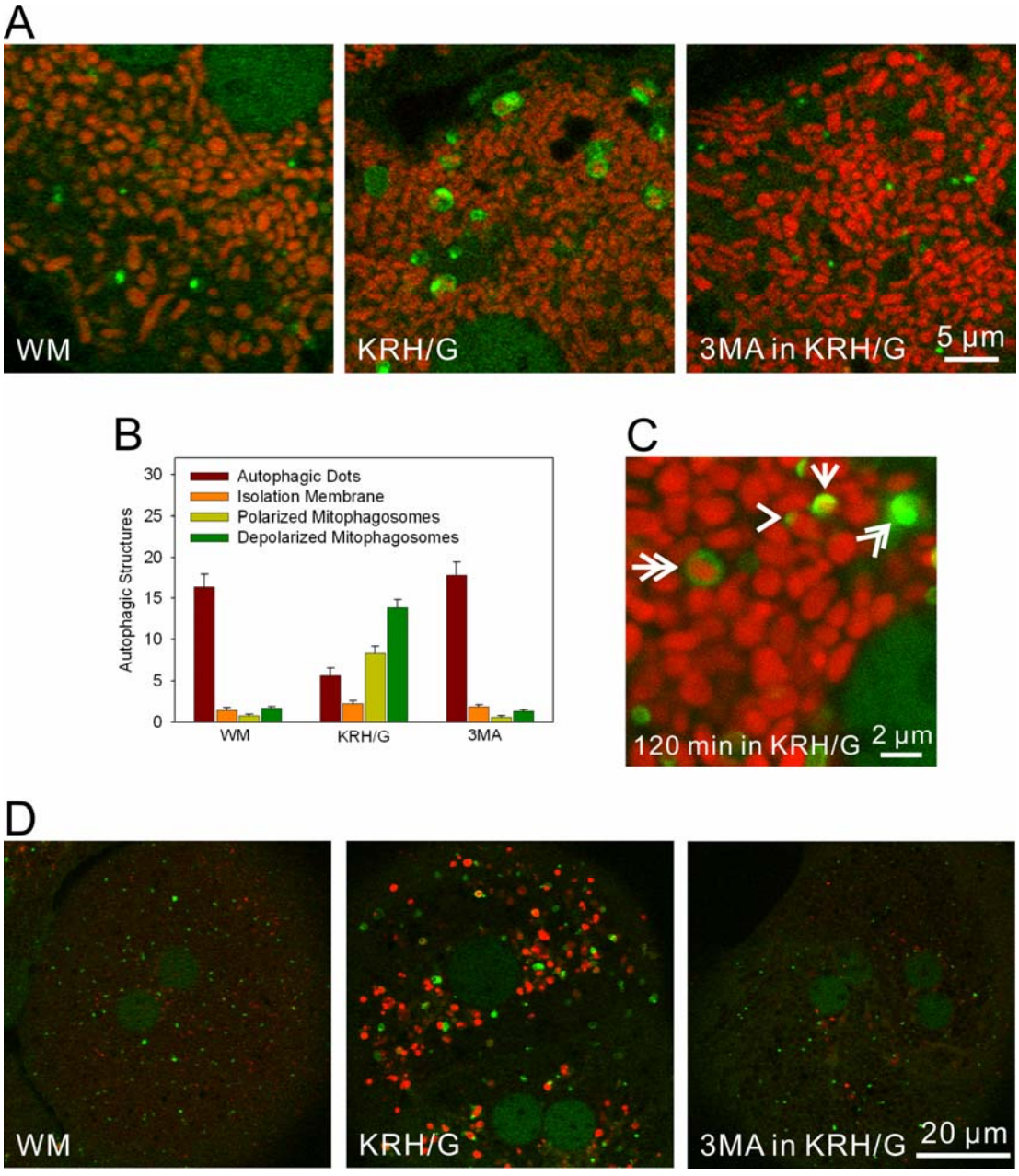
A
WM
KRH/G
3MA in KRH/G
5 μm
B
Autophagic Dots
Isolation Membrane
Polarized Mitophagosomes
Depolarized Mitophagosomes
Autophagic Structures
30
25
20
15
10
5
0
WM
KRH/G
3MA
C
120 min in KRH/G
2 μm
D
WM
KRH/G
3MA in KRH/G
20 μm

Figure 2.2. **Confocal microscopy of mitophagy during nutrient deprivation plus glucagon in GFP-LC3 hepatocytes**. GFP-LC3 hepatocytes were loaded with TMRM (A, B, and C) or LTR(D) for 30 min in complete growth medium (WM), as described in Materials and Methods. In A, TMRM-loaded GFP-LC3 hepatocytes were incubated 90 min in WM (left), KRH/G (middle) or KRH/G plus10 mM 3MA (right), and confocal images were collected. in KRH/G was taken after 90 min. Panel B illustrates the numbers of GFP-LC3 patches (PAS), phagophores, polarized mitophagosomes (GFP-LC3 rings or disks containing TMRM fluorescence) and depolarized autophagosomes (GFP-LC3 rings or disks not containing TMRM) as quantified from confocal images of GFP-LC3 hepatocytes incubated as described in A (xx-yy images from 3 different Hepatocyte isolations for each treatment group). Panel C shows typical structure of GFP-LC3 patches (arrowhead), phagophores (arrow), polarized mitophagosomes (double arrow) and depolarized autophagosomes (double arrowhead). Panel D shows proliferation of acidic LTR-labeled autophagosomes (LTR vesicles labeled with GFP-LC3) and autolysosomes (LTR vesicles without GFP-LC3) after 90 min incubation in KRH/G compared to WM. 3MA prevented autophagosomal and autolysosomal proliferation.

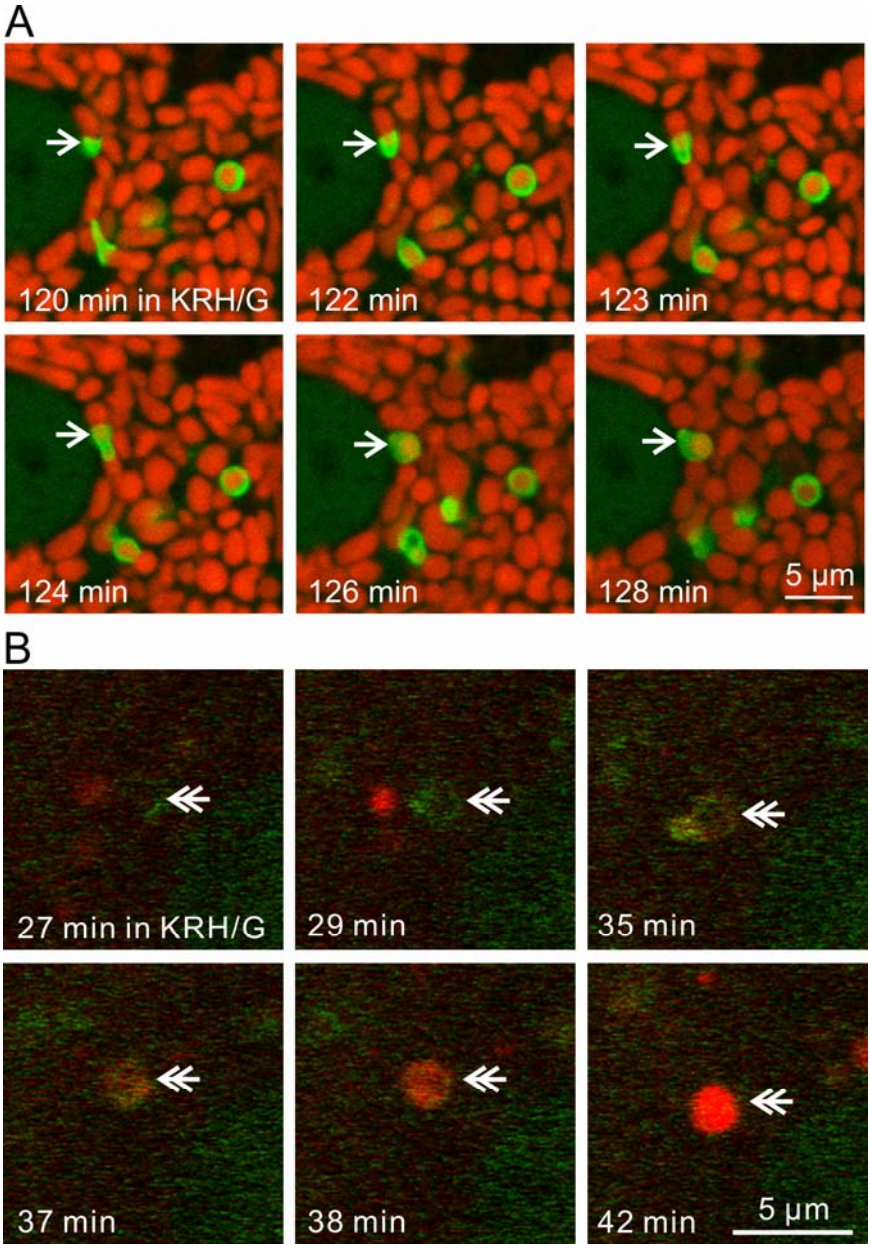

Figure 2.3. **Autophagic sequestration of mitochondria and acidification of autophagosomes.** In **A**, GFP-LC3 (green) hepatocytes were loaded with TMRM (red) for 30 min and incubated in KRH/G. Confocal image were taken every minute for 120 min. Arrow and double arrow illustrate the progression of formation of mitophagosomes (mitochondria-containing autophagosomes). In favorable sections along the axis of phagophores, note progression of mitophagy of TMRM-labeled polarized mitochondria from GFP-LC3 PAS patch to cup-shaped phagophore to fully sequestered autophagosomes (mitophagosomes). In **B**, GFP-LC3 hepatocytes were incubated in KRH/G containing LTR and confocal images were collected every mi. Note formation of an autophagosome (GFP-LC3 ring, arrow) after 29 min followed by LTR uptake (acidification) that became maximal after 42 min.

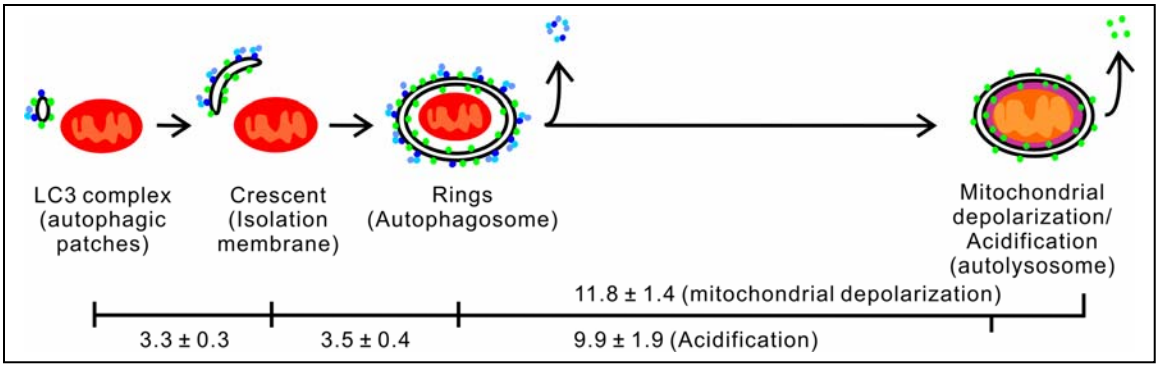

Figure 2.4. **Scheme of mitophasosome formation process.**
In nutrient deprivation (starvation), LC3 complex of other Atg proteins appears in close association with a mitochondrion forming isolation membrane in 3.3 min. The isolation membrane completely sequestrated the mitochondrion forming a ring in 6.8 min from the first appearance of dots. After ring closure, as mitochondria inside autophagosomes depolarize in 11.8 min, acidification occurs in 9.9 min. Typically, fusion with lysosomal precursors occurs at about this time, leading to formation of autolysosomes where mitochondrial contents are degraded.

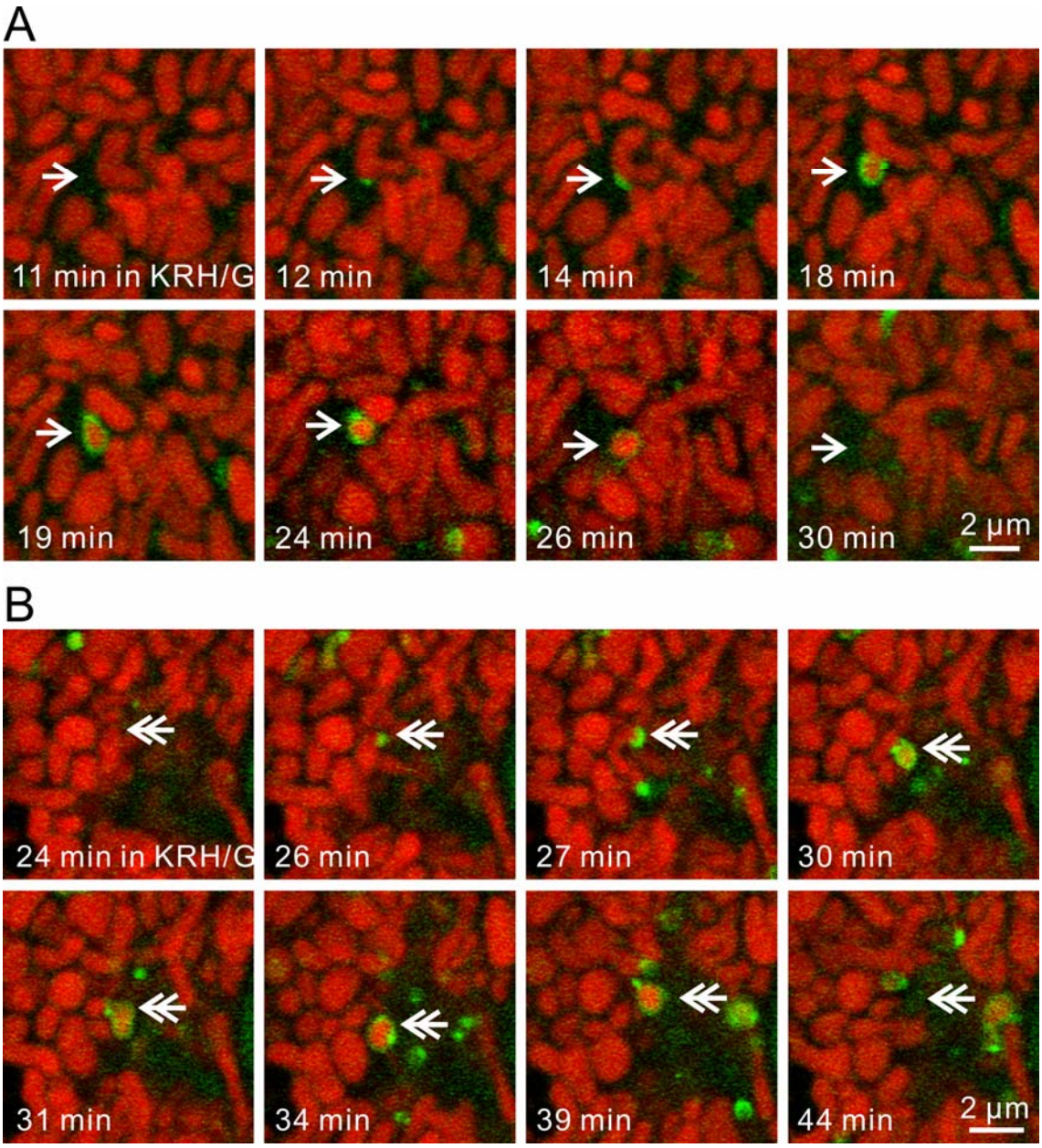

Figure 2.5. **Mitochondria fission during nutrient deprivation induced mitophagy.** GFP-LC3 hepatocytes were loaded with TMRM in WM and incubated in KRH/G as confocal images were collected every minute. In **A**, note fission of mitochondrion near its end as mitophagy proceeds (arrow). In **B**, fission near the middle of the mitochondrion occurred.

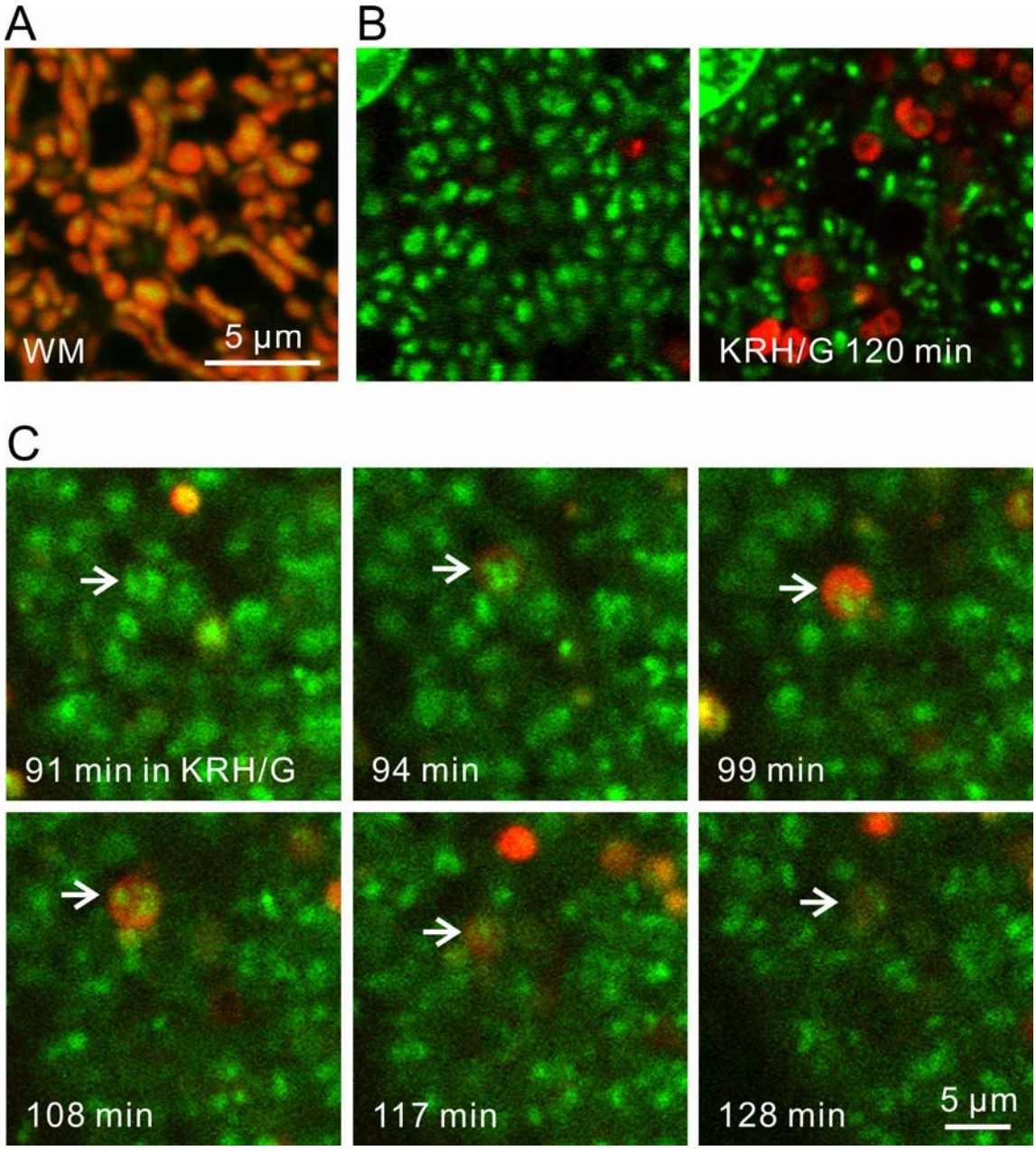

Figure 2.6. **Mitochondrial DNA (mtDNA) degradation by mitophagy.** Panel **A** shows a confocal image of a portion of a wildtype Hepatocyte co-loaded with PicoGreen (green) and TMRM (red) and incubated in WM. Yellow in the overlap represents PicoGreen-labeled mtDNA. In panel **B**, a PicoGreen and LTR co-labeled Hepatocyte was incubated in KRH/G for 120 min. In panel **C**, a PicoGreen and LTR co-labeled hepatocytes was incubated in KRH/G. Note sequestration of PicoGreen-labeled mtDNA into an LTR-labeled autolysosome and subsequent degradation of mtDNA.

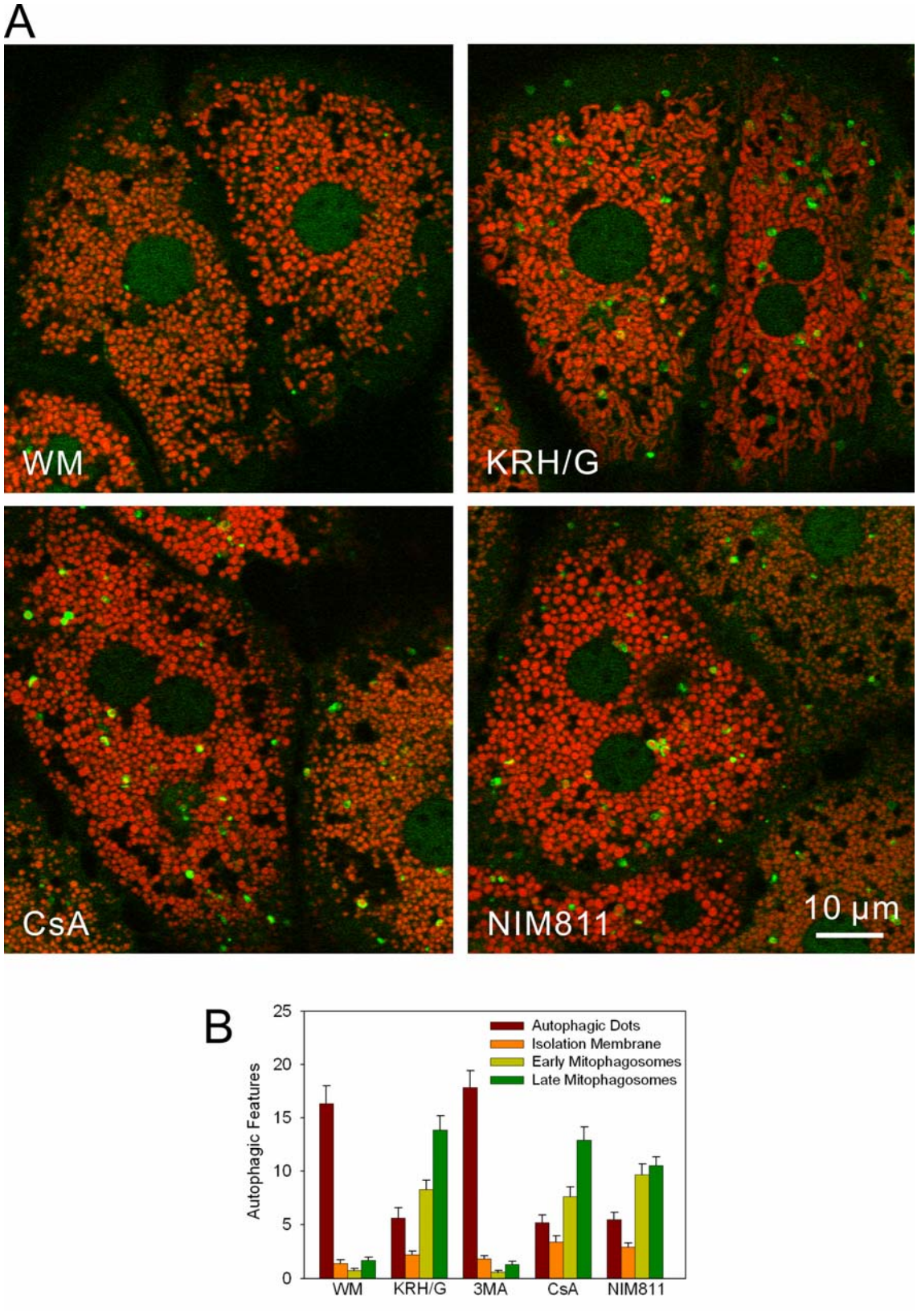
A
WM
KRH/G
CsA
NIM811
10 μm
B
Autophagic Features
25
20
15
10
5
0
Autophagic Dots
Isolation Membrane
Early Mitophagosomes
Late Mitophagosomes
WM
KRH/G
3MA
CsA
NIM811

Figure 2.7. **Lack of CsA and NIM811 on autophagic sequestration of mitochondria after nutrient deprivation.** In **A**, GFP-LC3 hepatocytes were loaded with TMRM and incubated for 90 min in WM (upper left), KRH/G (upper right) or KRH/G with 5 μM CsA (lower left) or 5 μM NIM811 (lower right). Note proliferation of GFP-LC3-decorated phagophores and autophagosomes in KRH/G that was not blocked by CsA or NIM811. Panel B plots the distribution of GFP-LC3 patches, phagophores, polarized mitophagosomes and depolarized autophagosomes for the 4 conditions of panel **A** from xx-yy images per groups of hepatocytes from three different isolations.

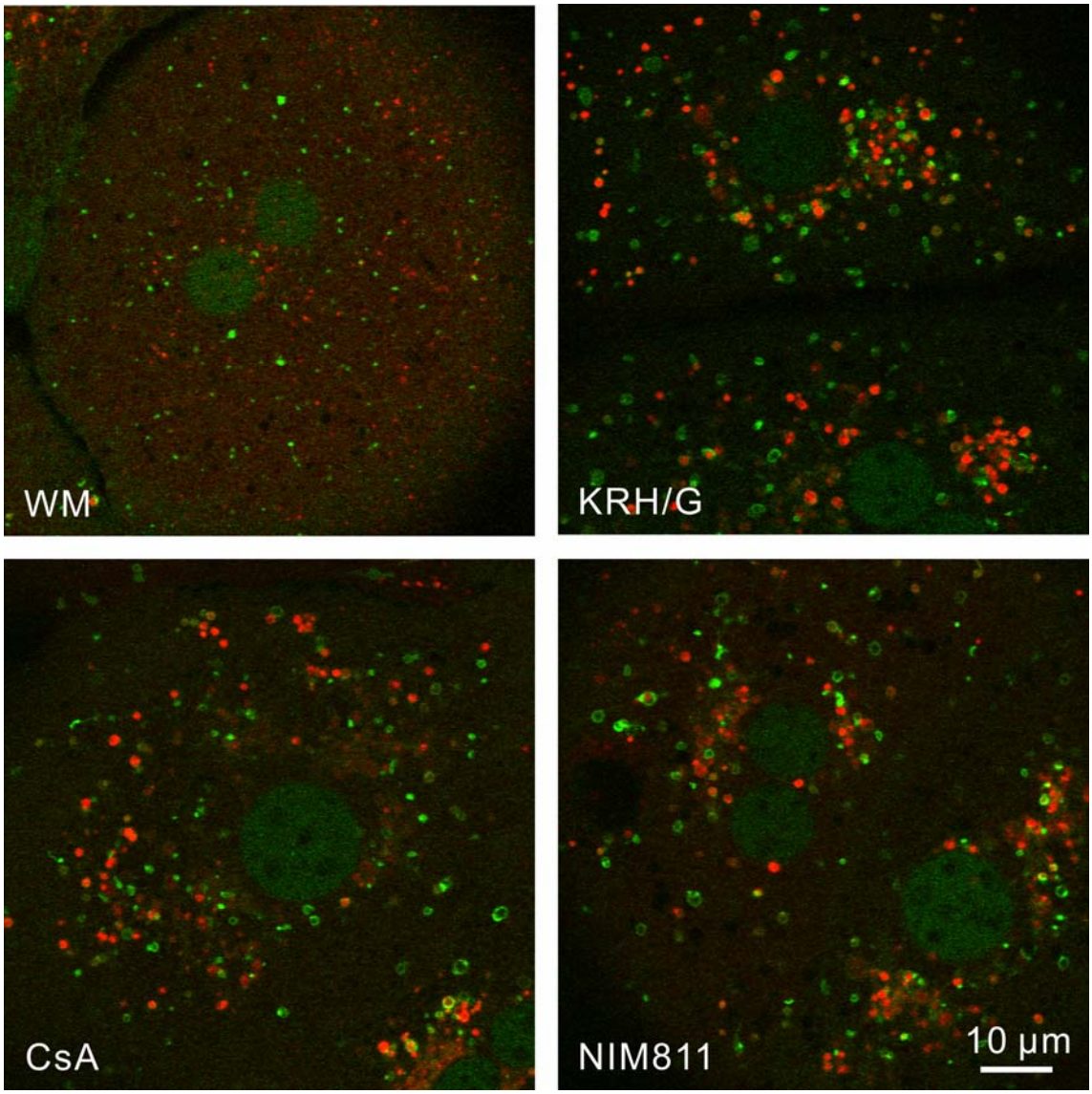

Figure 2.8. Lack of effect of **CsA and NIM autophagosomal proliferation after nutrient deprivation in GFP-LC3 hepatocytes.** GFP-LC3 hepatocytes were loaded with LTR and incubated for 90 min in WM (upper left), KRH/G (upper right) or KRH/G containing 5 µM CsA (lower left) or 5 µM NIM811 (lower right). Note proliferation of LTR-labeled acidic vesicles in KRH/G that was not blocked by CsA or NIM811.

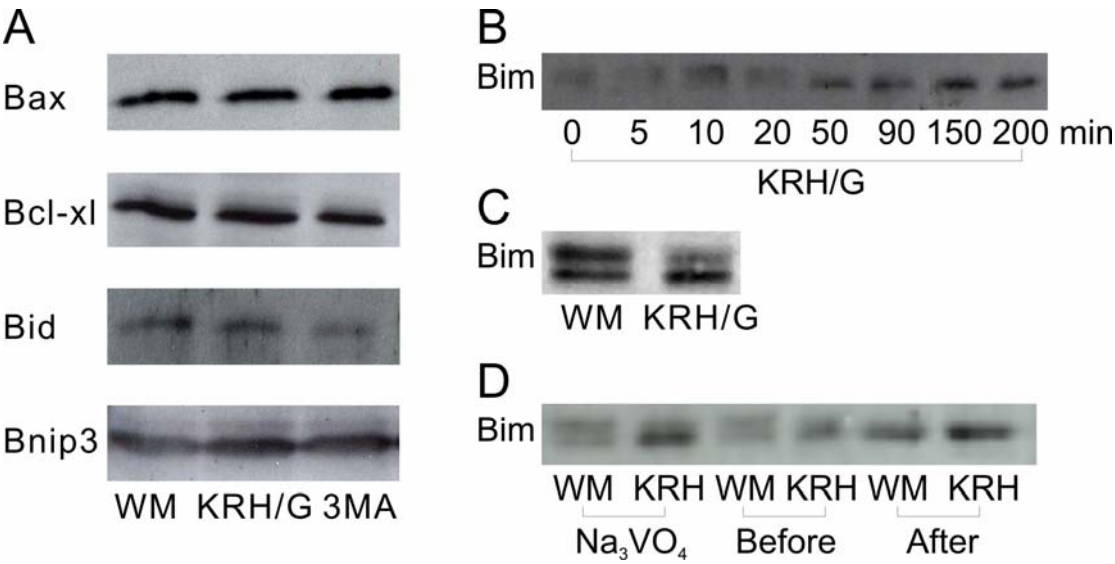

Figure 2.9. **Bim dephosphorylation during nutrient deprivation-induced autophagy.** In **A**, the lysates were obtained from rat hepatocytes incubated for 90 min in WM, KRH/G or KRH/G plus 10 mM 3MA and subjected to immunoblotting with antibodies against Bax, Bcl-xl, Bid, and Bnip3. In **B**, lysates of hepatocytes incubated in KRH/G for 0 to 200 min in KRH/G were immunoblotted with anti-Bim antibody. Note in A and B, 4-15% polyacrylamide gels were used. In **C**, lysates of hepatocytes incubated for 90 min in WM or KRH/G, were run on 20% polyacrylamide gels and immunoblotted with anti-Bim antibody. In **D**, cell lysates prepared for immunoblotting for Bim as above were harvested with and without sodium orthovanadate (Na_3VO_4), a phosphatase inhibitor. A portion of cell lysate not treated with sodium orthovanadate was exposed to lamda phosphatase and subjected to Western using 20% polyacrylamide gels.

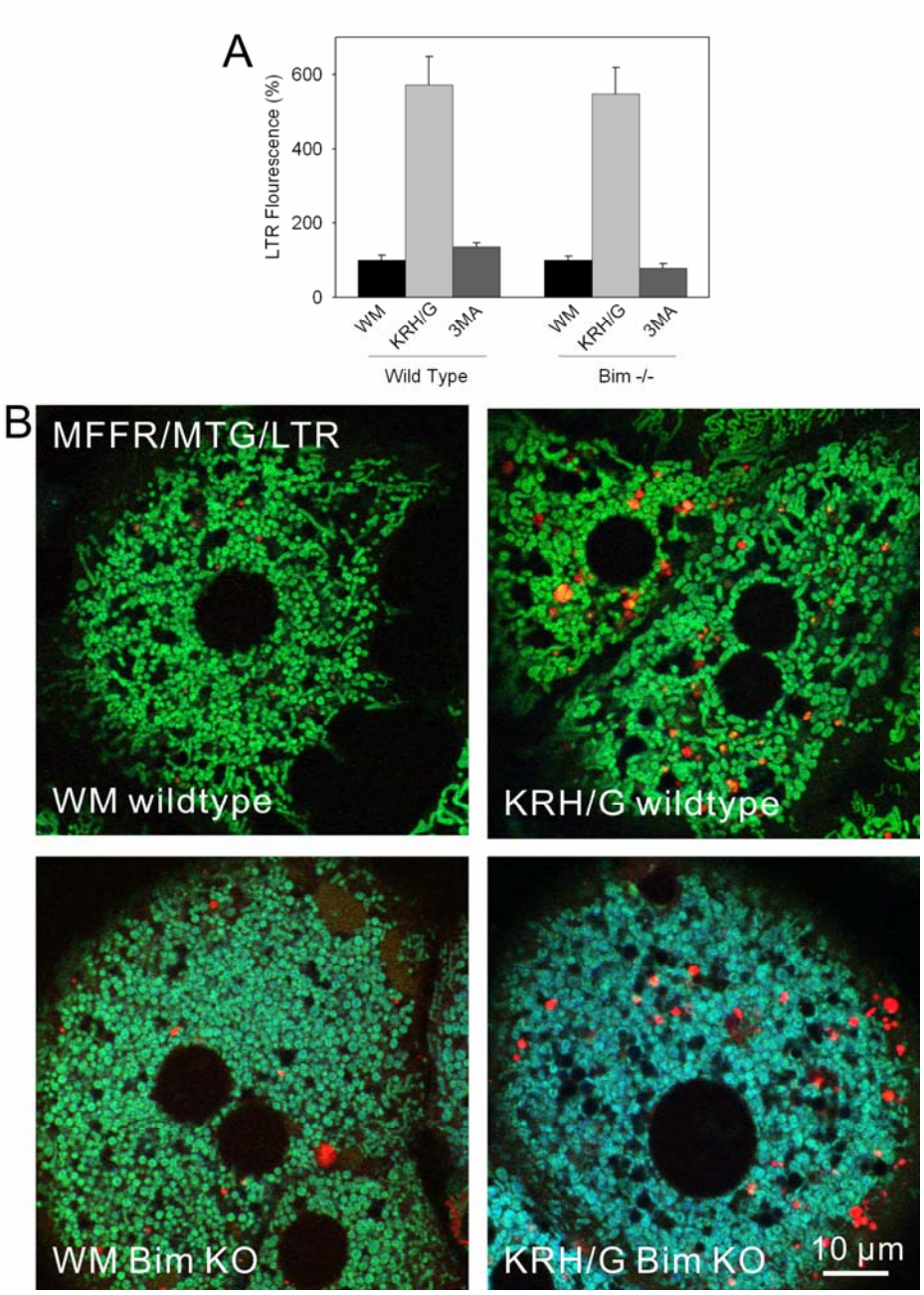

Figure 2.10. **Nutrient deprivation-induced autophagy in Bim deficient hepatocytes.** In **A**, hepatocytes isolated from wildtype and Bim knockout (Bim -/-) mice were incubated in WM, KRH/G and KRH/G plus 10 mM 3MA, and LTR uptake was after 90 min was measured by LTR multiwell assay. In **B**, wildtype and Bim -/- hepatocytes were co-loaded with LTR (red), MFFR (blue), and MTG (green) and incubated in WM or KRH/G for 90 min. Note similar proliferation of LTR-labeled autolysosomes in KRH/G in both wildtype and Bim -/- hepatocytes.

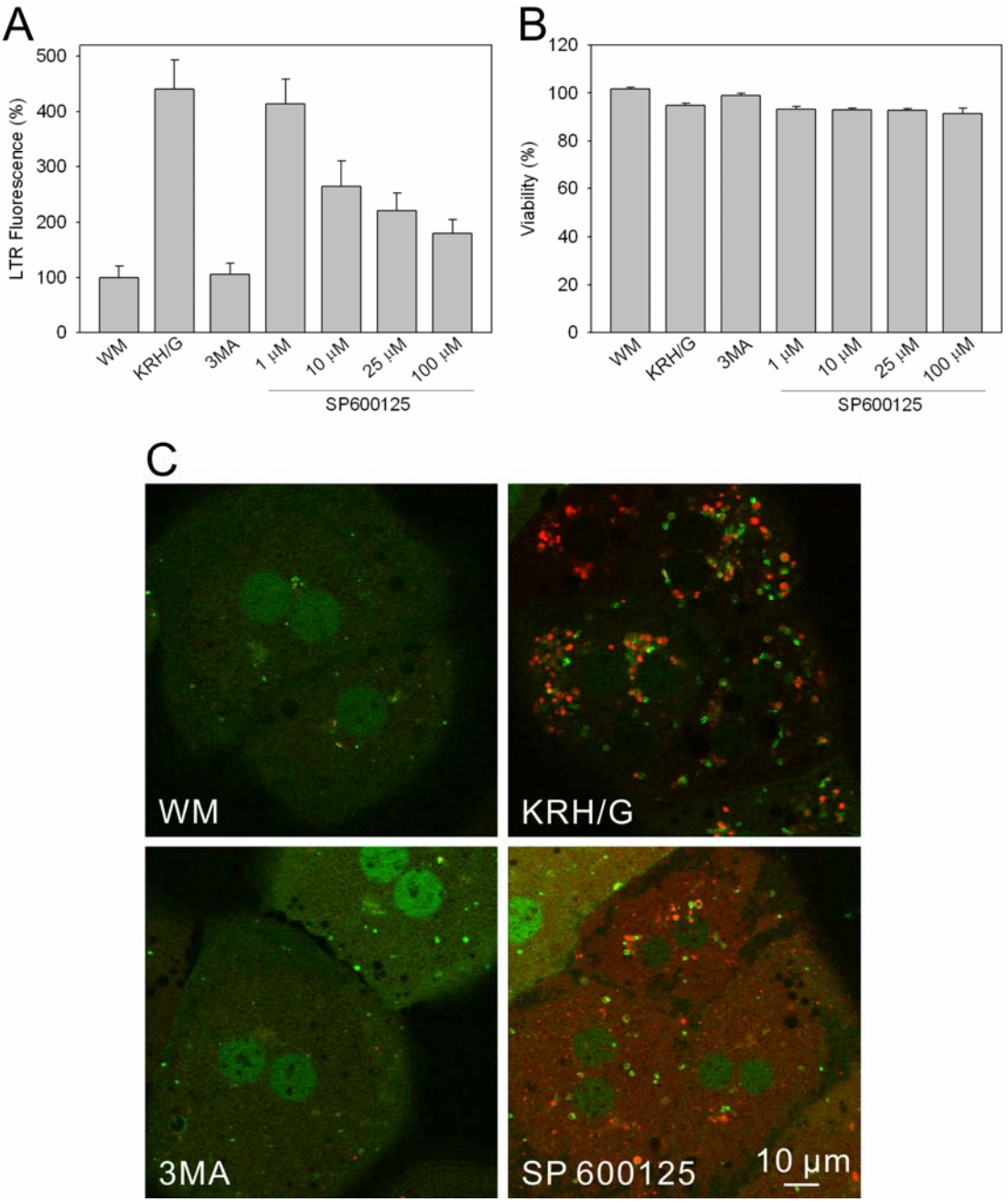

Figure 3.1. **Inhibition by SP600125 of nutrient deprivation-induced autophagy.** In A, primary hepatocytes were treated 90 min with 10 mM 3MA, 1, 10, 25, and 100 μM SP600125 or no addition in KRH/G in comparison to incubation in WM. The LTR fluorescence was measured using a multiwell plate reader. In B, the cell viability of 10 mM 3MA, 1, 10, 25, and 100 μM SP600125 in KRH/G was measured after 90 min incubation using PI fluorometry. In C, LTR (red) -loaded GFP-LC3 (green) hepatocytes were incubated 90 min in KRH/G with and without 25 μM SP600125. The green rings and solid red disc indicate autophagosomes and autolysosomes.

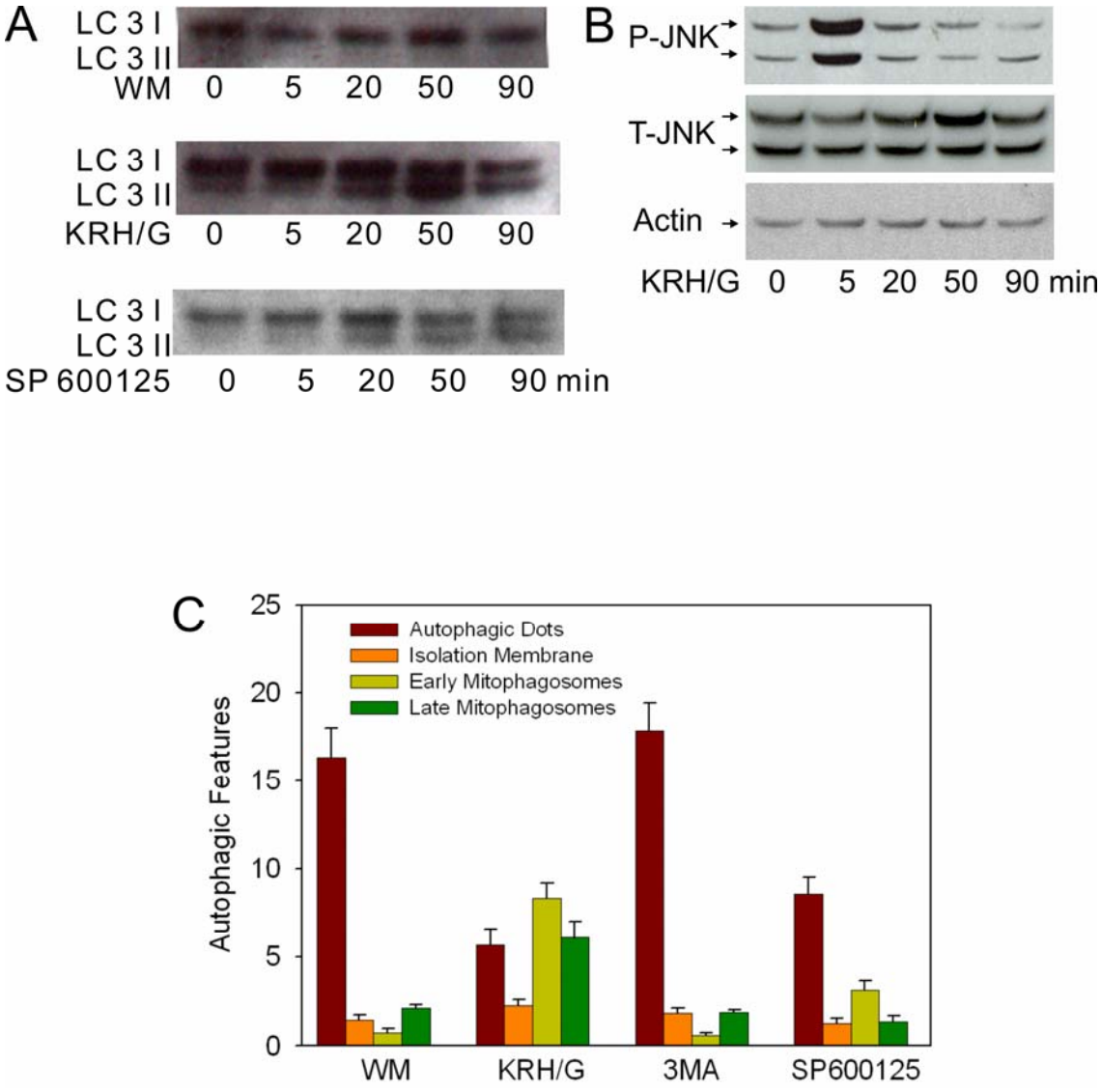

Figure 3.2. **JNK inhibits LC3-II and mitophagy after nutrient deprivation.**
The lysates of hepatocytes incubated in KRH/G for 0, 5, 20, 50, and 90 min were measured using (A) anti-LC3 antibody and (B) anti-phospho-JNK, anti-total JNK, and anti-actin. In A, the top bands indicates LC3 I, whereas the bottom bands indicates PE conjugated LC3, LC3 II. In B, both top and bottom bands indicates JNK1 and JNK2. Actin was used as loading control. In C, TMRM-loaded GFP-LC3 hepatocytes were for 90 min in WM or KRH/G alone or with 3MA. Autophagy-related structures - small GFP-LC3 dots (PAS-like structures), GFP-LC3 cup-shaped structures (phagophore), GFP-LC3 rings (late autophagosomes), and GFP-LC3 rings containing TMRM (early mitophagosomes).

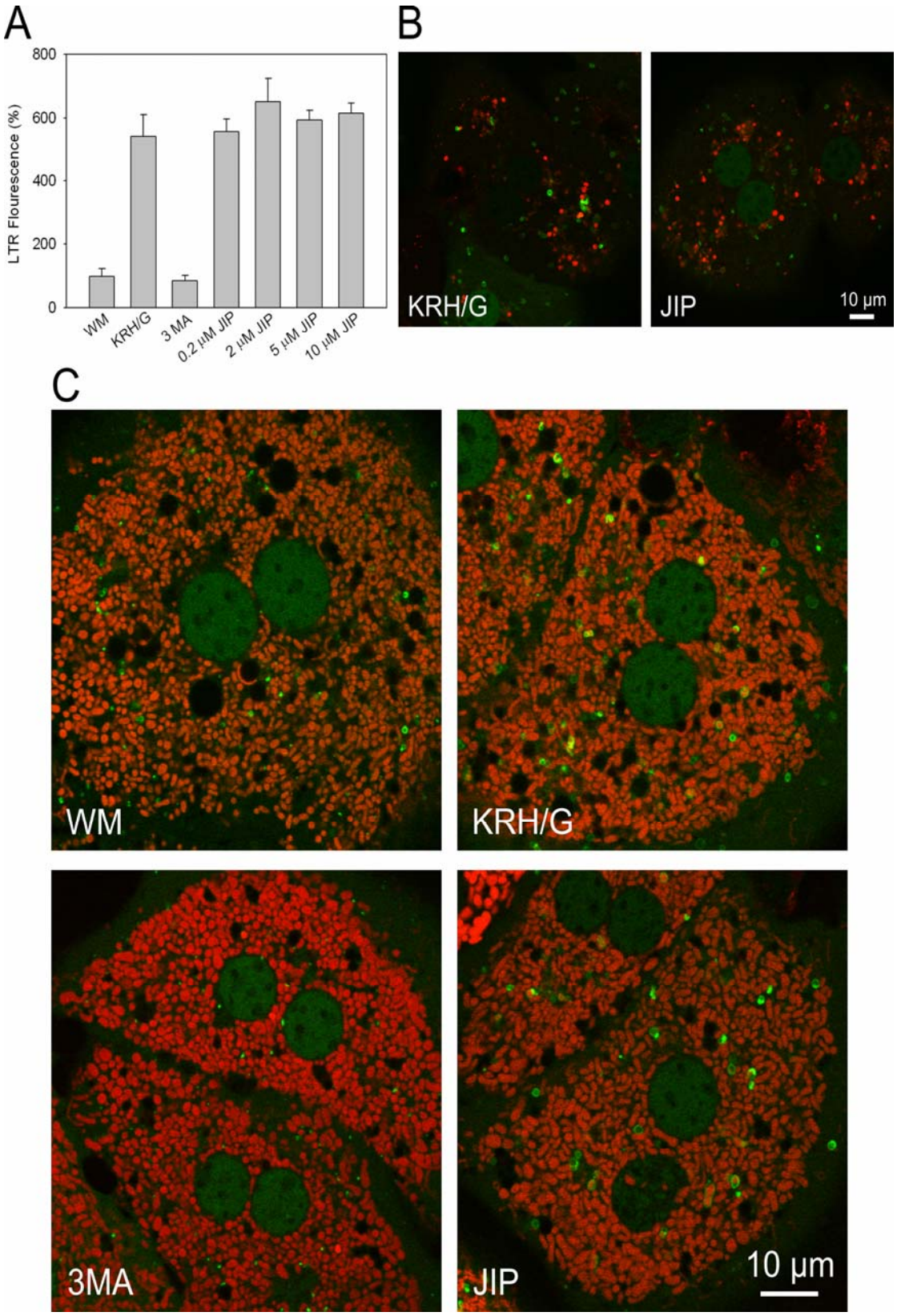
A
LTR Flourescence (%)
800
600
400
200
0
WM
KRH/G
3 MA
0.2 μM JIP
2 μM JIP
5 μM JIP
10 μM JIP
B
KRH/G
JIP
10 μm
C
WM
KRH/G
3MA
JIP
10 μm

Figure 3.3. **JIP does not block nutrient deprivation-induced autophagy and mitophagy.** In A, hepatocytes were incubated in KRH/G alone or in KRH/G with 10 mM 3MA, 0.2, 2, 5, 10 μM JIP for 70 min and loaded with 50 nM LTR for 20 min The LTR uptake was measured in comparison to incubation in WM using a multiwell plate reader. In B, LTR-labeled GFP-LC3 hepatocytes were incubated in KRH/G with and without 2 μM JIP for 90 min. Green rings and solid red vesicle indicates autophagosomes and autolysosomes. In C, TMRM-loaded hepatocytes were treated with or without 3MA and JIP after 90 min in KRH/G. Again, GFP-LC3 rings containing TMRM and GFP-LC3 rings indicates polarized mitophagosomes or depolarized mitophagosomes.

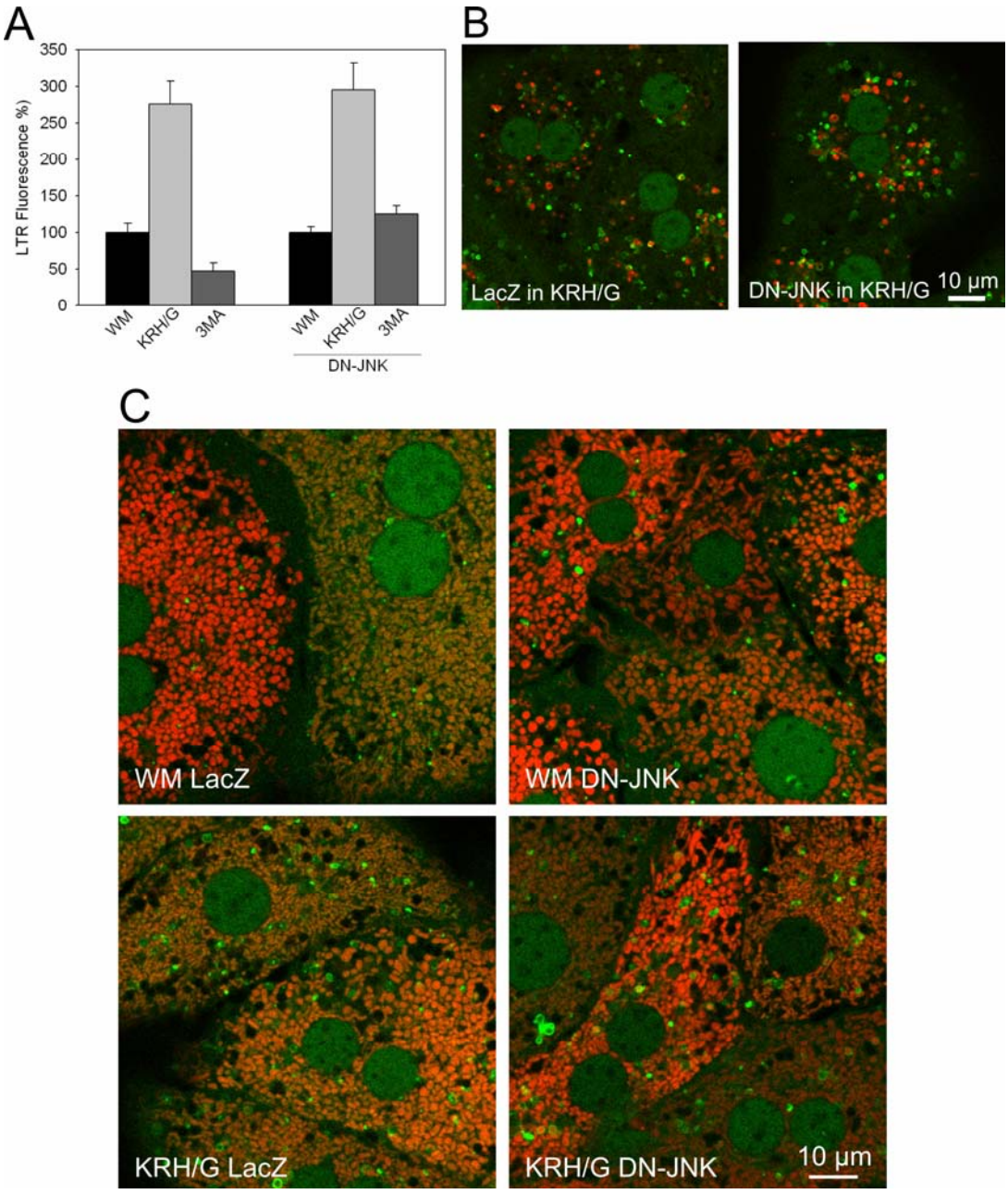

Figure 3.4. **DN-JNK does not affect nutrient deprivation-induced autophagy and mitophagy.** In A, hepatocytes infected with AdLacZ or AdDN-JNK were incubated in WM or KRH/G with or without 10 mM 3MA for 70 min and loaded with 50 nM LTR for 20 min. The LTR uptake was measured using a multiwell plate reader. In B, AdLacZ and AdDN-JNK infected GFP-LC3 hepatocytes were loaded with LTR and incubated in WM or KRH/G for 90 min. DN-JNK do not suppressed formation of autophagosomes (green rings) and autolysosomes (red vesicles). In C, AdLacZ and AdDN-JNK expression GFP-LC3 hepatocytes were loaded with TMRM and incubated in WM or KRH with or without 3MA for 90 min.

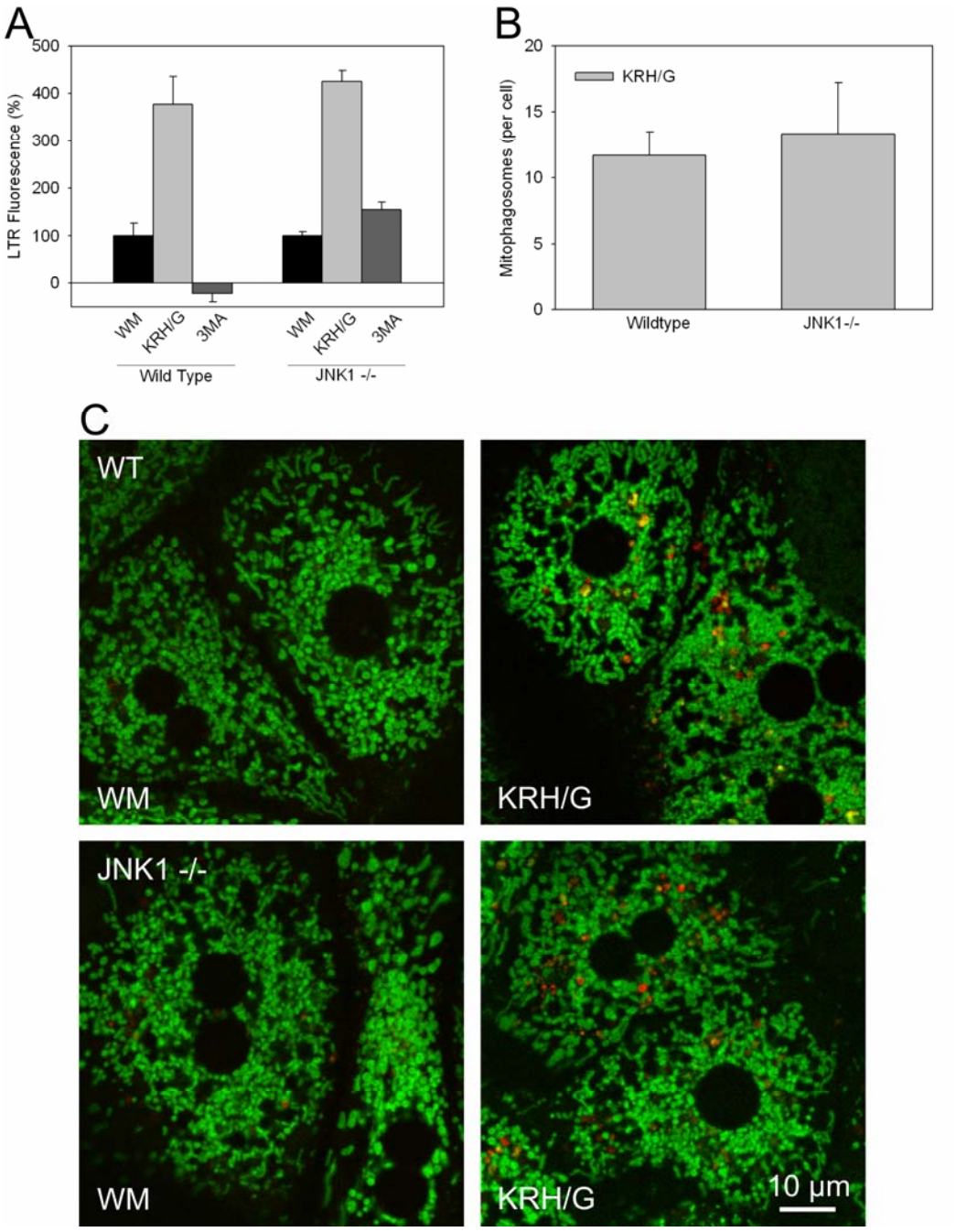

Figure 3.5. **JNK1 does not play a role in nutrient deprivation-induced autophagy and mitophagy.** In A, hepatocytes isolated from wildtype and JNK1 knockout (JNK1-/-) mice were incubated in WM or KRH/G with or without 10 mM 3MA for 70 min and loaded with 50 nM LTR for 20 min. The LTR uptake was measured using a multiwell plate reader. In B and C, wildtype and JNK1-/- hepatocytes were loaded with 500 nM LTR (red) or 300 nM MTG (green) and incubated in WM or KRH/G for 90 min. MTG-containing LTR vesicles and solid LTR vesicles indicated mitophagosomes. In B, the number of mitophagosomes of three independent confocal images (C) were counted.

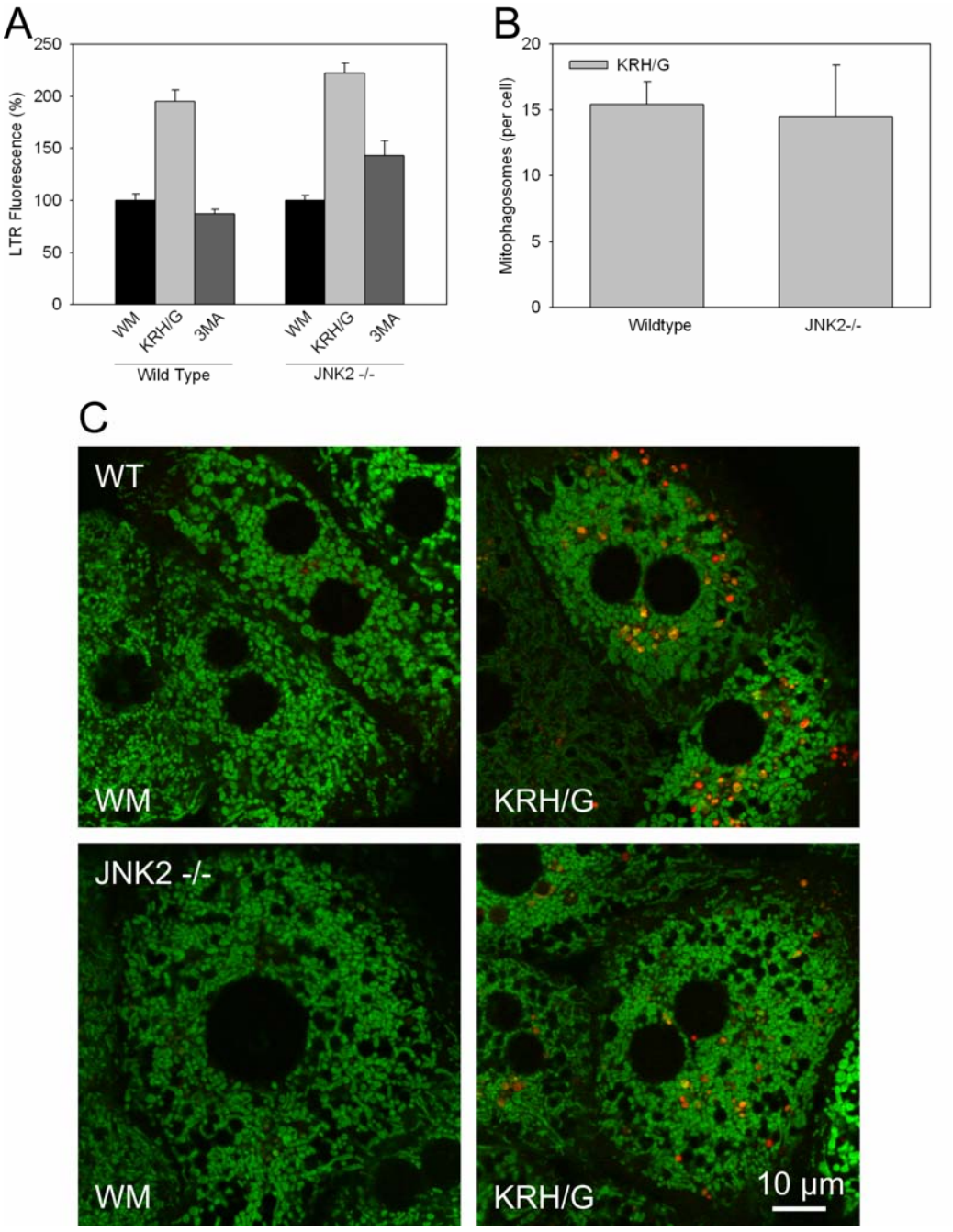

Figure 3.6. **JNK2 does not play a role in nutrient deprivation-induced autophagy and mitophagy.** In A, hepatocytes isolated from wildtype and JNK2 knockout (JNK2-/-) mice were incubated in WM or KRH/G with or without 10 mM 3MA for 70 min and loaded with 50 nM LTR for 20 min. The LTR fluorescence were measured afterward. In B and C, wildtype and JNK1-/- hepatocytes were loaded with LTR (red) or MTG (green) and incubated in WM or KRH/G for 90 min. MTG-containing LTR vesicles and solid LTR vesicles indicated mitophagosomes. In B, the number of mitophagosomes of three independent confocal images of C were counted.

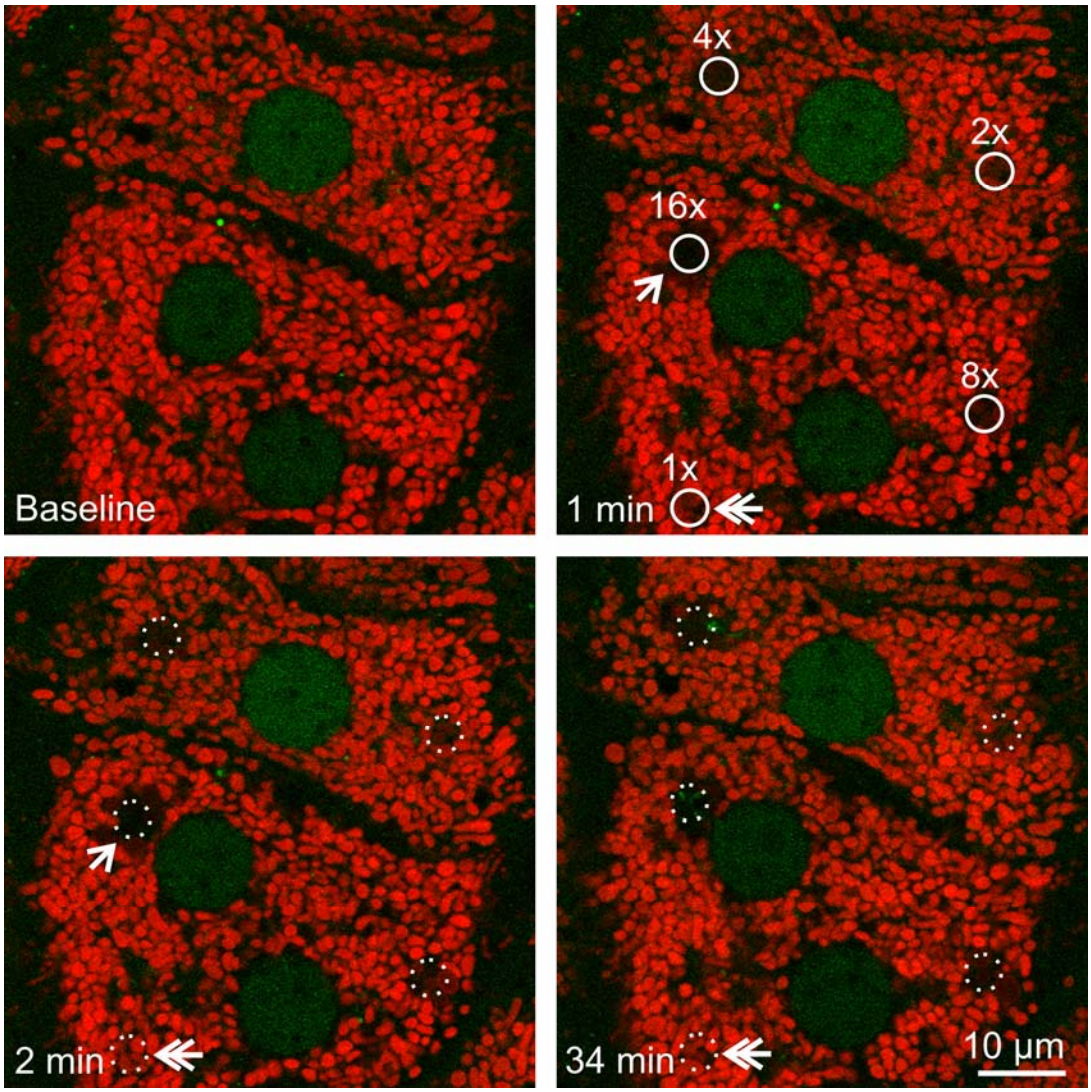

Figure 4.1. 488-nm light induced mitochondrial damage occurs in a dose dependent manner. The hepatocytes isolated from GFP-LC3 transgenic mice were loaded with 200 nM TMRM for 30 min. TMRM (red)-loaded GFP-LC3 hepatocytes of five mitochondria were exposed to different amount of 488 nm light at 100% power - 2.7 $x10^4$, 5.5 $x10^4$, 1.1 $x10^5$, 2.2 $x10^5$, and 4.4 $x10^5$ times per pixel higher than the pixel power used for imaging. These pixel powers were labeled in ascending order as 1x, 2x, 4x, 8x, and 16x. The solid and dotted circles represent photodamaged mitochondria. Images of red TMRM and green GFP-LC3 were collected every minute before (baseline) and after photodamage. The lost TMRM fluorescence indicates the complete depolarization of the mitochondria. The double arrow indicates transient TMRM loss after photodamage. The arrow indicates permanently TMRM loss of the mitochondria adjacent to photodamaged mitochondria.

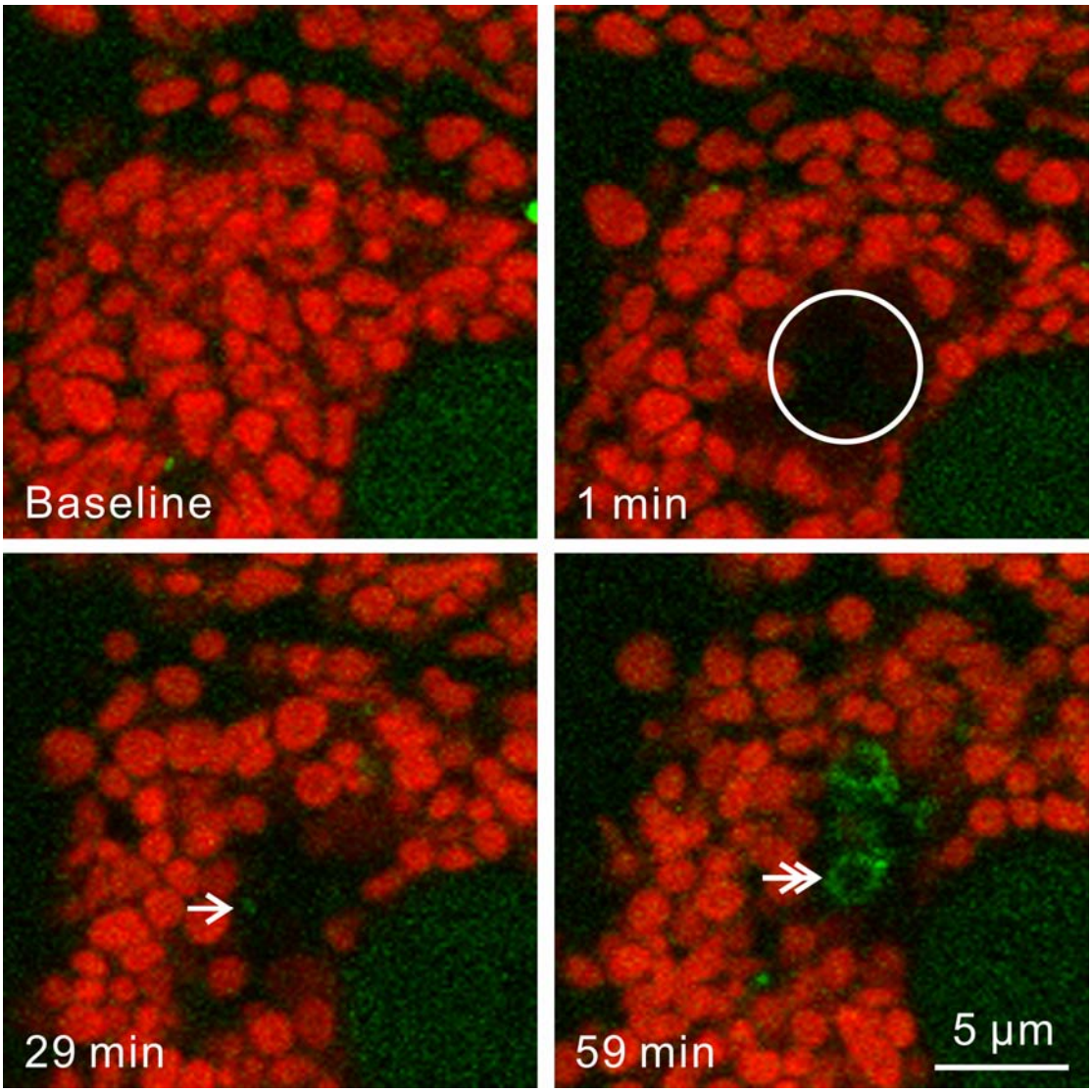

Figure 4.2. Photodamaged mitochondria are degraded by mitophagy. The higher magnification of the photodamaged mitochondria exposed to 16x light before and after 1, 29, and 59 min of Figure 4.1. The circled area indicates photodamaged mitochondria. Arrow indicates localization of GFP-LC3. Double arrow indicates GFP-LC3 ring formation.

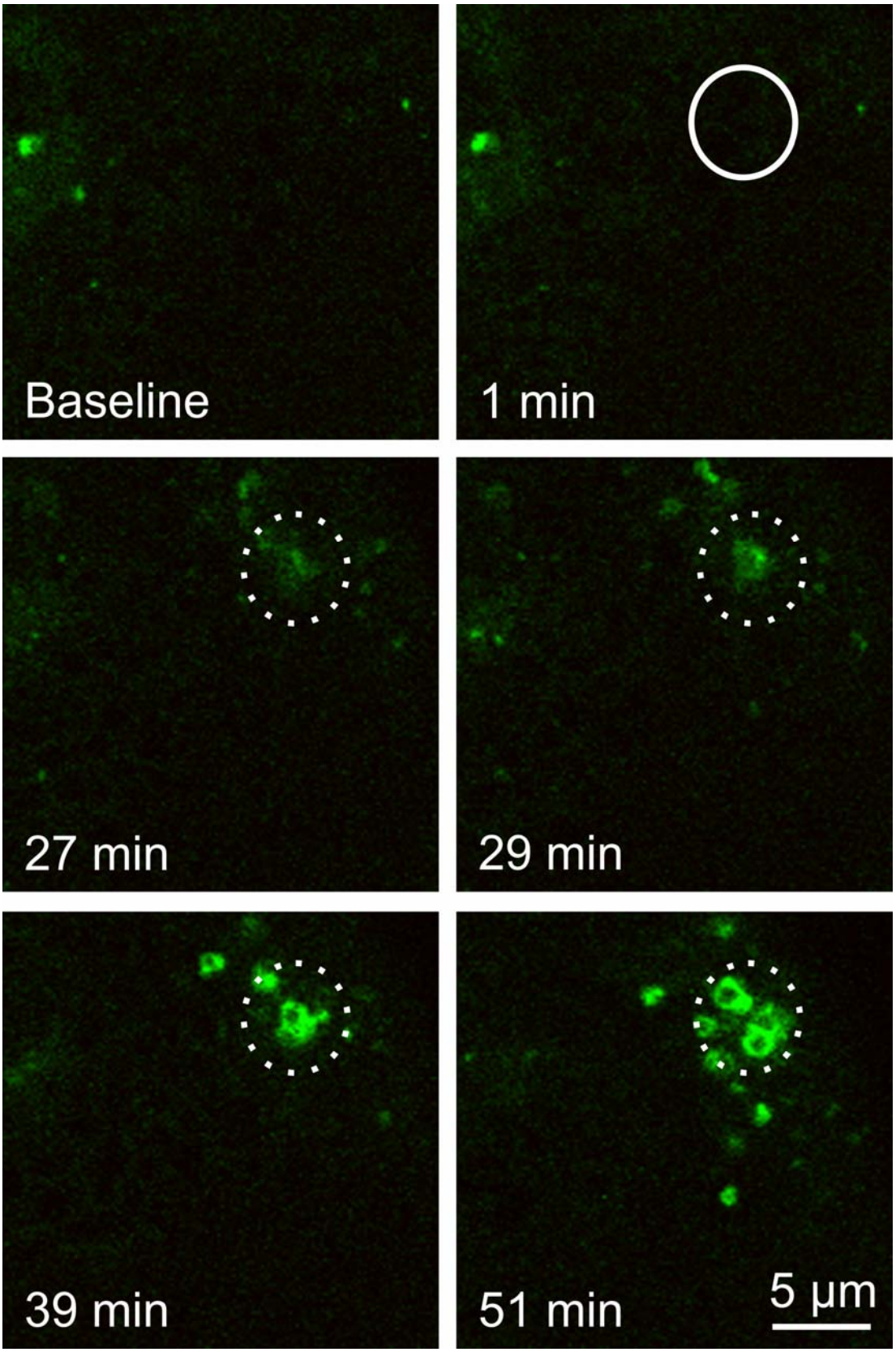
Baseline
1 min
27 min
29 min
39 min
51 min
5 µm

Figure 4.3. Photodamage-induced mitophagy is TMRM independent. Photodamaged area of GFP-LC3 hepatocytes before and every min for 120 min before and after exposed to 488-nm light at 16x light. The solid and dotted circles indicate photodamaged area. Images of green GFP-LC3 fluorescence were collected every min before (baseline) and after photodamage for 120 min.

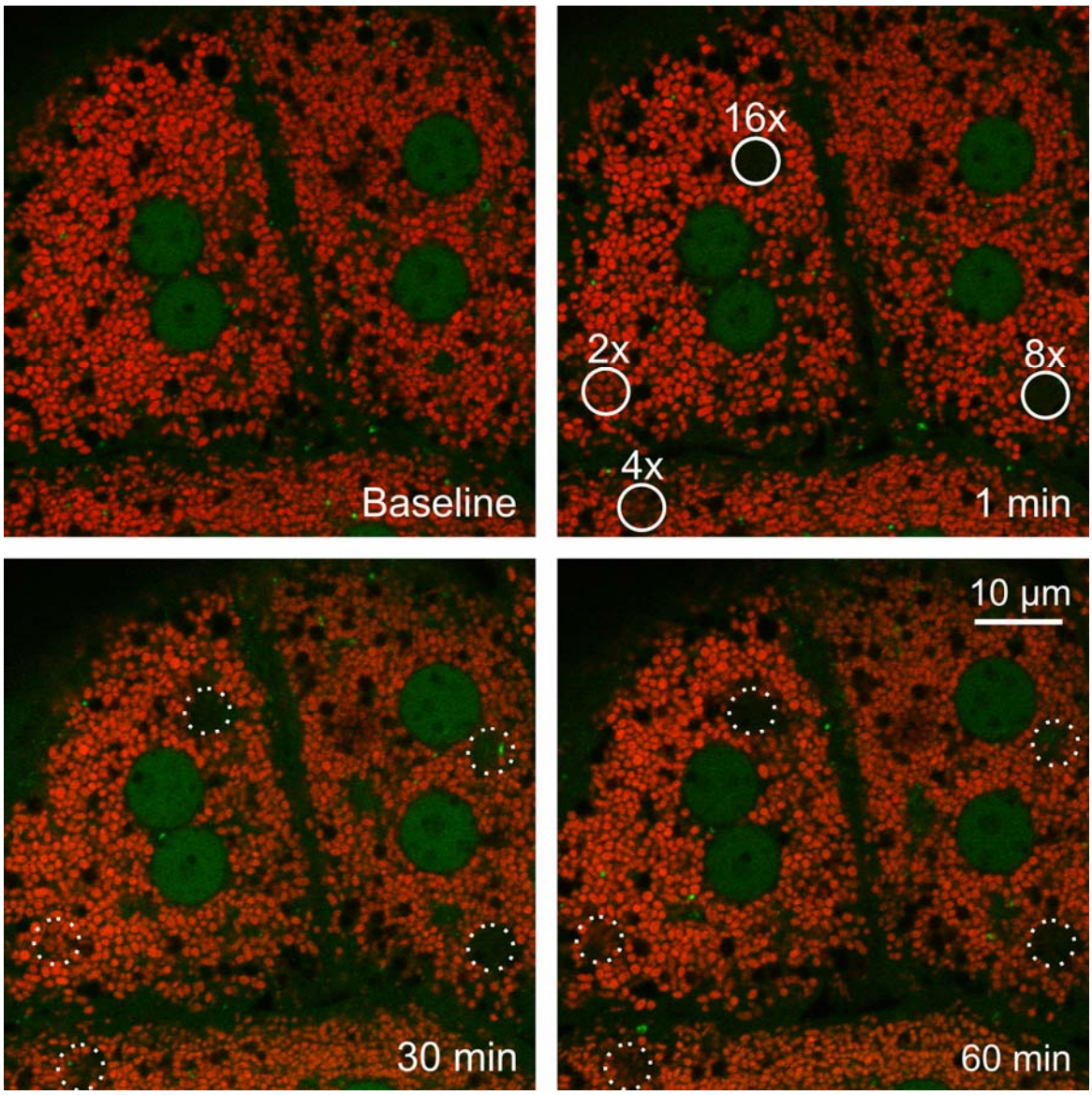

Figure 4.4. 543-nm light does not induce mitophagy. TMRM (red)-loaded GFP-LC3 hepatocytes of five mitochondria were exposed to different amount of 543-nm light at 100% power - 5.5 $x10^4$, 1.1 $x10^5$, 2.2 $x10^5$, and 4.4 $x10^5$ times per pixel higher than the pixel power used for imaging. These pixel powers were labeled in ascending order as 2x, 4x, 8x, and 16x. The solid and dotted circles represent photodamaged mitochondria. Images of red TMRM and green GFP-LC3 were collected every minute before (baseline) and after photodamage for 120 min.

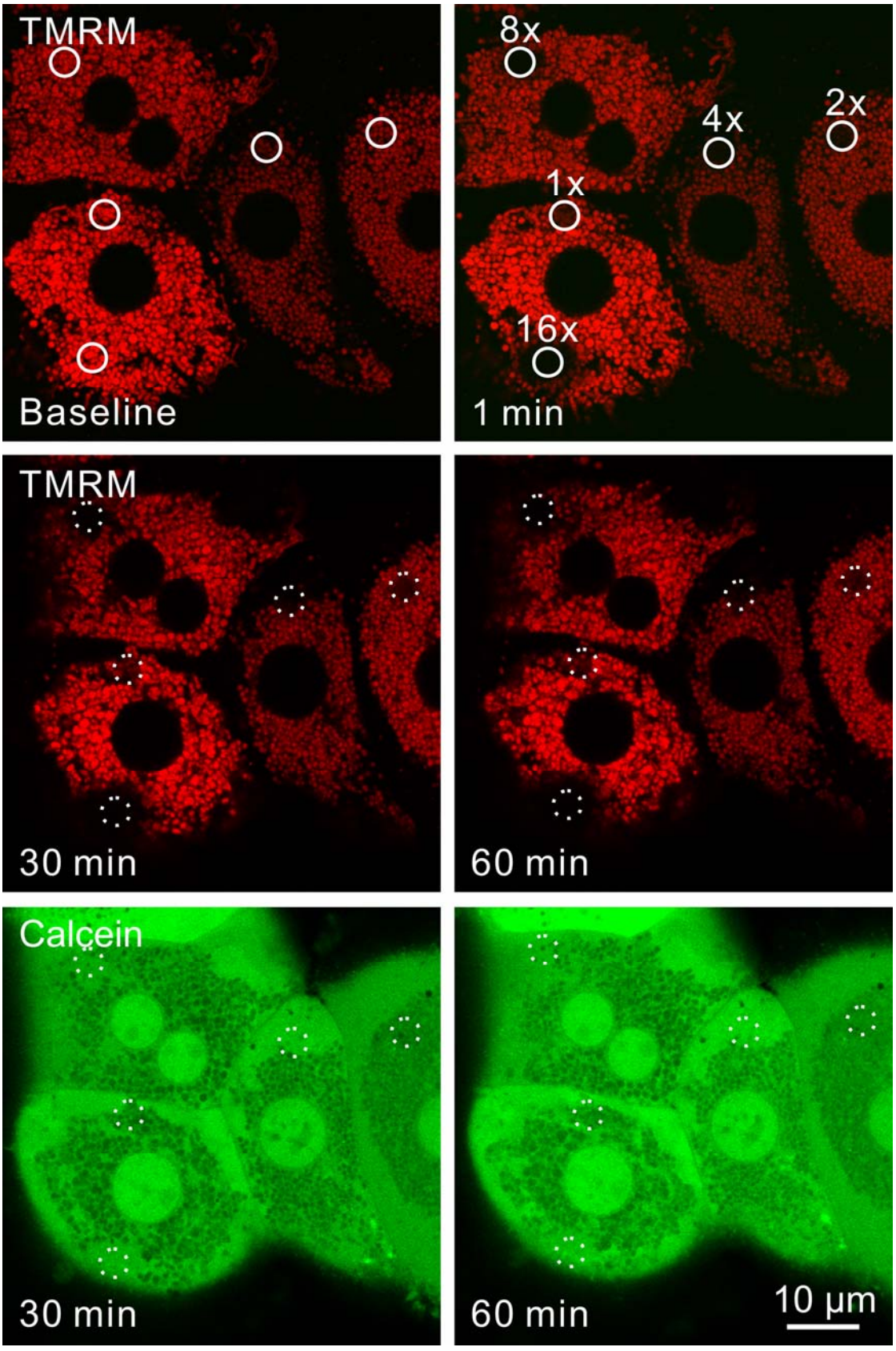
TMRM
8x
4x
2x
1x
16x
Baseline
1 min
TMRM
30 min
60 min
Calcein
30 min
60 min
10 μm

Figure 4.5. Inner membrane permeabilization occurs after photodamage. Hepatocytes from wildtype mouse were loaded with TMRM (red) and exposed to 488-nm laser light 1x, 2x, 4x, 8x, and 16x as descried in Figure1. Images were collected before (baseline) and after photodamage. The hepatocytes were then loaded with 1 μM calcein AM (green) for 10 min, and images of red TMRM and green calcein fluorescence were collected. The solid and dotted circles indicate photodamaged mitochondria.

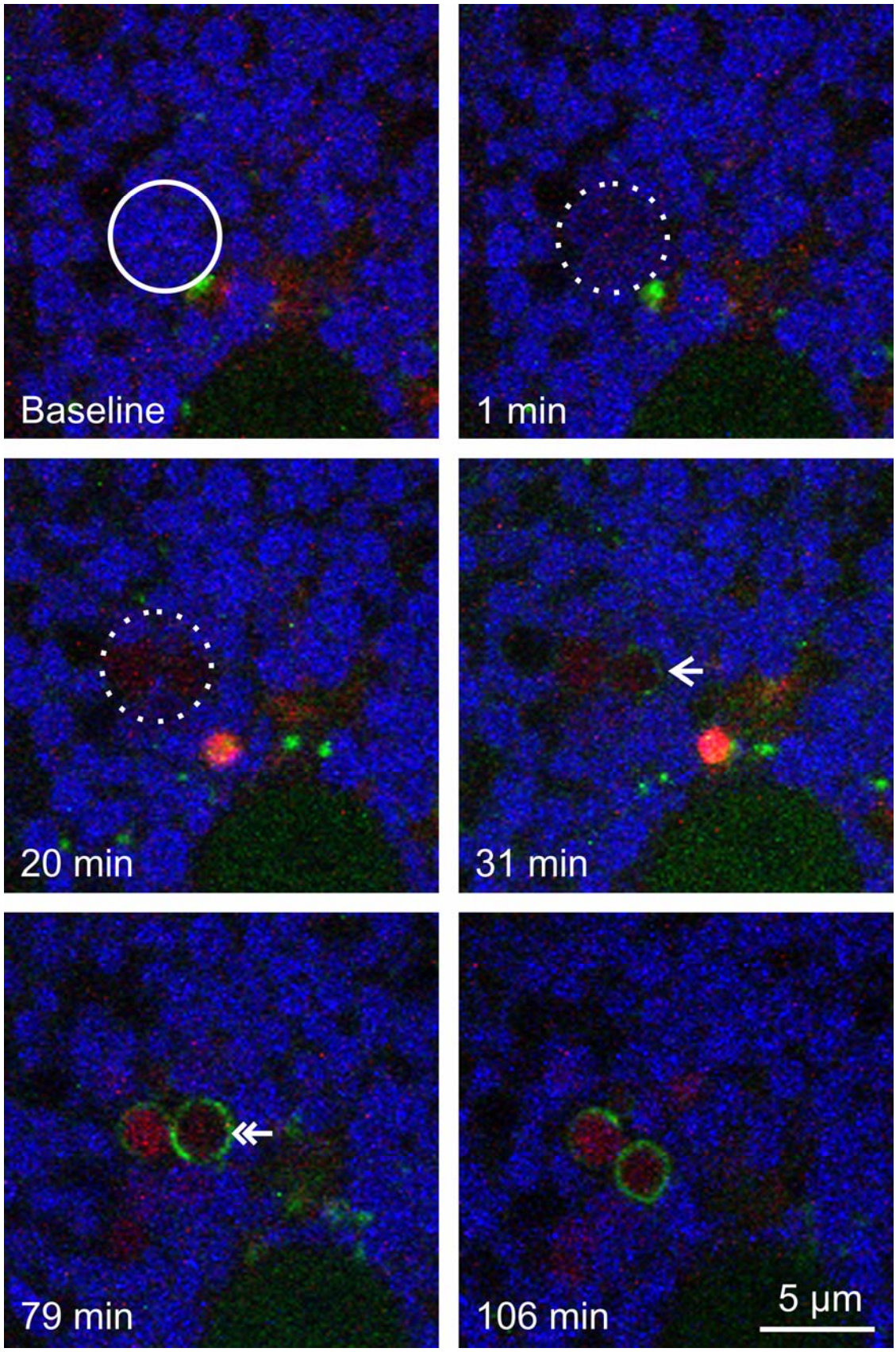
Baseline
1 min
20 min
31 min
79 min
106 min
5 µm

Figure 4.6. Photodamage-induced mitophagosomes acidify. GFP-LC3 (green) hepatocytes were loaded with 300 nM MFFR (blue) and 500 nM LTR for 30 min. Then five to ten mitochondria were photodamage by 488-nm light at the intensity of 16x (solid circle). The dotted circle indicates localization of LTR fluorescence at photodamaged mitochondria. Arrow indicates localization of GFP-LC3 to damaged mitochondria. Double arrow indicates GFP-LC3 rings (autophagosomes) around LTR-labeled photodamaged mitochondria.

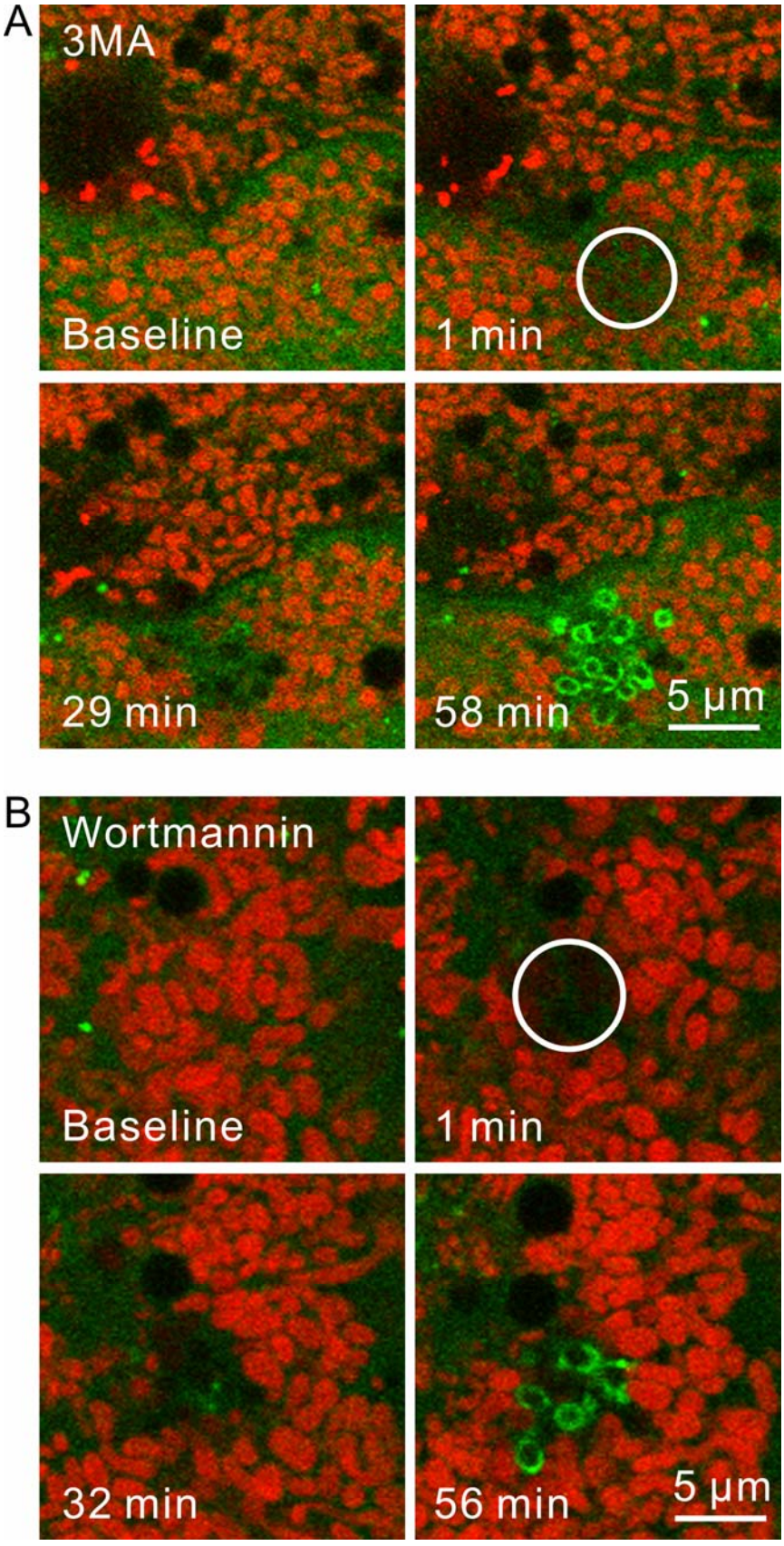
A
3MA
Baseline
1 min
29 min
58 min
5 μm
B
Wortmannin
Baseline
1 min
32 min
56 min
5 μm

Figure 4.7. 3-methyladenine and Wortmanin induce mitophagy after photodamage. GFP-LC3 transgenic hepatocytes were loaded with TMRM and pre-treated with 10 mM 3-methyladenine (3MA) (A) or 100 nM wortmannin (B) for 30 min. Then, five to ten mitochondria were photodamage by 488-nm laser at the intensity of 16x (circles) in the presence of 3MA and wortmannin. The images were taken every one minute for 120 min.

Appendix

Publications

Insil Kim, Rodriguez-Enriquez, S, and John J. Lemasters. "Minireview: Selective Degradation of Mitochondria by Mitophagy", Arch Biochem Biophys. 2007; 462(2): 245-253.

Insil Kim, Noboru Mizushima, and John Lemasters. "Mitochondrial Degradation by Autophagy in GFP-LC3 Transgenic Hepatocytes during Nutrient Deprivation", in preparation

Insil Kim, Noboru Mizushima, and John Lemasters. "Damaged Mitochondria are Selectively Removed by Mitophagy after Photodmage", in preparation

Sara Rodriguez-Enriquez, **Insil Kim**, Robert T. Currin, and John J. Lemasters. "Tracker Dyes to Probe Mitochondrial Autophagy (Mitophagy) in Rat Hepatocytes", Autophagy 2006; 2: 39-46.

Zhong, Z., Ramshesh, V.K., Currin, R.T., Sridharan, V., Rehman, H., **Kim, I**., Theruvath, T.P., Wright G.W., and John J. Lemasters. Activation of the Oxygen-Sensing Signal Cascade Prevents Mitochondrial Injury after Mouse Liver Ischemia-Reperfusion. /Gastroenterology,* */2007 (submitted)

Abstracts

Insil Kim, Noboru Mizushima, John Lemasters, "Dynamics of Mitophagy during Nutrient Deprivation to Hepatocytes", FASEB 2007; 21(5): A669

Insil Kim, Noboru Mizushima, John Lemasters. "Selective Removal of Damaged Mitochondria by Autophagy (Mitophagy)", Hepatology 2006; 44 (S1): 241A

Insil Kim, Noboru Mizushima, Yoshinori Ohsumi, and John J. Lemasters. "c-Jun N-Terminal Kinase (JNK) Inhibits Mitochondrial Autophagy in Nutrient-Deprived Hepatocytes", Hepatology 2005; 42 (S1): 1139

Insil Kim, Sara Rodriguez-Enriquez, Noboru Mizushima, Yoshinori Ohsumi, and John J. Lemasters. "Autophagic Degradation of Mitochondria in GFP-LC3 Transgenic Mouse Hepatocytes after Nutrient Deprivation", Hepatology 2004; 40 (S1): 292

Insil Kim, Sara Rodriguez-Enriquez, Noboru Mizushima, and John J. Lemasters. "Mechanisms of Mitophagy in Hepatocytes", *International Symposium on Autophagy*, Tokyo, Japan, October, 2006

JJ Lemasters, **I Kim**, S Rodriquez-Enriquez, H Lihua, P Pediaditakis[3], J.-S. Kim. "Mitochondrial Permeabilization in Cell Death and Mitophagy", *European Bioenergetics Conference*, Moscow, Russia, July, 2006

Reference List

Adams,J.M. and Cory,S. (2001). Life-or-death decisions by the Bcl-2 protein family. Trends Biochem. Sci. *26*, 61-66.

Aggarwal,B.B., Quintanilha,A.T., Cammack,R., and Packer,L. (1978). Damage to mitochondrial electron transport and energy coupling by visible light. Biochim. Biophys. Acta *502*, 367-382.

Alani,R., Brown,P., Binetruy,B., Dosaka,H., Rosenberg,R.K., Angel,P., Karin,M., and Birrer,M.J. (1991). The transactivating domain of the c-Jun proto-oncoprotein is required for cotransformation of rat embryo cells. Mol. Cell Biol. *11*, 6286-6295.

Alexandratou,E., Yova,D., Handris,P., Kletsas,D., and Loukas,S. (2002). Human fibroblast alterations induced by low power laser irradiation at the single cell level using confocal microscopy. Photochem. Photobiol. Sci. *1*, 547-552.

Arstila,A.U., Shelburne,J.D., and Trump,B.F. (1972). Studies on cellular autophagocytosis. A histochemical study on sequential alterations of mitochondria in the glucagon-induced autophagic vacuoles of rat liver. Lab Invest *27*, 317-323.

Arstila,A.U. and Trump,B.F. (1968). Studies on cellular autophagocytosis. The formation of autophagic vacuoles in the liver after glucagon administration. Am. J. Pathol. *53*, 687-733.

Ashley,N., Harris,D., and Poulton,J. (2005). Detection of mitochondrial DNA depletion in living human cells using PicoGreen staining. Exp. Cell Res. *303*, 432-446.

Attardi,G. and Schatz,G. (1988). Biogenesis of mitochondria. Annu. Rev. Cell Biol. *4*, 289-333.

Aubel,C., Dehez,S., Chabanon,H., Seva,C., Ferrara,M., and Brachet,P. (2001). Activation of c-Jun N-terminal kinase 1 (JNK-1) after amino acid deficiency in HeLa cells. Cell Signal. *13*, 417-423.

Austin,M. and Cook,S.J. (2005). Increased expression of Mcl-1 is required for protection against serum starvation in phosphatase and tensin homologue on chromosome 10 null mouse embryonic fibroblasts, but repression of Bim is favored in human glioblastomas. J. Biol. Chem. *280*, 33280-33288.

Bain,J., McLauchlan,H., Elliott,M., and Cohen,P. (2003). The specificities of protein kinase inhibitors: an update. Biochem. J. *371*, 199-204.

Bain,J., Plater,L., Elliott,M., Shpiro,N., Hastie,J., McLauchlan,H., Klevernic,I., Arthur,S., Alessi,D., and Cohen,P. (2007). The selectivity of protein kinase inhibitors; a further update. Biochem. J.

Barr,R.K., Boehm,I., Attwood,P.V., Watt,P.M., and Bogoyevitch,M.A. (2004a). The critical features and the mechanism of inhibition of a kinase interaction motif-based peptide inhibitor of JNK. J. Biol. Chem. *279*, 36327-36338.

Barr,R.K., Hopkins,R.M., Watt,P.M., and Bogoyevitch,M.A. (2004b). Reverse two-hybrid screening identifies residues of JNK required for interaction with the kinase interaction motif of JNK-interacting protein-1. J. Biol. Chem. *279*, 43178-43189.

Barr,R.K., Kendrick,T.S., and Bogoyevitch,M.A. (2002). Identification of the critical features of a small peptide inhibitor of JNK activity. J. Biol. Chem. *277*, 10987-10997.

Barsoum,M.J., Yuan,H., Gerencser,A.A., Liot,G., Kushnareva,Y., Graber,S., Kovacs,I., Lee,W.D., Waggoner,J., Cui,J., White,A.D., Bossy,B., Martinou,J.C., Youle,R.J., Lipton,S.A., Ellisman,M.H., Perkins,G.A., and Bossy-Wetzel,E. (2006). Nitric oxide-induced mitochondrial fission is regulated by dynamin-related GTPases in neurons. EMBO J. *25*, 3900-3911.

Basso,E., Fante,L., Fowlkes,J., Petronilli,V., Forte,M.A., and Bernardi,P. (2005). Properties of the permeability transition pore in mitochondria devoid of Cyclophilin D. J. Biol. Chem. *280*, 18558-18561.

Bellu,A.R., Kram,A.M., Kiel,J.A., Veenhuis,M., and van,d.K., I (2001). Glucose-induced and nitrogen-starvation-induced peroxisome degradation are distinct processes in Hansenula polymorpha that involve both common and unique genes. FEMS Yeast Res. *1*, 23-31.

Bennett,B.L., Sasaki,D.T., Murray,B.W., O'Leary,E.C., Sakata,S.T., Xu,W., Leisten,J.C., Motiwala,A., Pierce,S., Satoh,Y., Bhagwat,S.S., Manning,A.M., and Anderson,D.W. (2001). SP600125, an anthrapyrazolone inhibitor of Jun N-terminal kinase. Proc. Natl. Acad. Sci. U. S. A *98*, 13681-13686.

Beregi,E., Regius,O., Huttl,T., and Gobl,Z. (1988). Age-related changes in the skeletal muscle cells. Z. Gerontol. *21*, 83-86.

Bergamini,E. (2006). Autophagy: a cell repair mechanism that retards ageing and age-associated diseases and can be intensified pharmacologically. Mol. Aspects Med. *27*, 403-410.

Bergamini,E., Cavallini,G., Donati,A., and Gori,Z. (2003). The anti-ageing effects of caloric restriction may involve stimulation of macroautophagy and lysosomal degradation, and can be intensified pharmacologically. Biomed. Pharmacother. *57*, 203-208.

Beutner,G., Ruck,A., Riede,B., Welte,W., and Brdiczka,D. (1996). Complexes between kinases, mitochondrial porin and adenylate translocator in rat brain resemble the permeability transition pore. FEBS Lett. *396*, 189-195.

Blommaart,E.F., Krause,U., Schellens,J.P., Vreeling-Sindelarova,H., and Meijer,A.J. (1997). The phosphatidylinositol 3-kinase inhibitors wortmannin and LY294002 inhibit autophagy in isolated rat hepatocytes. Eur. J. Biochem. *243*, 240-246.

Bogoyevitch,M.A., Boehm,I., Oakley,A., Ketterman,A.J., and Barr,R.K. (2004). Targeting the JNK MAPK cascade for inhibition: basic science and therapeutic potential. Biochim. Biophys. Acta *1697*, 89-101.

Bohr,V.A. (2002). Repair of oxidative DNA damage in nuclear and mitochondrial DNA, and some changes with aging in mammalian cells. Free Radic. Biol. Med. *32*, 804-812.

Boya,P., Gonzalez-Polo,R.A., Casares,N., Perfettini,J.L., Dessen,P., Larochette,N., Metivier,D., Meley,D., Souquere,S., Yoshimori,T., Pierron,G., Codogno,P., and Kroemer,G. (2005). Inhibition of macroautophagy triggers apoptosis. Mol. Cell Biol. *25*, 1025-1040.

Bradham,C.A., Qian,T., Streetz,K., Trautwein,C., Brenner,D.A., and Lemasters,J.J. (1998). The mitochondrial permeability transition is required for tumor necrosis factor alpha-mediated apoptosis and cytochrome c release. Mol. Cell Biol. *18*, 6353-6364.

Brecht,S., Kirchhof,R., Chromik,A., Willesen,M., Nicolaus,T., Raivich,G., Wessig,J., Waetzig,V., Goetz,M., Claussen,M., Pearse,D., Kuan,C.Y., Vaudano,E., Behrens,A., Wagner,E., Flavell,R.A., Davis,R.J., and Herdegen,T. (2005). Specific pathophysiological functions of JNK isoforms in the brain. Eur. J. Neurosci. *21*, 363-377.

Brichese,L., Cazettes,G., and Valette,A. (2004). JNK is associated with Bcl-2 and PP1 in mitochondria: paclitaxel induces its activation and its association with the phosphorylated form of Bcl-2. Cell Cycle *3*, 1312-1319.

Bursch,W. (2001). The autophagosomal-lysosomal compartment in programmed cell death. Cell Death. Differ. *8*, 569-581.

Camougrand,N., Kissova,I., Velours,G., and Manon,S. (2004). Uth1p: a yeast mitochondrial protein at the crossroads of stress, degradation and cell death. FEMS Yeast Res. *5*, 133-140.

Charlotte,F., L'Hermine,A., Martin,N., Geleyn,Y., Nollet,M., Gaulard,P., and Zafrani,E.S. (1994). Immunohistochemical detection of bcl-2 protein in normal and pathological human liver. Am. J. Pathol. *144*, 460-465.

Chen,N., Nomura,M., She,Q.B., Ma,W.Y., Bode,A.M., Wang,L., Flavell,R.A., and Dong,Z. (2001). Suppression of skin tumorigenesis in c-Jun NH(2)-terminal kinase-2-deficient mice. Cancer Res. *61*, 3908-3912.

Chen,X.J. and Butow,R.A. (2005). The organization and inheritance of the mitochondrial genome. Nat. Rev. Genet. *6*, 815-825.

Coffey,E.T., Smiciene,G., Hongisto,V., Cao,J., Brecht,S., Herdegen,T., and Courtney,M.J. (2002). c-Jun N-terminal protein kinase (JNK) 2/3 is specifically activated by stress, mediating c-Jun activation, in the presence of constitutive JNK1 activity in cerebellar neurons. J. Neurosci. *22*, 4335-4345.

Crompton,M., Virji,S., and Ward,J.M. (1998). Cyclophilin-D binds strongly to complexes of the voltage-dependent anion channel and the adenine nucleotide translocase to form the permeability transition pore. Eur. J. Biochem. *258*, 729-735.

Cuervo,A.M. (2004). Autophagy: many paths to the same end. Mol. Cell Biochem. *263*, 55-72.

Davis,R.J. (2000). Signal transduction by the JNK group of MAP kinases. Cell *103*, 239-252.

de Grey,A.D. (1997). A proposed refinement of the mitochondrial free radical theory of aging. BioEssays *19*, 161-166.

DE,D.C. (1963). The lysosome. Sci. Am. *208*, 64-72.

Debnath,J., Baehrecke,E.H., and Kroemer,G. (2005). Does autophagy contribute to cell death? Autophagy. *1*, 66-74.

Dickens,M., Rogers,J.S., Cavanagh,J., Raitano,A., Xia,Z., Halpern,J.R., Greenberg,M.E., Sawyers,C.L., and Davis,R.J. (1997). A cytoplasmic inhibitor of the JNK signal transduction pathway. Science *277*, 693-696.

Ding,W.X., Ni,H.M., Gao,W., Yoshimori,T., Stolz,D.B., Ron,D., and Yin,X.M. (2007). Linking of autophagy to ubiquitin-proteasome system is important for the regulation of endoplasmic reticulum stress and cell viability. Am. J. Pathol. *171*, 513-524.

Dorn,B.R., Dunn,W.A., Jr., and Progulske-Fox,A. (2002). Bacterial interactions with the autophagic pathway. Cell Microbiol. *4*, 1-10.

Dunn,W.A., Jr. (1990). Studies on the mechanisms of autophagy: formation of the autophagic vacuole. J. Cell Biol. *110*, 1923-1933.

Elmore,S.P., Qian,T., Grissom,S.F., and Lemasters,J.J. (2001). The mitochondrial permeability transition initiates autophagy in rat hepatocytes. FASEB J. *15*, 2286-2287.

Eminel,S., Klettner,A., Roemer,L., Herdegen,T., and Waetzig,V. (2004). JNK2 translocates to the mitochondria and mediates cytochrome c release in PC12 cells in response to 6-hydroxydopamine. J. Biol. Chem. *279*, 55385-55392.

Ermini,M. (1976). Ageing changes in mammalian skeletal muscle: biochemical studies. Gerontology *22*, 301-316.

Fengsrud,M., Roos,N., Berg,T., Liou,W., Slot,J.W., and Seglen,P.O. (1995). Ultrastructural and immunocytochemical characterization of autophagic vacuoles in isolated hepatocytes: effects of vinblastine and asparagine on vacuole distributions. Exp. Cell Res. *221*, 504-519.

Fontenay,M., Cathelin,S., Amiot,M., Gyan,E., and Solary,E. (2006). Mitochondria in hematopoiesis and hematological diseases. Oncogene *25*, 4757-4767.

Forte,M. and Bernardi,P. (2005). Genetic dissection of the permeability transition pore. J. Bioenerg. Biomembr. *37*, 121-128.

Furuno,K., Ishikawa,T., Akasaki,K., Lee,S., Nishimura,Y., Tsuji,H., Himeno,M., and Kato,K. (1990). Immunocytochemical study of the surrounding envelope of autophagic vacuoles in cultured rat hepatocytes. Exp. Cell Res. *189*, 261-268.

Furuya,N., Yu,J., Byfield,M., Pattingre,S., and Levine,B. (2005). The evolutionarily conserved domain of Beclin 1 is required for Vps34 binding, autophagy and tumor suppressor function. Autophagy. *1*, 46-52.

Goldberg,A.L. (2003). Protein degradation and protection against misfolded or damaged proteins. Nature *426*, 895-899.

Golstein,P. and Kroemer,G. (2007). A multiplicity of cell death pathways. Symposium on apoptotic and non-apoptotic cell death pathways. EMBO Rep. *8*, 829-833.

Gores,G.J., Nieminen,A.L., Fleishman,K.E., Dawson,T.L., Herman,B., and Lemasters,J.J. (1988). Extracellular acidosis delays onset of cell death in ATP-depleted hepatocytes. Am. J. Physiol *255*, C315-C322.

Gozuacik,D. and Kimchi,A. (2004). Autophagy as a cell death and tumor suppressor mechanism. Oncogene *23*, 2891-2906.

Gronostajski,R.M., Pardee,A.B., and Goldberg,A.L. (1985). The ATP dependence of the degradation of short- and long-lived proteins in growing fibroblasts. J. Biol. Chem. *260*, 3344-3349.

Gunter,T.E. and Pfeiffer,D.R. (1990). Mechanisms by which mitochondria transport calcium. Am. J. Physiol *258*, C755-C786.

Gupta,S., Barrett,T., Whitmarsh,A.J., Cavanagh,J., Sluss,H.K., Derijard,B., and Davis,R.J. (1996). Selective interaction of JNK protein kinase isoforms with transcription factors. EMBO J. *15*, 2760-2770.

Halestrap,A.P. and Davidson,A.M. (1990). Inhibition of Ca2(+)-induced large-amplitude swelling of liver and heart mitochondria by cyclosporin is probably caused by the inhibitor binding to mitochondrial-matrix peptidyl-prolyl cis-trans isomerase and preventing it interacting with the adenine nucleotide translocase. Biochem. J. *268*, 153-160.

Harada,H., Quearry,B., Ruiz-Vela,A., and Korsmeyer,S.J. (2004). Survival factor-induced extracellular signal-regulated kinase phosphorylates BIM, inhibiting its association with BAX and proapoptotic activity. Proc. Natl. Acad. Sci. U. S. A *101*, 15313-15317.

Harding,T.M., Hefner-Gravink,A., Thumm,M., and Klionsky,D.J. (1996). Genetic and phenotypic overlap between autophagy and the cytoplasm to vacuole protein targeting pathway. J. Biol. Chem. *271*, 17621-17624.

Hatano,E., Bradham,C.A., Stark,A., Iimuro,Y., Lemasters,J.J., and Brenner,D.A. (2000). The mitochondrial permeability transition augments Fas-induced apoptosis in mouse hepatocytes. J. Biol. Chem. *275*, 11814-11823.

He,L. and Lemasters,J.J. (2002). Regulated and unregulated mitochondrial permeability transition pores: a new paradigm of pore structure and function? FEBS Lett. *512*, 1-7.

He,L. and Lemasters,J.J. (2003). Heat shock suppresses the permeability transition in rat liver mitochondria. J. Biol. Chem. *278*, 16755-16760.

He,L. and Lemasters,J.J. (2005). Dephosphorylation of the Rieske iron-sulfur protein after induction of the mitochondrial permeability transition. Biochem. Biophys. Res. Commun. *334*, 829-837.

Hibi,M., Lin,A., Smeal,T., Minden,A., and Karin,M. (1993). Identification of an oncoprotein- and UV-responsive protein kinase that binds and potentiates the c-Jun activation domain. Genes Dev. *7*, 2135-2148.

Hirosumi,J., Tuncman,G., Chang,L., Gorgun,C.Z., Uysal,K.T., Maeda,K., Karin,M., and Hotamisligil,G.S. (2002). A central role for JNK in obesity and insulin resistance. Nature *420*, 333-336.

Hsu,V.L. and Armitage,I.M. (1992). Solution structure of cyclosporin A and a nonimmunosuppressive analog bound to fully deuterated cyclophilin. Biochemistry *31*, 12778-12784.

Hunter,D.R., Haworth,R.A., and Southard,J.H. (1976). Relationship between configuration, function, and permeability in calcium-treated mitochondria. J. Biol. Chem. *251*, 5069-5077.

Jager,S., Bucci,C., Tanida,I., Ueno,T., Kominami,E., Saftig,P., and Eskelinen,E.L. (2004). Role for Rab7 in maturation of late autophagic vacuoles. J. Cell Sci. *117*, 4837-4848.

Jou,M.J., Jou,S.B., Chen,H.M., Lin,C.H., and Peng,T.I. (2002). Critical role of mitochondrial reactive oxygen species formation in visible laser irradiation-induced apoptosis in rat brain astrocytes (RBA-1). J. Biomed. Sci. *9*, 507-516.

Kabeya,Y., Mizushima,N., Ueno,T., Yamamoto,A., Kirisako,T., Noda,T., Kominami,E., Ohsumi,Y., and Yoshimori,T. (2000). LC3, a mammalian homologue of yeast Apg8p, is localized in autophagosome membranes after processing. EMBO J. *19*, 5720-5728.

Kadowaki,M., Venerando,R., Miotto,G., and Mortimore,G.E. (1996). Mechanism of autophagy in permeabilized hepatocytes: evidence for regulation by GTP binding proteins. Adv. Exp. Med. Biol. *389*, 113-119.

Kawai,A., Takano,S., Nakamura,N., and Ohkuma,S. (2006). Quantitative monitoring of autophagic degradation. Biochem. Biophys. Res. Commun. *351*, 71-77.

Kennedy,B.K. and Guarente,L. (1996). Genetic analysis of aging in Saccharomyces cerevisiae. Trends Genet. *12*, 355-359.

Kiel,J.A., Komduur,J.A., van,d.K., I, and Veenhuis,M. (2003). Macropexophagy in Hansenula polymorpha: facts and views. FEBS Lett. *549*, 1-6.

Kim, I., Mizushima, N., and Lemasters, J. J. Selective removal of damaged mitochondria by autophagy (mitophagy). Hepatology 44 (Suppl. 1), 241A. 2006.
Ref Type: Abstract

Kim,I., Rodriguez-Enriquez,S., and Lemasters,J.J. (2007). Selective degradation of mitochondria by mitophagy. Arch. Biochem. Biophys. *462*, 245-253.

Kim, I., Rodriguez-Enriquez, S., Mizushima, N., Ohsumi, Y., and Lemasters, J. J. Autophagic degradation of mitochondria in GFP-LC3 transgenic mouse hepatocytes after nutrient deprivation. Hepatology 40 (Suppl. 1), 291A. 2004.
Ref Type: Abstract

Kim,J., Huang,W.P., Stromhaug,P.E., and Klionsky,D.J. (2002). Convergence of multiple autophagy and cytoplasm to vacuole targeting components to a perivacuolar membrane compartment prior to de novo vesicle formation. J. Biol. Chem. *277*, 763-773.

Kim,J. and Klionsky,D.J. (2000). Autophagy, cytoplasm-to-vacuole targeting pathway, and pexophagy in yeast and mammalian cells. Annu. Rev. Biochem. *69*, 303-342.

Kissova,I., Deffieu,M., Manon,S., and Camougrand,N. (2004). Uth1p is involved in the autophagic degradation of mitochondria. J. Biol. Chem. *279*, 39068-39074.

Kokoszka,J.E., Waymire,K.G., Levy,S.E., Sligh,J.E., Cai,J., Jones,D.P., MacGregor,G.R., and Wallace,D.C. (2004). The ADP/ATP translocator is not essential for the mitochondrial permeability transition pore. Nature *427*, 461-465.

Kon,K., Kim,J.S., Jaeschke,H., and Lemasters,J.J. (2004). Mitochondrial permeability transition in acetaminophen-induced necrosis and apoptosis of cultured mouse hepatocytes. Hepatology *40*, 1170-1179.

Kopitz,J., Kisen,G.O., Gordon,P.B., Bohley,P., and Seglen,P.O. (1990). Nonselective autophagy of cytosolic enzymes by isolated rat hepatocytes. J. Cell Biol. *111*, 941-953.

Kotoulas,O.B., Kalamidas,S.A., and Kondomerkos,D.J. (2006). Glycogen autophagy in glucose homeostasis. Pathol. Res. Pract. *202*, 631-638.

Kuan,C.Y., Yang,D.D., Samanta Roy,D.R., Davis,R.J., Rakic,P., and Flavell,R.A. (1999). The Jnk1 and Jnk2 protein kinases are required for regional specific apoptosis during early brain development. Neuron *22*, 667-676.

Kuma,A., Hatano,M., Matsui,M., Yamamoto,A., Nakaya,H., Yoshimori,T., Ohsumi,Y., Tokuhisa,T., and Mizushima,N. (2004). The role of autophagy during the early neonatal starvation period. Nature *432*, 1032-1036.

Kuma,A., Mizushima,N., Ishihara,N., and Ohsumi,Y. (2002). Formation of the approximately 350-kDa Apg12-Apg5.Apg16 multimeric complex, mediated by Apg16 oligomerization, is essential for autophagy in yeast. J. Biol. Chem. *277*, 18619-18625.

Lam,M., Oleinick,N.L., and Nieminen,A.L. (2001). Photodynamic therapy-induced apoptosis in epidermoid carcinoma cells. Reactive oxygen species and mitochondrial inner membrane permeabilization. J. Biol. Chem. *276*, 47379-47386.

Lei,K. and Davis,R.J. (2003). JNK phosphorylation of Bim-related members of the Bcl2 family induces Bax-dependent apoptosis. Proc. Natl. Acad. Sci. U. S. A *100*, 2432-2437.

Leicht,M., Marx,G., Karbach,D., Gekle,M., Kohler,T., and Zimmer,H.G. (2003). Mechanism of cell death of rat cardiac fibroblasts induced by serum depletion. Mol. Cell Biochem. *251*, 119-126.

Lemasters,J.J. (2005). Selective mitochondrial autophagy, or mitophagy, as a targeted defense against oxidative stress, mitochondrial dysfunction, and aging. Rejuvenation. Res. *8*, 3-5.

Lemasters,J.J., Nieminen,A.L., Qian,T., Trost,L.C., Elmore,S.P., Nishimura,Y., Crowe,R.A., Cascio,W.E., Bradham,C.A., Brenner,D.A., and Herman,B. (1998). The mitochondrial permeability transition in cell death: a common mechanism in necrosis, apoptosis and autophagy. Biochim. Biophys. Acta *1366*, 177-196.

Levine,B. and Klionsky,D.J. (2004). Development by self-digestion: molecular mechanisms and biological functions of autophagy. Dev. Cell *6*, 463-477.

Levine,B. and Yuan,J. (2005). Autophagy in cell death: an innocent convict? J. Clin. Invest *115*, 2679-2688.

Li,C., Capan,E., Zhao,Y., Zhao,J., Stolz,D., Watkins,S.C., Jin,S., and Lu,B. (2006). Autophagy is induced in CD4+ T cells and important for the growth factor-withdrawal cell death. J. Immunol. *177*, 5163-5168.

Liu,X., Dai,S., Zhu,Y., Marrack,P., and Kappler,J.W. (2003). The structure of a Bcl-xL/Bim fragment complex: implications for Bim function. Immunity. *19*, 341-352.

Luciano,F., Jacquel,A., Colosetti,P., Herrant,M., Cagnol,S., Pages,G., and Auberger,P. (2003). Phosphorylation of Bim-EL by Erk1/2 on serine 69 promotes its degradation via the proteasome pathway and regulates its proapoptotic function. Oncogene *22*, 6785-6793.

Lutz,R.J. (2000). Role of the BH3 (Bcl-2 homology 3) domain in the regulation of apoptosis and Bcl-2-related proteins. Biochem. Soc. Trans. *28*, 51-56.

Malhi,H., Gores,G.J., and Lemasters,J.J. (2006). Apoptosis and necrosis in the liver: a tale of two deaths? Hepatology *43*, S31-S44.

Marzo,I., Brenner,C., Zamzami,N., Susin,S.A., Beutner,G., Brdiczka,D., Remy,R., Xie,Z.H., Reed,J.C., and Kroemer,G. (1998). The permeability transition pore complex: a target for apoptosis regulation by caspases and bcl-2-related proteins. J. Exp. Med. *187*, 1261-1271.

Matsushita,M., Suzuki,N.N., Obara,K., Fujioka,Y., Ohsumi,Y., and Inagaki,F. (2007). Structure of Atg5.Atg16, a complex essential for autophagy. J. Biol. Chem. *282*, 6763-6772.

Maundrell,K., Antonsson,B., Magnenat,E., Camps,M., Muda,M., Chabert,C., Gillieron,C., Boschert,U., Vial-Knecht,E., Martinou,J.C., and Arkinstall,S. (1997). Bcl-2 undergoes phosphorylation by c-Jun N-terminal kinase/stress-activated protein kinases in the presence of the constitutively active GTP-binding protein Rac1. J. Biol. Chem. *272*, 25238-25242.

Meijer,A.J. and Codogno,P. (2004). Regulation and role of autophagy in mammalian cells. Int. J. Biochem. Cell Biol. *36*, 2445-2462.

Meijer,A.J. and Codogno,P. (2006). Signalling and autophagy regulation in health, aging and disease. Mol. Aspects Med. *27*, 411-425.

Menzies,R.A. and Gold,P.H. (1971). The turnover of mitochondria in a variety of tissues of young adult and aged rats. J. Biol. Chem. *246*, 2425-2429.

Minden,A., Lin,A., McMahon,M., Lange-Carter,C., Derijard,B., Davis,R.J., Johnson,G.L., and Karin,M. (1994a). Differential activation of ERK and JNK mitogen-activated protein kinases by Raf-1 and MEKK. Science *266*, 1719-1723.

Minden,A., Lin,A., Smeal,T., Derijard,B., Cobb,M., Davis,R., and Karin,M. (1994b). c-Jun N-terminal phosphorylation correlates with activation of the JNK subgroup but not the ERK subgroup of mitogen-activated protein kinases. Mol. Cell Biol. *14*, 6683-6688.

Mitchener,J.S., Shelburne,J.D., Bradford,W.D., and Hawkins,H.K. (1976). Cellular autophagocytosis induced by deprivation of serum and amino acids in HeLa cells. Am. J. Pathol. *83*, 485-492.

Mizushima,N., Yamamoto,A., Matsui,M., Yoshimori,T., and Ohsumi,Y. (2004). In vivo analysis of autophagy in response to nutrient starvation using transgenic mice expressing a fluorescent autophagosome marker. Mol. Biol. Cell *15*, 1101-1111.

Mousavi,S.A., Brech,A., Berg,T., and Kjeken,R. (2003). Phosphoinositide 3-kinase regulates maturation of lysosomes in rat hepatocytes. Biochem. J. *372*, 861-869.

Nakagawa,I., Amano,A., Mizushima,N., Yamamoto,A., Yamaguchi,H., Kamimoto,T., Nara,A., Funao,J., Nakata,M., Tsuda,K., Hamada,S., and Yoshimori,T. (2004). Autophagy defends cells against invading group A Streptococcus. Science *306*, 1037-1040.

Nieminen,A.L., Byrne,A.M., Herman,B., and Lemasters,J.J. (1997). Mitochondrial permeability transition in hepatocytes induced by t-BuOOH: NAD(P)H and reactive oxygen species. Am. J. Physiol *272*, C1286-C1294.

Noda,T. and Ohsumi,Y. (1998). Tor, a phosphatidylinositol kinase homologue, controls autophagy in yeast. J. Biol. Chem. *273*, 3963-3966.

O'Reilly,L.A., Cullen,L., Visvader,J., Lindeman,G.J., Print,C., Bath,M.L., Huang,D.C., and Strasser,A. (2000). The proapoptotic BH3-only protein bim is expressed in hematopoietic, epithelial, neuronal, and germ cells. Am. J. Pathol. *157*, 449-461.

Ogata,M., Hino,S., Saito,A., Morikawa,K., Kondo,S., Kanemoto,S., Murakami,T., Taniguchi,M., Tanii,I., Yoshinaga,K., Shiosaka,S., Hammarback,J.A., Urano,F., and Imaizumi,K. (2006). Autophagy is activated for cell survival after endoplasmic reticulum stress. Mol. Cell Biol. *26*, 9220-9231.

Ogawa,M., Yoshimori,T., Suzuki,T., Sagara,H., Mizushima,N., and Sasakawa,C. (2005). Escape of intracellular Shigella from autophagy. Science *307*, 727-731.

Ohsumi,Y. and Mizushima,N. (2004). Two ubiquitin-like conjugation systems essential for autophagy. Semin. Cell Dev. Biol. *15*, 231-236.

Pattingre,S., Tassa,A., Qu,X., Garuti,R., Liang,X.H., Mizushima,N., Packer,M., Schneider,M.D., and Levine,B. (2005). Bcl-2 antiapoptotic proteins inhibit Beclin 1-dependent autophagy. Cell *122*, 927-939.

Petiot,A., Pattingre,S., Arico,S., Meley,D., and Codogno,P. (2002). Diversity of signaling controls of macroautophagy in mammalian cells. Cell Struct. Funct. *27*, 431-441.

Pfeifer,U. (1978). Inhibition by insulin of the formation of autophagic vacuoles in rat liver. A morphometric approach to the kinetics of intracellular degradation by autophagy. J. Cell Biol. *78*, 152-167.

Pfeiffer,D.R., Gudz,T.I., Novgorodov,S.A., and Erdahl,W.L. (1995). The peptide mastoparan is a potent facilitator of the mitochondrial permeability transition. J. Biol. Chem. *270*, 4923-4932.

Punnonen,E.L., Autio,S., Marjomaki,V.S., and Reunanen,H. (1992). Autophagy, cathepsin L transport, and acidification in cultured rat fibroblasts. J. Histochem. Cytochem. *40*, 1579-1587.

Putcha,G.V., Le,S., Frank,S., Besirli,C.G., Clark,K., Chu,B., Alix,S., Youle,R.J., LaMarche,A., Maroney,A.C., and Johnson,E.M., Jr. (2003). JNK-mediated BIM phosphorylation potentiates BAX-dependent apoptosis. Neuron *38*, 899-914.

Puthalakath,H., Huang,D.C., O'Reilly,L.A., King,S.M., and Strasser,A. (1999). The proapoptotic activity of the Bcl-2 family member Bim is regulated by interaction with the dynein motor complex. Mol. Cell *3*, 287-296.

Qian,T., Herman,B., and Lemasters,J.J. (1999). The mitochondrial permeability transition mediates both necrotic and apoptotic death of hepatocytes exposed to Br-A23187. Toxicol. Appl. Pharmacol. *154*, 117-125.

Qian,T., Nieminen,A.L., Herman,B., and Lemasters,J.J. (1997). Mitochondrial permeability transition in pH-dependent reperfusion injury to rat hepatocytes. Am. J. Physiol *273*, C1783-C1792.

Quadros,M.R., Connelly,S., Kari,C., Abrams,M.T., Wickstrom,E., and Rodeck,U. (2006). EGFR-dependent downregulation of Bim in epithelial cells requires MAPK and PKC-delta activities. Cancer Biol. Ther. *5*, 498-504.

Reggiori,F., Shintani,T., Nair,U., and Klionsky,D.J. (2005). Atg9 cycles between mitochondria and the pre-autophagosomal structure in yeasts. Autophagy. *1*, 101-109.

Rodriguez-Enriquez,S., Kim,I., Currin,R.T., and Lemasters,J.J. (2006). Tracker dyes to probe mitochondrial autophagy (mitophagy) in rat hepatocytes. Autophagy. *2*, 39-46.

Rosette,C. and Karin,M. (1996). Ultraviolet light and osmotic stress: activation of the JNK cascade through multiple growth factor and cytokine receptors. Science *274*, 1194-1197.

Sabapathy,K., Jochum,W., Hochedlinger,K., Chang,L., Karin,M., and Wagner,E.F. (1999). Defective neural tube morphogenesis and altered apoptosis in the absence of both JNK1 and JNK2. Mech. Dev. *89*, 115-124.

Sakanoue,J., Ichikawa,K., Nomura,Y., and Tamura,M. (1997). Rhodamine 800 as a probe of energization of cells and tissues in the near-infrared region: a study with isolated rat liver mitochondria and hepatocytes. J. Biochem. *121*, 29-37.

Schworer,C.M. and Mortimore,G.E. (1979). Glucagon-induced autophagy and proteolysis in rat liver: mediation by selective deprivation of intracellular amino acids. Proc. Natl. Acad. Sci. U. S. A *76*, 3169-3173.

Seglen,P.O., Berg,T.O., Blankson,H., Fengsrud,M., Holen,I., and Stromhaug,P.E. (1996). Structural aspects of autophagy. Adv. Exp. Med. Biol. *389*, 103-111.

Seglen,P.O. and Bohley,P. (1992). Autophagy and other vacuolar protein degradation mechanisms. Experientia *48*, 158-172.

Seglen,P.O. and Gordon,P.B. (1982). 3-Methyladenine: specific inhibitor of autophagic/lysosomal protein degradation in isolated rat hepatocytes. Proc. Natl. Acad. Sci. U. S. A *79*, 1889-1892.

Seglen,P.O., Gordon,P.B., and Holen,I. (1990). Non-selective autophagy. Semin. Cell Biol. *1*, 441-448.

Seward,R.J., von Haller,P.D., Aebersold,R., and Huber,B.T. (2003). Phosphorylation of the pro-apoptotic protein Bim in lymphocytes is associated with protection from apoptosis. Mol. Immunol. *39*, 983-993.

She,Q.B., Chen,N., Bode,A.M., Flavell,R.A., and Dong,Z. (2002). Deficiency of c-Jun-NH(2)-terminal kinase-1 in mice enhances skin tumor development by 12-O-tetradecanoylphorbol-13-acetate. Cancer Res. *62*, 1343-1348.

Simizu,S., Tamura,Y., and Osada,H. (2004). Dephosphorylation of Bcl-2 by protein phosphatase 2A results in apoptosis resistance. Cancer Sci. *95*, 266-270.

Stromhaug,P.E., Berg,T.O., Fengsrud,M., and Seglen,P.O. (1998). Purification and characterization of autophagosomes from rat hepatocytes. Biochem. J. *335 (Pt 2)*, 217-224.

Suzuki,K., Kirisako,T., Kamada,Y., Mizushima,N., Noda,T., and Ohsumi,Y. (2001). The pre-autophagosomal structure organized by concerted functions of APG genes is essential for autophagosome formation. EMBO J. *20*, 5971-5981.

Tal,R., Winter,G., Ecker,N., Klionsky,D.J., and Abeliovich,H. (2007). Aup1p, a yeast mitochondrial protein phosphatase homolog, is required for efficient stationary phase mitophagy and cell survival. J. Biol. Chem. *282*, 5617-5624.

Tanida,I., Ueno,T., and Kominami,E. (2004). LC3 conjugation system in mammalian autophagy. Int. J. Biochem. Cell Biol. *36*, 2503-2518.

Tassa,A., Roux,M.P., Attaix,D., and Bechet,D.M. (2003). Class III phosphoinositide 3-kinase--Beclin1 complex mediates the amino acid-dependent regulation of autophagy in C2C12 myotubes. Biochem. J. *376*, 577-586.

Terman,A. (1995). The effect of age on formation and elimination of autophagic vacuoles in mouse hepatocytes. Gerontology *41 Suppl 2*, 319-326.

Thumm,M., Egner,R., Koch,B., Schlumpberger,M., Straub,M., Veenhuis,M., and Wolf,D.H. (1994). Isolation of autophagocytosis mutants of Saccharomyces cerevisiae. FEBS Lett. *349*, 275-280.

Tournier,C., Hess,P., Yang,D.D., Xu,J., Turner,T.K., Nimnual,A., Bar-Sagi,D., Jones,S.N., Flavell,R.A., and Davis,R.J. (2000). Requirement of JNK for stress-induced activation of the cytochrome c-mediated death pathway. Science *288*, 870-874.

Tracy,K., Dibling,B.C., Spike,B.T., Knabb,J.R., Schumacker,P., and Macleod,K.F. (2007). BNIP3 is an RB/E2F target gene required for hypoxia-induced autophagy. Mol. Cell Biol. *27*, 6229-6242.

Trifunovic,A., Wredenberg,A., Falkenberg,M., Spelbrink,J.N., Rovio,A.T., Bruder,C.E., Bohlooly,Y., Gidlof,S., Oldfors,A., Wibom,R., Tornell,J., Jacobs,H.T., and Larsson,N.G. (2004). Premature ageing in mice expressing defective mitochondrial DNA polymerase. Nature *429*, 417-423.

Tsujimoto,Y. (2003). Cell death regulation by the Bcl-2 protein family in the mitochondria. J. Cell Physiol *195*, 158-167.

Tsujimoto,Y. and Shimizu,S. (2000). VDAC regulation by the Bcl-2 family of proteins. Cell Death. Differ. *7*, 1174-1181.

Tsujimoto,Y. and Shimizu,S. (2005). Another way to die: autophagic programmed cell death. Cell Death. Differ. *12 Suppl 2*, 1528-1534.

Tsukada,M. and Ohsumi,Y. (1993). Isolation and characterization of autophagy-defective mutants of Saccharomyces cerevisiae. FEBS Lett. *333*, 169-174.

Tsuruta,F., Sunayama,J., Mori,Y., Hattori,S., Shimizu,S., Tsujimoto,Y., Yoshioka,K., Masuyama,N., and Gotoh,Y. (2004). JNK promotes Bax translocation to mitochondria through phosphorylation of 14-3-3 proteins. EMBO J. *23*, 1889-1899.

Turk,B., Stoka,V., Rozman-Pungercar,J., Cirman,T., Droga-Mazovec,G., Oresic,K., and Turk,V. (2002). Apoptotic pathways: involvement of lysosomal proteases. Biol. Chem. *383*, 1035-1044.

Tuttle,D.L., Lewin,A.S., and Dunn,W.A., Jr. (1993). Selective autophagy of peroxisomes in methylotrophic yeasts. Eur. J. Cell Biol. *60*, 283-290.

Waldmeier,P.C., Zimmermann,K., Qian,T., Tintelnot-Blomley,M., and Lemasters,J.J. (2003). Cyclophilin D as a drug target. Curr. Med. Chem. *10*, 1485-1506.

Wang,Y., Singh,R., Lefkowitch,J.H., Rigoli,R.M., and Czaja,M.J. (2006). Tumor necrosis factor-induced toxic liver injury results from JNK2-dependent activation of caspase-8 and the mitochondrial death pathway. J. Biol. Chem. *281*, 15258-15267.

Weston,C.R., Balmanno,K., Chalmers,C., Hadfield,K., Molton,S.A., Ley,R., Wagner,E.F., and Cook,S.J. (2003). Activation of ERK1/2 by deltaRaf-1:ER* represses Bim expression independently of the JNK or PI3K pathways. Oncogene *22*, 1281-1293.

Xue,L., Fletcher,G.C., and Tolkovsky,A.M. (1999). Autophagy is activated by apoptotic signalling in sympathetic neurons: an alternative mechanism of death execution. Mol. Cell Neurosci. *14*, 180-198.

Xue,L., Fletcher,G.C., and Tolkovsky,A.M. (2001). Mitochondria are selectively eliminated from eukaryotic cells after blockade of caspases during apoptosis. Curr. Biol. *11*, 361-365.

Yakes,F.M. and Van,H.B. (1997). Mitochondrial DNA damage is more extensive and persists longer than nuclear DNA damage in human cells following oxidative stress. Proc. Natl. Acad. Sci. U. S. A *94*, 514-519.

Yamamoto,A., Masaki,R., and Tashiro,Y. (1990). Characterization of the isolation membranes and the limiting membranes of autophagosomes in rat hepatocytes by lectin cytochemistry. J. Histochem. Cytochem. *38*, 573-580.

Yamamoto,K., Ichijo,H., and Korsmeyer,S.J. (1999). BCL-2 is phosphorylated and inactivated by an ASK1/Jun N-terminal protein kinase pathway normally activated at G(2)/M. Mol. Cell Biol. *19*, 8469-8478.

Yokota,S. (2003). Degradation of normal and proliferated peroxisomes in rat hepatocytes: regulation of peroxisomes quantity in cells. Microsc. Res. Tech. *61*, 151-160.

Yorimitsu,T. and Klionsky,D.J. (2005). Autophagy: molecular machinery for self-eating. Cell Death. Differ. *12 Suppl 2*, 1542-1552.

Yu,L., Alva,A., Su,H., Dutt,P., Freundt,E., Welsh,S., Baehrecke,E.H., and Lenardo,M.J. (2004). Regulation of an ATG7-beclin 1 program of autophagic cell death by caspase-8. Science *304*, 1500-1502.

Yu,Q.C. and Marzella,L. (1988). Response of autophagic protein degradation to physiologic and pathologic stimuli in rat hepatocyte monolayer cultures. Lab Invest *58*, 643-652.

Yuan,J., Lipinski,M., and Degterev,A. (2003). Diversity in the mechanisms of neuronal cell death. Neuron *40*, 401-413.

Yue,Z., Jin,S., Yang,C., Levine,A.J., and Heintz,N. (2003). Beclin 1, an autophagy gene essential for early embryonic development, is a haploinsufficient tumor suppressor. Proc. Natl. Acad. Sci. U. S. A *100*, 15077-15082.

Zahrebelski,G., Nieminen,A.L., al-Ghoul,K., Qian,T., Herman,B., and Lemasters,J.J. (1995). Progression of subcellular changes during chemical hypoxia to cultured rat hepatocytes: a laser scanning confocal microscopic study. Hepatology *21*, 1361-1372.

Zoratti,M. and Szabo,I. (1995). The mitochondrial permeability transition. Biochim. Biophys. Acta *1241*, 139-176.

Zorov,D.B., Juhaszova,M., and Sollott,S.J. (2006). Mitochondrial ROS-induced ROS release: an update and review. Biochim. Biophys. Acta *1757*, 509-517.